# Soil Moisture Analysis Based On Microwave Brightness Temperatures: A Study on Systematic and Random Errors

**Dissertation**

zur

Erlangung des Doktorgrades (Dr. rer. nat.)

der

Mathematisch-Naturwissenschaftlichen Fakultät

der

Rheinischen Friedrich-Wilhelms-Universität Bonn

vorgelegt von

**Henning Wilker**

aus

Bassum

Bonn 2006

Angefertigt mit Genehmigung der Mathematisch-Naturwissenschaftlichen Fakultät der Rheinischen Friedrich-Wilhelms-Universität Bonn

1. Referent: Prof. Dr. Clemens Simmer
2. Referent: Privatdozent Dr. Hendrik Elbern

Tag der Promotion: 10. April 2007

Diese Dissertation ist auf dem Hochschulschriftenserver der ULB Bonn
`http://hss.ulb.uni-bonn.de/diss_online` elektronisch publiziert.

Erscheinungsjahr: 2007

**Abstract**

The soil moisture analysis systems of current operational weather prediction models mainly rely on observations of screen-level (2-metre) air temperature and humidity and thus require a strong coupling between the soil and the atmospheric boundary layer by the latent and sensible heat fluxes. Satellite-borne brightness temperature observations in the low-frequency microwave range are independent of the weather situation and can provide land surface soil moisture information from regional to global scales. In the context of the European Union research project ELDAS (complete title: *Development of a European Land Data Assimilation System to predict floods and droughts*), the European Centre for Medium-Range Weather Forecasts (ECMWF) developed an experimental soil moisture analysis system which, embedded in the single-column version of the ECMWF weather forecast model, is able to assimilate both screen-level variables and microwave brightness temperatures. The Meteorological Institute of the University of Bonn contributed to this system by incorporating the Land Surface Microwave Emissivity Model (LSMEM). Based on measurements from the Southern Great Plains Hydrology Experiments (SGP97 and SGP99), this dissertation investigates the impact of potential systematic and random errors on the performance of the ELDAS soil moisture analysis and discusses how to cope with these errors in operational applications. Three topics are addressed in detail:

(a) An error propagation experiment simulates the effects of erroneous precipitation forcing on the soil moisture of different model layers. The non-systematic, depth-dependent errors found are integrated into the model error covariance matrix. Analysed soil moisture and modelled surface heat fluxes from assimilation runs using this covariance matrix are compared to results from reference runs using a vertically uniform model error. The different model error covariance matrices significantly affect model soil moisture and fluxes; a preferable setting, however, can not be identified.

(b) An easy-to-apply method of accounting for systematic errors of observations, forward operators and the background soil moisture in an operational large-scale forecast environment is to correct the observations used for the assimilation procedure by the so-called innovation bias (the systematic deviation of the observations from the model equivalents). Such a correction is carried out based on data from an SGP97 site and is shown to improve the performance of the soil moisture analysis. The simulation of the surface latent and sensible

heat fluxes, however, does not benefit from the improved analysis. Significant contributions to the innovation biases are shown to result from the microwave forward operator (the LSMEM) and a dry bias of the modelled near-surface soil moisture.

(c) Land surface schemes of current weather forecast models do not sufficiently resolve the top few centimetres of the soil from where the main brightness temperature signal originates. In case of non-uniform near-surface soil moisture and temperature profiles in reality, the assimilation of the corresponding brightness temperature observations can lead to misinterpretations by the soil moisture analysis. The relevance of this model shortcoming is investigated with artificial profiles created on the basis of SGP99 soil moisture and temperature measurements. Mean brightness temperature errors of up to $\pm$ 5 K are found depending on the days elapsed after a rainfall event. A simple bias correction method is presented and applied for the SGP97 period.

The assimilation studies prove that microwave brightness temperature observations are a valuable information source for analysing model soil moisture. However, accurate knowledge of the accompanying systematic and random errors is needed.

**Zusammenfassung**

Die Bodenfeuchteanalyseverfahren in gegenwärtigen operationellen Wettervorhersagemodellen beruhen hauptsächlich auf Beobachtungen der 2m-Temperatur und -Feuchte und erfordern daher eine ausgeprägte Kopplung zwischen dem Erdboden und der atmosphärischen Grenzschicht über die latenten und fühlbaren Wärmeflüsse. Satellitengetragene Beobachtungen der Helligkeitstemperatur im unteren Mikrowellenfrequenzbereich sind unabhängig von der Wettersituation und können Informationen über die regionale bis globale Bodenfeuchteverteilung liefern. Im Rahmen des EU-Forschungsprojektes ELDAS (vollständiger übersetzter Titel: *Entwicklung eines Europäischen Landdatenassimilationssystems zur Vorhersage von Hochwassern und Trockenheiten*) hat das Europäische Zentrum für mittelfristige Wettervorhersage (EZMW) ein experimentelles Bodenfeuchteanalysesystem entwickelt, mit dem, eingebettet in die eindimensionale Version des EZWM-Wettervorhersagemodells, die Ausnutzung sowohl von operationellen Beobachtungen der 2m-Temperatur und -Feuchte als auch von Mikrowellenhelligkeitstemperaturen möglich ist. Das Meteorologische Institut der Universität Bonn ergänzte dazu das EZMW-Modell mit einem Mikrowellenemissivitätsmodell für Landoberflächen (LSMEM). Basierend auf Feldmessungen der Southern Great Plains Hydrology Experiments (SGP97 und SGP99) untersucht diese Dissertation, welche Auswirkungen potentielle systematische und zufällige Fehler auf die Güte der ELDAS-Bodenfeuchteanalyse haben und wie diese Fehler im operationellen Modellbetrieb berücksichtigt werden können. Drei Themenschwerpunkte werden diskutiert:

(a) In einem Fehlerausbreitungsexperiment werden die Auswirkungen von fehlerhaften Niederschlagsdaten auf die Bodenfeuchte in verschiedenen Modellschichten simuliert. Die dabei gefundenen, von der Bodentiefe abhängigen Unsicherheiten werden in die Kovarianzmatrix des Modellfehlers integriert. Die auf Basis dieser Kovarianzmatrix berechneten Bodenfeuchten und Flüsse latenter und sensibler Wärme werden mit entsprechenden Ergebnissen aus Referenzläufen, bei denen ein vertikal konstanter Modellfehler angenommen wurde, verglichen. Die unterschiedlichen Kovarianzmatrizen des Modellfehlers beeinflussen signifikant die Modellbodenfeuchte und -flüsse. Welche Festlegung der Kovarianzmatrix insgesamt besser ist, kann aber anhand der vorhandenen Ergebnisse nicht festgestellt werden.

(b) Eine einfach anzuwendende Methode, um systematische Fehler der Beobachtungen, der Vorwärtsoperatoren und der Hintergrundbodenfeuchte im operationellen Betrieb eines großskaligen Vorhersagemodells zu berücksichtigen, ist die Korrektur der zu assimilierenden Beobachtungen um den Betrag des so genannten Innovationsbias (die systematische Abweichung der Beobachtungen von den entsprechenden Modellwerten). Eine solche Korrektur wurde anhand von Daten eines SGP97-Messfeldes durchgeführt. Die Güte der Bodenfeuchteanalyse (verglichen mit Messungen) konnte dadurch verbessert werden. Die Simulation der oberflächennahen latenten und fühlbaren Wärmeflüsse profitiert jedoch nicht von der verbesserten Bodenfeuchteanalyse. Es wird gezeigt, dass der Mikrowellen-Vorwärtsoperator (das LSMEM) und ein trockener Bias der modellierten oberflächennahen Bodenfeuchte die wesentlichen Beiträge zum Innovationsbias liefern.

(c) Die Bodenmodelle in gegenwärtigen Wettervorhersagemodellen erfassen die obersten Zentimeter des Bodens nur ungenügend. Aus diesem Bereich kommt allerdings der wesentliche Beitrag zum Helligkeitstemperatursignal. Wenn der Boden in der Realität kein konstantes Feuchte- oder Temperaturprofil aufweist, kann deshalb die Assimilation der entsprechenden Helligkeitstemperaturbeobachtungen zu falschen Interpretationen durch die Bodenfeuchteanalyse führen. Die Relevanz dieser Modellunzulänglichkeit wird anhand von künstlichen Profilen, die auf Basis von SGP99-Messungen der Bodenfeuchte und Bodentemperatur erzeugt wurden, untersucht. Bei den modellierten Helligkeitstemperaturen ergeben sich durchschnittliche Fehler von bis zu $\pm$ 5 K, abhängig von der Anzahl der Tage, die seit dem Auftreten eines Regenereignisses vergangen sind. Es wird eine einfache Biaskorrektur vorgeschlagen und für den SGP97-Zeitraum angewendet.

Insgesamt zeigen die Assimilationsstudien, dass Beobachtungen von Mikrowellenhelligkeitstemperaturen eine wertvolle Informationsquelle für die Analyse der Modellbodenfeuchte sind. Eine genaue Kenntnis der damit verbundenen systematischen und zufälligen Fehler ist aber unerlässlich.

# Contents

# List of Figures

# List of Tables

# List of Acronyms

**AMSR-E** Advanced Microwave Scanning Radiometer – EOS

**ARM** Atmospheric Radiation Measurement Program

**ARS** Agricultural Research Service

**ATDD** Atmospheric Turbulence and Diffusion Division

**BCO** Assimilation runs using observations corrected by innovation biases

**CART** Cloud and Radiation Testbed

**CF** Central Facility

**CF**** SGP site identifier in the Central Facility area, e.g. CF01

**CTRL** Control run

**DFG** Deutsche Forschungsgemeinschaft (German Research Foundation)

**DMSP** Defense Meteorological Satellite Program

**DWD** Deutscher Wetterdienst (German Weather Service)

**ECMWF** European Centre for Medium-Range Weather Forecasts

**ELDAS** European Land Data Assimilation System

**EOS** NASA's Earth Observing System

**ER** El Reno

**ER*** SGP site identifier in the El Reno area, e.g. ER5

**ERA-40** ECMWF 40-Year Re-Analysis

**ESA** European Space Agency

**ESTAR** Electronically Scanned Thinned Array Radiometer

**EU** European Union

**GVMP** Control run with model soil moisture re-initialised with retrievals from matric potential observations and gravimetric measurements at SGP97 site LW02

**HYDROS** Hydrosphere State Mission

**IFS** ECMWF's Integrated Forecast System

**KB** Extended Kalman filter soil moisture analysis assimilating brightness temperature alone

**KTR** Extended Kalman filter soil moisture analysis assimilating 2-metre temperature and relative humidity alone

**KTRB** Extended Kalman filter soil moisture analysis assimilating 2-metre temperature, relative humidity and brightness temperature together

**LDAS** North American Land Data Assimilation System

**LITFASS** Lindenberg Inhomogeneous Terrain — Fluxes between Atmosphere and Surface: a long-term Study

**LSMEM** Land Surface Microwave Emissivity Model

**LST** Local Standard Time

**LW** Little Washita Watershed

**LW**** SGP site identifier in the Little Washita Watershed, e.g. LW02

**MP** Control run with model soil moisture re-initialised with retrievals from matric potential observations at SGP97 site LW02

**MSMA** Measurement-forced Soil Moisture Analysis

**NASA** National Aeronautics and Space Administration of the U.S.A

**NASDA** National Space Development Agency of Japan

**NDVI** Normalised Difference Vegetation Index

**NOAA** National Oceanic and Atmospheric Administration of the U.S.A.

**OBS** Observations

**OI** Optimal Interpolation

**PCB** Assimilation runs applying a systematic error correction due to the profile sensitivity study

**Q** Assimilation runs applying the revised model error

**REF** Reference assimilation experiments (Seuffert et al., 2004)

**SCM** Single-Column Model

**SGP97** Southern Great Plains Hydrology Experiment 1997

**SGP99** Southern Great Plains Hydrology Experiment 1999

**SHAWMS** Soil Heat And Water Measurement System

**SMOS** Soil Moisture and Ocean Salinity Mission

**SSM/I** Special Sensor Microwave Imager

**STATSGO** State Soil Geographic Database

**TBA** Mean brightness temperature calculated from the artificial profile ensembles

**TBU** Brightness temperature calculated from the mean, vertically uniform model soil moisture

**TESSEL** Tiled ECMWF Scheme for Surface Exchanges over Land

**TMI** TRMM Microwave Imager

**TRMM** Tropical Rainfall Measuring Mission

**USDA** United States Department of Agriculture

# Chapter 1

# Motivation and objectives

## 1.1 Relevance of soil moisture

Water is an essential component of the Earth's climate system: almost 71 % of the Earth's surface is covered by oceans; the continents are characterised by a variety of surface and subsurface water reservoirs (e.g. rivers, lakes, and groundwater); during winter, snow and ice spread over up to 42 % of the Northern Hemispheric land area (Robinson et al., 1993); two-thirds of the planet are on average cloud-covered (Peixoto and Oort, 1992; Rossow and Schiffer, 1999); and the troposphere contains a varying portion of water vapor (up to a few percent by volume). Water thus naturally occurs in the solid (ice), liquid and gaseous (water vapor) phase under the prevailing pressure and temperature conditions on Earth. Evapotranspiration, condensation and sublimation processes, precipitation, ocean currents, atmospheric winds and land surface streams build a complex system of persistent water and energy transports on our planet, driven by the solar insolation. A schematic diagram of this global water cycle, also referred to as hydrological cycle, is shown in Fig. 1.1. The quantities of water volumes and fluxes are estimates adopted from Oki (1999). Precise values are not known yet; therefore, the specified numbers can differ from others given in the literature (see e.g. Peixoto and Oort (1992) and Hartmann (1994)). However, Fig. 1.1 illustrates the qualitative proportions of the global water reservoirs and transports.

A fraction of the water at land is held in the soil between the surface and the groundwater level due to hygroscopic and capillary forces. The volume or mass ratio of the bound water to the soil media is called soil moisture or soil water content. Although comparatively small in the absolute amount (see Fig. 1.1), the soil water can be of significant importance to human activities:

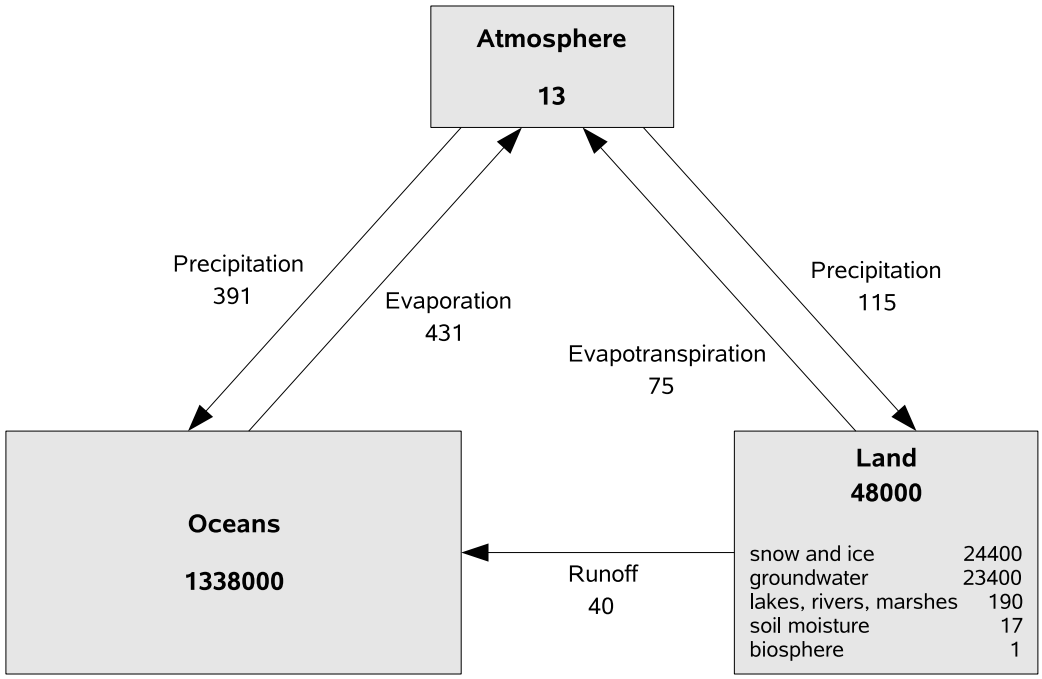


Figure 1.1: Schematic diagram of the Earth's water cycle. Reservoir volumes (boxes) are stated in $10^3$ km$^3$, water fluxes (arrows) in $10^3$ km$^3$ per year. Values are adopted from Oki (1999).

a) Plants extract water from the soil through their roots. Depending on vegetation type, soil type, and water availability, the roots reach depths from a few centimetres to several metres. An appropriate soil water content of the root zone, i.e. not too dry and not too wet over a longer time period, is essential for plants to survive. Therefore, the cultivation of plants requires knowledge of their appropriate root zone moisture and of the prevalent soil water content, e.g. in order to effectively irrigate crop fields.

b) The ability of the soil to take up a certain amount of water can have a significant influence on the occurrence and intensity of floodings. The field capacity, which is the soil water content below which the soil can hold back water against the force of gravity, varies from about 0.10 m$^3$/m$^3$ for very sandy soils to about 0.35 m$^3$/m$^3$ for heavy clay (Dingman, 2002). Consequently, a cubic metre of dry soil media is able to absorb a water volume of several ten to a few hundred litres. The ability of the soil to take up rainwater decreases when the soil media is very dry and compact, partly frozen, or when the precipitation is too intense. Nevertheless, a dry soil can act as a significant detention reservoir in case of heavy rain, extenuating the runoff into rivers. If the soil was already saturated all precipitating water would be directly discharged at the surface or underground, enhancing the possibility or aggravating the intensity of floodings

(e.g. Bundesanstalt für Gewässerkunde, 2002). Therefore, not only an accurate precipitation forecast but also the knowledge of the actual soil moisture is important for the prediction of flooding events.

c) As long as enough water is available in the upper soil layers and the atmosphere on top is not saturated, evaporation takes place at the soil surface. Plants also continuously release water into the air mainly from their leaf surfaces, although they are able to control this process by their stomata. In general, the rate of evapotranspiration depends on the temperature and water content of the soil surface, of the vegetation, and of the atmosphere on top, on the wind speed, and on the ability of the soil (by hygroscopic and capillary forces) and the plants (by closing their leaf pores) to hold back the water (Hartmann, 1994). The higher the evapotranspiration rate, the more energy is needed for the transition from the liquid to the gaseous phase. Therefore, the soil water content affects the energy budget at the soil surface, namely the partitioning of the available energy into the sensible and latent heat fluxes. Soil moisture thus has an indirect influence on the dynamics of the planetary boundary layer and therefore on the weather. This relation was demonstrated by several sensitivity simulations with numerical models. Seuffert et al. (2002), for instance, showed in a late-summer case study over the Sieg catchment that the precipitation forecast can significantly depend on the initialisation and spatial representation of the model soil moisture. Schär et al. (1999) found similar results in a sensitivity study covering Europe during midsummer of 1990 and 1993. However, the regional effects of area-wide variations in initial soil moisture on the precipitation amount were quite different. In some regions, doubling the soil water content or reducing it by half accounts for precipitation modifications of the same factor, while no significant changes in precipitation were simulated at other locations. Dirmeyer et al. (2000) showed that the sensitivity of the turbulent surface fluxes to the soil moisture strongly depends on the type of vegetation cover and on the wetness of the soil itself. They found that the correlation of the evaporative fraction, which is the ratio of latent heat flux to the sum of latent and sensible heat flux, with the soil water content is largest for regions with sparse vegetation and dry soils. The turbulent fluxes over forested or wet surfaces revealed the smallest sensitivity to soil water variations. Ament and Simmer (2006) demonstrated on the basis of measurements from the LITFASS domain near Berlin, Germany, that surface flux simulations with the Lokal-Modell (LM) of the German Weather Service (Deutscher Wetterdienst, DWD) significantly improve when (a) the operational soil moisture analysis, which is solely based on 2-metre temperature and relative humdity (Hess, 2001), is replaced by a measurement-forced soil moisture analysis (MSMA), which also uses wind, radiation and radar-retrieved precipiation obser-

vations, and (b) when the vegetation stomatal resistance and albedo is defined land-use-dependent. These selected studies show that an accurate knowledge of the soil water content, in conjunction with a proper definition of the vegetation characteristics, is essential for the simulation of the land surface turbulent fluxes and therefore for the numerical prediction of weather conditions.

## 1.2 Current simulation of soil moisture in numerical weather prediction models

Provided that nearly all of the soil water that plants take up in the root zone is transpired and only a negligible fraction is used for the plant's growth, the change of soil water storage at an arbitrary location is the sum of precipitation, evapotranspiration, surface runoff, percolation, and horizontal water transports within the soil (e.g. Peixoto and Oort, 1992). The water balance equation for the land surface can therefore be written as follows:

$$S = P - E - R_0 - R_u \tag{1.1}$$

Here $S$ denotes the change of soil water storage, $P$ precipitation, $E$ evapotranspiration, $R_0$ surface runoff, and $R_u$ subsurface runoff including percolation. In principle, numerical land surface schemes simply have to solve Eq. (1.1) to calculate the spatial distribution and temporal evolution of the soil water content. However, the simulation of soil moisture in atmospheric models is still unsatisfying (e.g. Richter et al., 2004; Ament and Simmer, 2006). The deficiencies can be traced back to the following issues:

a) The modelled values of surface net radiation and precipitation are often inaccurate because the forecast models still have problems with properly simulating the development and movement of low-pressure systems, of convective systems inducing showers and thunderstorms, and of low-level clouds often occurring in winterly high-pressure inversion conditions (e.g. Jung and Tompkins, 2003).

b) A couple of static or slowly varying soil and vegetation characteristics (e.g. soil texture, rooting depth, and leaf area index) affect the amount of water the soil can absorb and hold back against evaporation and percolation and determine how much water the plants take up through their roots and transpire from their leafs. The absolute values and the spatial distribution of these parameters are only approximately known.

c) Physical, chemical and biological processes usually take place on much smaller scales than a numerical model used for weather prediction or climate

simulations is able to resolve. These processes thus have to be represented by approximate equations, the so-called parameterisations. Parts of these parameterisations and the process coefficients they contain cannot be deduced from theory. Hence, they are often derived from a limited number of measurements which have been recorded under certain conditions at selected locations or in a laboratory, and thus might be valid for specific situations only. Additionally, the complexity of atmospheric and land surface processes and the still limited computing power requires compromises between simulation quality and efficiency in weather forecast models (e.g. radiative transfer calculations and cloud physics).

These error sources can cause drifts in the simulated soil moisture away from reality over weeks and months. Consequently, modelled root zone soil moisture has to be regularly corrected by measurements. A widely-used procedure to incorporate observations into numerical models is the technique of data assimilation. It combines the information content of measurements with the mathematical and physical constraints of the models so that a physically consistent image of the state of the system under consideration (e.g. the atmosphere) can be retrieved. However, a global network of in-situ soil moisture measurements that could provide data on the model's grid scale does not exist at present. Consequently, proxy observations for root zone soil moisture are used. Current operational analysis systems rely on observations of screen-level variables, namely 2-metre temperature and 2-metre relative humidity, which are coupled to the land surface by the turbulent fluxes of sensible and latent heat. At Météo France and the European Centre for Medium-Range Weather Forecasts (ECMWF), an Optimal Interpolation method (Douville et al., 2000) is used to initialise soil moisture operationally, while the German Weather Service (DWD) applies an Extended Kalman filter as described by Hess (2001). Another helpful proxy observation type is the land surface heating rate derived from satellite temperature observations (e.g. Jones et al., 1998a,b). This method makes use of the temperature increase during the morning hours which is higher for a dry soil than for a wet one.

Soil moisture analysis systems using proxy observations of air temperature and humidity rely on strong thermal interactions between the soil surface and the atmospheric layers on top. In case of a weak coupling, i.e. during strong horizontal winds and weak insolation, the application of these analysis methods might even adjust the model soil moisture into the wrong direction. Therefore, theses types of soil moisture analysis systems are modified for these specific meteorological conditions (e.g. Douville et al., 2000; Mahfouf, 1991). The use of satellite-observed heating rates requires clear skies so that several days or even weeks might pass between two soil moisture analyses. In contrast to these current

soil moisture analysis systems, the impact of weather conditions on the information from passive microwave remote sensing is negligible. Therefore, microwave data might prove to be an additional valuable data source for soil moisture analysis as described in the next section.

## 1.3 Potential benefits from passive microwave remote sensing

The brightness temperature of a body is defined by the mathematical product of its emissivity and its temperature. In passive microwave remote sensing applications, the brightness temperature is usually used as a measure of the radiation intensity, to which it is proportional for typical Earth surface temperatures and frequencies in the microwave range (1 – 300 GHz) according to the radiation law of Rayleigh and Jeans (e.g. Ulaby et al., 1981). Passive microwave brightness temperature observations of the land surface from satellites are a more direct information source of the near-surface soil moisture than 2-metre temperature, 2-metre humidity and heating rates and are not subject to the constraints of these proxy observation types discussed in the previous section (e.g. Jackson et al., 1999; Njoku and Entekhabi, 1996; Ulaby et al., 1981, 1982, 1986).

What makes microwave radiation interesting for soil moisture sensing is the fact that the real part of the dielectric constant of water and dry soil material significantly differ at microwave frequencies. Fig. 1.2(a) shows an example of this difference. As a result, the emissivity of a soil volume varies significantly with its water content. Fig. 1.2(b) shows an example for a loamy soil with a smooth surface at 1.4 GHz. The emissivity for the microwave radiation decreases from nearly 0.9 for a dry case to less than 0.6 for a high water content. This results in brightness temperature variations of up to 90 K for a soil temperature of 300 K.

Microwaves below 2 GHz (L-band) are especially well-suited for the remote sensing of soil moisture because the soil penetration depth significantly increases towards lower frequencies (e.g. Njoku and Entekhabi, 1996). Moreover, the impact of the atmosphere and clouds on the low-frequency microwave radiation is negligible (Barrett and Kniveton, 1995; Drusch et al., 2001; Ulaby et al., 1981). Since purely from the technical point of view microwave brightness temperatures can be measured with an accuracy of better than 1 K (Njoku and Entekhabi, 1996), the signal-to-noise ratio is large and illustrates the potential of passive microwave remote sensing for monitoring the land surface soil moisture. However, a dense vegetation canopy can obscure the soil moisture signal in the microwave radiation received by a satellite-borne or air-borne sensor although the impact

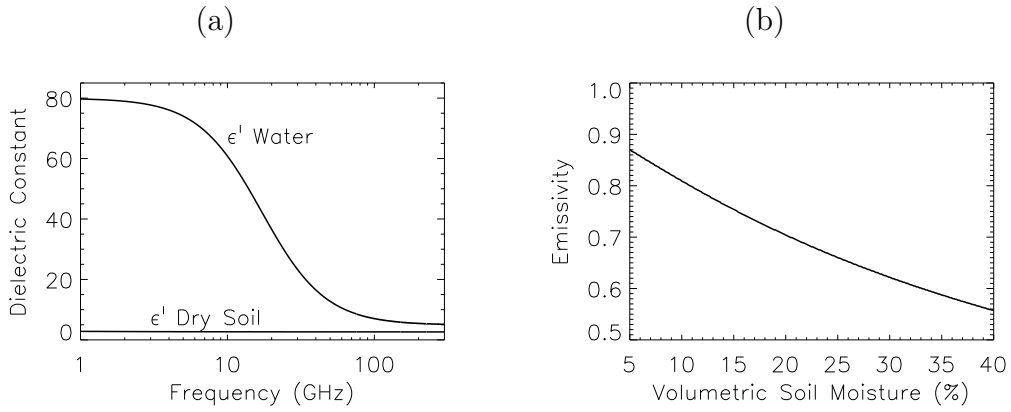


Figure 1.2: Examples of (a) the real part of the dielectric constants of water and dry soil and (b) the soil emissivity with varying water content. (The curves are calculated with the Land Surface Microwave Emissivity Model (LSMEM, section 2.1.3) for a loamy soil with a bulk density of 1.35 g/cm$^3$ and water with a salinity of 0.65 psu and a temperature of 20 °C. Viewing angle and frequency used for plot (b) are 0° and 1.4 GHz, respectively.)

of vegetation on the microwave emission of a soil surface decreases towards lower microwave frequencies (Ulaby et al., 1986; Wegmüller et al., 1995). Vegetation effects thus need to be taken into account in data assimilation applications using microwave remote sensing data (also see Sec. 2.1.3).

Current passive microwave sensors flying onboard satellites are the Special Sensor Microwave Imager (SSM/I; Hollinger et al., 1987), the Advanced Microwave Scanning Radiometer (AMSR-E; Kawanishi et al., 2003), and the Tropical Rainfall Measuring Mission (TRMM) Microwave Imager (TMI; Kummerow et al., 1998). SSM/I sensors fly onboard satellites of the United States Air Force Defense Meteorological Satellite Program (DMSP) since 1987. They globally observe brightness temperatures at four channels and two polarisations between 19 and 85 GHz. TMI is a similar instrument onboard the TRMM satellite, which is jointly operated by the National Aeronautics and Space Administration (NASA) of the United States and the National Space Development Agency (NASDA) of Japan since 1998, with an additional channel at 10.7 GHz. It provides passive microwave observations at latitudes between 40° North and 40° South. The AMSR-E sensor finally was launched onboard NASA's Earth Observing System (EOS) Aqua satellite in 2002 in cooperation with NASDA. This instrument provides, in addition to frequencies similar to TMI, global observations at 6.9 GHz.

The available frequencies are not optimal for soil moisture retrieval applications (see above). Therefore, the European Space Agency (ESA) is preparing to launch the Soil Moisture and Ocean Salinity (SMOS) mission (Kerr et al.,

2001) — currently scheduled for 2007 — which will provide 1.4 GHz brightness temperature observations on a global scale for at least 3 years. Data will be delivered with a spatial resolution of about 50 kilometres and a revisit time of 3 days at the equator. This project will provide the opportunity to assess the benefits of supplementing current land data assimilation systems with passive microwave brightness temperatures as another source of proxy observations of surface soil moisture. It is expected that this method can further improve the soil moisture analysis in weather forecast systems leading to a better representation of the planetary boundary layer dynamics. Another satellite project, NASA's Hydrosphere State (HYDROS) mission (Entekhabi et al., 2004), was planned to start operation in 2010 in order to provide global L-band brightness temperatures, too. The funding for this project has however been ceased recently (`http://hydros.gsfc.nasa.gov/`).

## 1.4 Thesis objectives and outline

Publications in the reviewed literature have already demonstrated the usefulness of passive microwave observations in land data assimilation applications (Margulis et al., 2002; Crow and Wood, 2003; Seuffert et al., 2003, 2004; Reichle and Koster, 2005). However, very little research has been done on the effects of inevitable systematic and random errors of observations, models, and forcing data on the outcome of the soil moisture analysis systems. The quality of the analysis strongly depends on an accurate determination of these errors for two reasons (Bouttier and Courtier, 1999; Talagrand, 1997): a) Assimilation techniques rely on bias-free observations and model formulations. Any systematic error must be corrected before the analysis is performed. b) Assimilation techniques weight the information from the observations and from the model background, which e.g. can be the results of an antecedent forecast, by their uncertainties. The larger the mean random error of an observation or background variable is, the less it shall influence the analysis. Incorrect assumptions or non-consideration of these errors can significantly degrade the performance of a soil moisture analysis as recently shown by Crow and van Loon (2006) for the model error in an ensemble Kalman filter system.

In preparation for the use of L-band microwave brightness temperatures in land data assimilation systems, this thesis examines:

- Errors occurring in both the observations and the model.
- How these errors effect the analysed soil moisture and the resulting surface fluxes of latent and sensible heat.

- How to take these errors into account in the soil moisture analysis.

These questions are addressed using ECMWF's European Land Data Assimilation System (ELDAS) soil moisture analysis.

Section 4.1 quantifies the effect of erroneous precipitation forcing on the model's first guess of the soil water content profile. The difficulties of current numerical weather prediction models to accurately forecast the intensity of precipitation events are represented by performing a set of forecasts with randomly perturbed rain amounts. The resulting soil moisture uncertainties are integrated into the model error covariance matrix which has then been applied in a 4-week assimilation run using data from the Southern Great Plains 1997 Hydrology Experiment (SGP97). Section 4.2 addresses the so-called innovation vector, which contains the differences between the observations and their equivalent model values. The innovation vector needs to be unbiased for a well-defined assimilation system. On the basis of SGP97 data, sources for biases are discussed and the impact of a bias correction, which can be easily applied in operational forecast systems, on the performance of the soil moisture analysis and the resulting turbulent surface heat fluxes is examined.

In section 4.3, this thesis focuses on the systematic error which is introduced by the insufficient vertical resolution of the soil close to the surface in current large-scale meteorological and hydrological land surface models. Passive microwave measurements are most sensitive to the moisture profile in the top few centimeters of the soil, but in models, this zone is often represented by only one layer. In this case, the modelled brightness temperature in the data assimilation system, which is based on the modelled soil moisture value of the top layer of the land surface model, will be equal to the observation only if the true soil moisture profile is uniform. In case of a non-uniform profile a vertically integrated mean soil moisture content will introduce errors. The model will compute too high brightness temperatures from the uniform model profile whenever, in reality, the top of that particular layer is wetter than the average and too low brightness temperatures for the opposite situation. This study quantifies this systematic error based on in-situ observations from the SGP99 experiment. The most sophisticated approach to eliminate profile biases in the assimilation of microwave brightness temperatures would be to include more soil layers in the hydrological land surface model. However, land surface model modifications always affect a range of parameters and processes which then would need additional elaborate testing and learning. A more practical way to cope with these systematic errors is to correct the observed brightness temperatures for the effect of a non-uniform soil moisture profile. Therefore, a correction method in observation space is presented and applied to the ELDAS (European Land Data Assimilation System)

soil moisture analysis system. It has been tested with SGP97 data based on assimilation experiments performed by Seuffert et al. (2004).

# Chapter 2

# ELDAS data assimilation system

In the context of the European Union's Fifth Framework Program, the research project ELDAS, an acronym for *Development of a European Land Data Assimilation System to predict floods and droughts*, was carried out "to develop a general data assimilation infrastructure for estimating soil moisture fields on the regional (continental) scale, and to assess the added value of these fields for the prediction of the land surface hydrology in models used for numerical weather prediction and climate studies" (cited from `http://www.knmi.nl/samenw/eldas/`). Several European hydrological and meteorological institutions and weather centres (e.g. the European Centre for Medium-Range Weather Forecasts (ECMWF), Météo France, and the German Weather Service (DWD)) exchanged their expertise in land data assimilation and worked on coordinated and efficient enhancements of their land data assimilation systems. As a part of ELDAS, ECMWF developed an experimental soil moisture analysis system which is able to process both screen-level observations (air temperature and humidity at 2 m height) and microwave brightness temperatures observed from satellite or aircraft. The Meteorological Institute of the University of Bonn contributed to this system by integrating the microwave forward operator. The purpose was to test the possible future usage of remotely sensed passive microwave observations in land data assimilation systems. The soil moisture analyis has been coupled with ECMWF's single-column model (SCM) which is a limited version of ECMWF's operational Integrated Forecast System (IFS, version number Cy23r4). The SCM only addresses interactions and processes active in the vertical direction so that changes in the atmospheric column due to horizontal advection have to be specified as input. Apart from that, it comprises the complete physical package of the IFS and therefore is a useful tool for computing-time-effective testing of new physical parameterisations. This chapter introduces selected characteristics of the SCM (atmospheric model plus land surface scheme). A detailed description of the

IFS can be found under `http://www.ecmwf.int/research/ifsdocs/`. Furthermore, this chapter addresses the newly implemented microwave radiative transfer model and details the ELDAS soil moisture analysis.

## 2.1 Single-column model

### 2.1.1 Atmosphere

The single-column model is a hydrostatic model based on the primitive equations incorporating 60 atmospheric vertical levels (ECMWF, 2001). Since single-column models by definition have no information about the spatial distribution of meteorological variables, the SCM needs to be regularly provided with data from a separate four-dimensional model. In this study, the SCM has been driven every six hours by the geostrophic wind vector, the vertical velocity, and the advection tendencies of wind components, temperature, and specific humidity, which have been taken from the ERA-40 reanalysis (Uppala et al., 2005). Additionally, in order to prevent drifts away from reality during a simulation period, the horizontal wind vector, temperature, surface pressure, specific humidity, specific cloud liquid and ice water content, and cloud fraction have been initialised every 24 hours.

### 2.1.2 Land surface

The turbulent fluxes of momentum, sensible heat and latent heat at the bottom boundary of the atmosphere are simulated with the Tiled ECMWF Scheme for Surface Exchanges over Land (TESSEL). Fig. 2.1 shows a schematic diagram of this model. It includes four soil layers with a thickness of 7 cm (surface layer), 21, 72 and 189 cm, respectively, labeled layer 1 to layer 4 throughout this thesis. Most of the vegetation root zone is represented by the three top layers (van den Hurk et al., 2000; ECMWF, 2001), which together equal a depth of one metre and are summarised as the root zone layer in the following. Each model grid box can be subdivided into up to 6 surface types (tiles) over land, which are bare ground, low and high vegetation, intercepted water, shaded and exposed snow, and up to two types over sea and freshwater, which are open and frozen water. A mixing of the two water tiles with land surface tiles is not possible, i.e. a grid box is either 100 % land or 100 % ocean. For each tile the surface turbulent fluxes are calculated separately based on a resistance parameterisation which depends on the characteristics of the surface type. The resulting surface fluxes are then

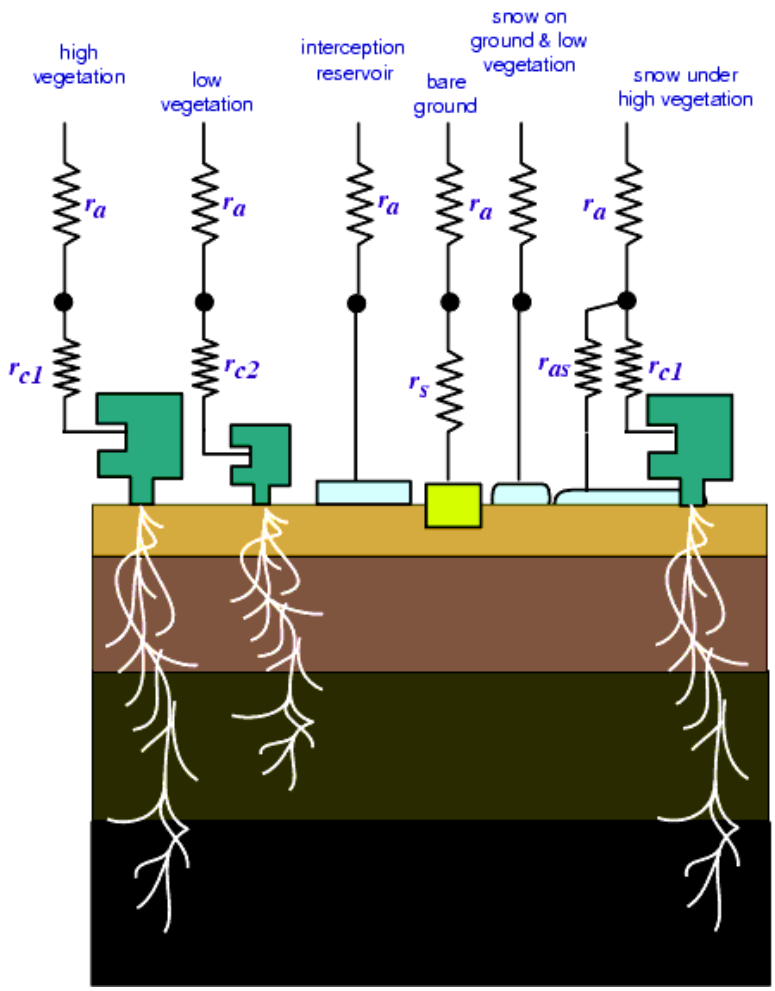


Figure 2.1: Schematic diagram of the Tiled ECMWF Scheme for Surface Exchanges over Land (TESSEL, ECMWF (2001)).

weighted by the area fractions of the corresponding tiles to obtain mean values of the grid box fluxes.

The resistance approches applied in TESSEL can mainly be subdivided into three categories (van den Hurk et al., 2000; ECMWF, 2001): a) surfaces at which the real evaporation is equal to the potential evaporation (open and frozen water, snow on low vegetation), b) surfaces at which the real evaporation (evapotranspiration) is generally lower than the potential values due to the ability of plants and soil material to hold back water (low and high vegetation, bare soil, interception reservoir), and c) the case of snow under high vegetation which is a mixture of the categories above. For the assimilation studies presented in this thesis only the approaches under b) need to be used. They are described in more detail in the following.

The turbulent flux of latent heat $E$ at a bare soil surface is calculated with

$$E = \frac{\rho_a}{r_a + r_s} \left[ q_L - q_{sat}(T_{sk}) \right] \tag{2.1}$$

where $q_L$ denotes the specific air humidity at the lowest atmospheric model level (about 10 m above the surface), $q_{sat}$ the saturation humidity at the surface skin temperature $T_{sk}$, and $\rho_a$ the air density. The atmospheric resistance term $r_a$ controls that the flux becomes stronger with increasing wind speed and an increasing exchange coefficient[1]. The exchange coefficient varies from tile to tile depending on the surface roughness lengths of momentum and moisture and on the atmospheric layering (stability) above the surface (see ECMWF, 2001, for more details). $r_s$ stands for the soil's resistance against evaporation and is a function of a predefined minimum resistance value $r_{s,min}$ and the soil water content:

$$r_s = r_{s,min}\, f_s \tag{2.2}$$

with

$$\frac{1}{f_s} = \begin{cases} 0 & \theta < \theta_{pwp} \\ \frac{\theta - \theta_{pwp}}{\theta_{cap} - \theta_{pwp}} & \theta_{pwp} \leq \theta \leq \theta_{cap} \\ 1 & \theta > \theta_{cap} \end{cases} \tag{2.3}$$

Here, $\theta$, $\theta_{pwp}$, and $\theta_{cap}$ are the soil water contents of the first soil model layer, at the permanent wilting point, and at the field capacity of the soil, respectively. The standard values for $\theta_{pwp}$ and $\theta_{cap}$ within TESSEL are 0.171 $m^3/m^3$ and 0.323 $m^3/m^3$. It can be seen from Eqs. (2.2) and (2.3) that the resistance receives its maximum (infinity) for soil moisture values at or below the permanent wilting point, i.e. that evaporation is cut off completely for dry soils. This limitation is recognised as a shortcoming of the approach. However, an alternative parameterisation that has been tested until this work started shows other serious deficiencies (ECMWF, 2001). At or above field capacity, evaporation over bare soil reaches its maximum.

For high and low vegetation, the latent heat flux is calculated similar to Eq. (2.1); only $r_s$ is replaced by a canopy resistance $r_c$ which is a complex function of the downward shortwave radiation $R_s$, the leaf area index $LAI$, the average unfrozen root zone soil moisture $\overline{\theta}$, the atmospheric water vapor deficit $D_a$, and a minimum stomatal resistance $r_{st,min}$ (see ECMWF, 2001, for details):

$$r_c = \frac{r_{st,min}}{LAI}\, f_1(R_s)\, f_2(\overline{\theta})\, f_3(D_a) \tag{2.4}$$

[1]The atmospheric resistance term is the inverse of the product of the horizontal wind speed and the turbulent exchange coefficient.

The term $f_2$ is determined similarly to $f_s$ in Eq. (2.3) but additionally includes the water content and the root zone fractions in all four layers.

In case of an interception reservoir, $r_s$ in Eq. (2.1) is replaced by a resistance term that accounts for the amount of water available. If this amount is sufficient to sustain potential evaporation the resistance term is set to zero.

The sensible heat flux is calculated as a function of the gradient of the dry static energy:

$$H = \frac{\rho_a}{r_a} \left[ c_p T_L - c_p T_{sk} + gz \right] \tag{2.5}$$

Here $c_p$ denotes the heat capacity of the moist air, $T_L$ the temperature at the lowest atmospheric level, and $gz$ the geopotential at the height $z$ with an acceleration due to gravity $g$ (all other variables as in Eq. (2.1)).

The coupling between the two heat fluxes takes place in a model skin layer, which represents the soil-atmosphere interface, through the skin temperature, which in turn is determined by the surface energy balance equation:

$$(1 - f_{Rs})(1 - \alpha) R_s + \epsilon (R_T - \sigma T_{sk}^4) + H + LE = \Lambda_{sk} (T_{sk} - T_1) \tag{2.6}$$

The first and second term on the left side represent the net shortwave and longwave radiation, respectively, the third and fourth term the sensible and latent heat flux while the heat conductance from the soil is included on the right. In more detail, $\alpha$ and $R_s$ denote the surface reflectivity and the incoming shortwave radiation, respectively. The term $1 - f_{Rs}$ accounts for partial absorption of the net shortwave radiation $(1 - \alpha)R_s$ in the skin layer (ECMWF, 2001). Furthermore, $\epsilon$ is the longwave surface emissivity, $R_T$ the incoming longwave radiation, $\sigma$ the Stefan-Boltzmann constant, $L$ the latent heat of evaporation, $\Lambda_{sk}$ the heat conductivity of the skin layer (predefined for each tile), and $T_1$ the temperature of the top soil layer.

Analogue to the surface fluxes, the model values of air temperature and relative humdity at 2 m height depend on the near-surface gradients of the dry static energy and the specific humidity, respectively. The 2-metre temperature is interpolated from the surface temperature and the one of the lowest atmospheric level, accounting for the stability of the atmospheric layering and the roughness lengths of heat and momentum. Correspondingly, the 2-metre humidity is a function of the specific humidity at the lowest atmospheric model layer, the saturation humidity for the skin temperature, the atmospheric stability and the roughness lenghts of momentum and moisture. A detailed description of the underlying equations is given in the IFS documentation (ECMWF, 2001).

The change of water storage in a soil layer is calculated with

$$\rho_w \frac{\partial \theta}{\partial t} = -\frac{\partial F_w}{\partial z} + \rho_w S_\theta \tag{2.7}$$

where $\rho_w$ denotes the water density, $\theta$ the volumetric water content, $t$ time, $z$ the soil depth, $F_w$ the vertical water flux (positive downwards), and $S_\theta$ a sink term due to root extraction. The vertical water flux is determined according to Darcy's law by

$$F_w = \rho_w \left( \lambda \frac{\partial \theta}{\partial z} - \gamma \right) \tag{2.8}$$

where $\lambda$ and $\gamma$ are the hydraulic diffusivity and hydraulic conductivity, respectively, which are calculated as a function of the soil water content according to the formulations by Clapp and Hornberger (see ECMWF, 2001, for details). For the determination of the sink term $S_\theta$ it is assumed that the water amount bound by the plants for their growth is negligible so that all the water extracted from the soil by the vegetation roots is transpired. The water extraction in each layer can then be calculated from the total evapotranspiration, the soil fraction covered by vegetation, the vertical root distribution (predefined for each vegetation type) and the vertical soil moisture distribution. Infiltration (e.g. from rainfall or snow melt) and evapotranspiration are the boundary condition for the water transports at the top of the soil. At the bottom of the deepest layer, excessive water can freely drain.

### 2.1.3 Microwave radiative transfer

In order to be able to use remotely sensed microwave brightness temperatures in the ELDAS land data assimilation system, we upgraded the ECMWF weather forecast model (in this early experimental state the SCM) with a microwave radiative transfer model which calculates the model equivalents of the brightness temperature observations from the model's soil, vegetation and atmospheric state variables and parameters. The radiative transfer model LSMEM (Land Surface Microwave Emissivity Model) chosen as the observation operator has already been applied in several other studies (e.g. Drusch, 1998; Drusch et al., 2001; Seuffert et al., 2003, 2004; Gao et al., 2004, 2006).

The LSMEM is designed to simulate the measurements of passive microwave sensors on satellites or aircraft over land surfaces with sparse to medium vegetation at frequencies between 1 and about 20 GHz. It accounts for radiation polarisation, viewing geometry as well as scattering, absorption and emission at the rough soil surface, by an idealized vegetation layer, and by atmospheric gases.

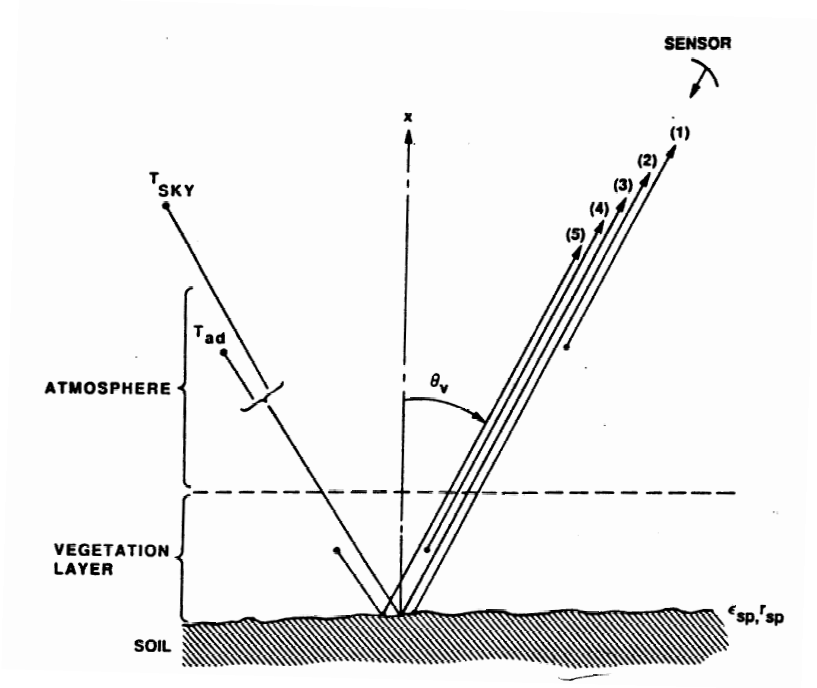


Figure 2.2: Schematic diagram of the radiation components of the LSMEM (Kerr and Njoku, 1990).

Fig. 2.2 shows a schematic diagram of the radiation components included in the LSMEM: (1) Upwelling atmospheric emission: Its intensity can be expressed by the effective brightness temperature $T_{B,au}$ which accounts for the atmospheric temperature and water vapor profile. (2) Microwave radiation emitted from the soil surface and attenuated by the vegetation layer and the atmosphere: If the degree of attenuation is expressed by the optical thicknesses $\tau_{veg}$ and $\tau_{atm}$, this radiation component is denoted by $T_{B,s,p} \cdot \exp(-\tau_{veg}) \cdot \exp(-\tau_{atm})$, where $T_{B,s,p}$ stands for the radiation intensity emitted from the bare soil. It is polarisation-dependent as indicated by the index $p$. (3) Downwelling cosmic background radiation attenuated by the atmosphere plus the atmospheric emission which both are attenuated by the vegetation layer, partly reflected at the surface, again attenuated by the vegetation layer, and finally attenuated by the atmosphere: This can be expressed by the term $(T_{sky} \exp(-\tau_{atm}) + T_{B,ad}) \cdot r_{s,p} \cdot \exp(-2\tau_{veg}) \cdot \exp(-\tau_{atm})$ where $T_{sky}$ denotes the cosmic background radiation, $T_{B,ad}$ the downwelling atmospheric radiation, and $r_{s,p}$ the soil surface reflectivity. (4) Upwelling emission from the vegetation layer attenuated by the atmosphere: Similar to the soil and the atmosphere, the radiation intensity emitted from the vegetation layer can be expressed by an effective brightness temperature $T_{B,veg}$. The radiation component then is $T_{B,veg} \cdot \exp(-\tau_{atm})$. (5) Downwelling vegetation emission partly

reflected at the soil surface and then attenuated by the vegetation layer and the atmosphere: In terms of the preceding specifications, this component is denoted by $T_{B,veg} \cdot r_{s,p} \cdot \exp(-\tau_{veg}) \cdot \exp(-\tau_{atm})$. The brightness temperature seen from the microwave sensor $T_{B,p}$ can then be calculated with

$$\begin{aligned} T_{B,p} = & T_{B,au} + \left(T_{B,s,p} e^{-\tau_{veg}} + T_{B,veg}\right) e^{-\tau_{atm}} \\ & + \left(\left[T_{sky} e^{-\tau_{atm}} + T_{B,ad}\right] e^{-\tau_{veg}}\right) r_{s,p} e^{-(\tau_{veg}+\tau_{atm})} \end{aligned} \tag{2.9}$$

Each radiation component depends on the frequency and the viewing angle $\theta_v$. If vegetation does not completely cover the soil (as it is generally the case) the brightness temperature observed by the microwave sensor is determined by a linear combination of the bare soil contribution and the one coming from the vegetation-covered soil

$$T_{B,p} = (1 - c_{veg})\, T_{B,bs,p} + c_{veg}\, T_{B,vs,p} \tag{2.10}$$

where $c_{veg}$ denotes the fraction of the soil covered with vegetation. $T_{B,bs,p}$ and $T_{B,vs,p}$ are the brightness temperature over bare soil and over vegetation-covered soil, respectively.

The emission contribution of the soil is determined by the soil's temperature profile, which can be summarised in an effective temperature $T_{s\_eff,p}$, and the soil's emissivity $\epsilon_{s,p}$:

$$T_{B,s,p} = \epsilon_{s,p}\, T_{seff,p} = (1 - r_{s,p})\, T_{s\_eff,p} \tag{2.11}$$

Two options exist in the LSMEM for calculating the soil reflectivity. In the first approach the soil is represented by one semi-infinite layer. Reflection only takes place at the soil's surface and is calculated with the Fresnel equations (e.g. Ulaby et al., 1981). It depends only on the sensor's viewing angle and the soil's complex dielectric constant. This one-layer approach is accurate under the assumption that the vertical soil moisture and temperature distributions are uniform so that no gradients in the dielectric constant exist and therefore no reflections occur within the soil. In order to accurately represent vertically inhomogeneous soils the multi-layer approach of Wilheit (1978) is implemented in the LSMEM. It calculates the surface microwave emission based on the contributions of each soil layer and explicitly takes into account the reflections occurring at the interfaces between adjacent layers. Reflections at the soil-air interface or at inner-soil inhomogeneities are determined by the complex dielectric constants of the soil layers. These dielectric constants are calculated as a function of the layer's temperature, water content, texture, density, and water salinity following a parameterisation

proposed by Dobson et al. (1985).

Natural land surfaces are generally not smooth but show varying degrees of roughness. The height fluctuations on distances of the order of the microwave wavelength significantly affect the radiative characteristics of a land surface at this wavelength. The reflectivity of a surface decreases with increasing roughness (Choudhury et al., 1979; Wang and Choudhury, 1981; Njoku and Entekhabi, 1996). This implies an increase in emissivity and therefore in brightness temperature. Additionally, the radiation intensity at each polarisation is differently affected by the soil surface roughness. The difference between the vertically and horizontally polarised brightness temperatures is lower for a rough surface than for a smooth one and highest for large viewing angles, while it becomes zero at zenith. In order to account for the surface roughness effects on the microwave emission of the soil, two different parameterisations are implemented in the microwave radiative transfer model (Choudhury et al. (1979); Wang and Choudhury (1981); and Wegmüller and Mätzler (1999)). Both calculate the reflectivity of a rough surface as a function of the smooth surface reflectivity (given by the Fresnel equations), the incidence angle, and a characteristic roughness height of the surface. While Wegmüller and Mätzler (1999) use the standard deviation of the surface height which can be directly measured, the formulation of Choudhury et al. (1979) and Wang and Choudhury (1981) is based on a roughness parameter $h$ which needs to be derived from measurements by regression methods. Since $h$ was derived for the SGP97 region, the latter approach was used in our assimilation experiments.

The effective soil temperature in Eq. (2.11) is either the temperature of the semi-infinite soil layer or calculated by Wilheit's multi-layer model which weights the emission contributions of each soil layer.

Eq. 2.9 requires the radiation intensity emitted from the vegetation layer (i.e. its brightness temperature) and its optical thickness. The brightness temperature can be determined with (Kerr and Njoku, 1990)

$$T_{B,veg} = (1 - \omega)(1 - e^{-\tau_{veg}})T_{veg} \tag{2.12}$$

where $\omega$ is the effective single scattering albedo, which accounts for reflections at leaves, stalks, etc. and has to be defined as input in the LSMEM. Two parameterisations can be used to calculate the canopy optical thickness (Kirdyashev et al., 1979; Wegmüller et al., 1995). Both approaches strongly depend on a coefficient which accounts for the vegetation structure. Since a vegetation canopy generally is a chaotic-arranged composition of plant components, this structure coefficient needs to be derived from brightness temperature measurements, which is not

feasible for operational large-scale applications, or estimated based on the vegetation type. It can be a significant source of uncertainty for microwave radiative transfer calculations which has to be taken into account in the ELDAS assimilation system (a bias analysis is presented in Sec. 4.2.2). The results of the two parameterisations differ only marginally below 5 Ghz, and since the formulation of Kirdyashev et al. (1979) requires less input parameters, it was used in our assimilation studies.

In the atmosphere, microwave radiation can significantly be influenced by the gases oxygen and water vapor as well as by water droplets in clouds and precipitation. However, these effects become negligible at frequencies below 5 GHz (Barrett and Kniveton, 1995; Ulaby et al., 1981). Therefore, this part of the LSMEM is only addressed in brief here. Atmospheric absorption is based on the millimeter-wave propagation model of Liebe (1989) which includes the absorption lines of oxygen and water vapor. Water droplets are so far not included in the LSMEM. The atmospheric part requires the vertical profiles of temperature, humidity and pressure as input for an arbitrary number of layers. An overview of all necessary input data for the LSMEM is listed in Appendix A.

## 2.2 Soil moisture analysis

The aim of any assimilation system is to find a solution for a state vector $\mathbf{x}$ that optimally combines (modelled) background data and observations by weighting all information sources depending on their uncertainties. According to variational analysis, the best estimate of $\mathbf{x}$ is achieved by minimising the so-called cost function (e.g. Courtier, 1997)

$$J(\mathbf{x}) = (\mathbf{y} - H\mathbf{x})^{\mathrm{T}} \mathbf{R}^{-1} (\mathbf{y} - H\mathbf{x}) + (\mathbf{x} - \mathbf{x}_b)^{\mathrm{T}} \mathbf{B}^{-1} (\mathbf{x} - \mathbf{x}_b) \tag{2.13}$$

which means to solve $\nabla J = 0$. The vectors $\mathbf{x}_b$ and $\mathbf{y}$ contain the background state vector and the observations, respectively. The first guess equivalents of the observations are calculated from the model state vector $\mathbf{x}$ with the generally non-linear forward operator $H$ (also called observation operator). The random observation and background errors are taken into account by the covariance matrices

$$\mathbf{R} = \overline{(\mathbf{y} - H\mathbf{x}_t)(\mathbf{y} - H\mathbf{x}_t)^{\mathrm{T}}} \tag{2.14}$$

and

$$\mathbf{B} = \overline{(\mathbf{x}_b - \mathbf{x}_t)(\mathbf{x}_b - \mathbf{x}_t)^{\mathrm{T}}} \tag{2.15}$$

where the index $t$ denotes the true values of $\mathbf{x}$, the exponent T stands for the transpose and the overbar indicates the expectation value of the term underneath. The mean errors $\overline{\mathbf{y} - H\mathbf{x}_t}$ and $\overline{\mathbf{x}_b - \mathbf{x}_t}$ are assumed to be zero.

$\nabla J = 0$ represents a non-linear system of equations, a solution can only be deduced iteratively. However, an analytical solution of the system can be found by linearising the forward operator $H$, i.e. it is assumed that small perturbations of the initial state $\mathbf{x}_b$ result in only linear changes of the parameters calculated by the forward operator. This can be mathematically expressed by

$$H\mathbf{x} - H\mathbf{x}_b = \mathbf{H}(\mathbf{x} - \mathbf{x}_b) \tag{2.16}$$

where $\mathbf{H}$ denotes the linearised forward operator.

The soil moisture analysis in the ELDAS data assimilation system is based on the extended Kalman filter (see e.g. Bouttier and Courtier, 1999). The system is designed to perform an analysis every 24 hours by using the microwave brightness temperature, 2-metre air temperature and 2-metre relative humidity observations available from between two analyses. The best estimate of the model soil moisture state vector $\mathbf{x}_a$, which results from minimising the cost function (2.13), is

$$\mathbf{x}_a(t) = \mathbf{x}_b(t) + \mathbf{K}_{[t-24\mathrm{h},t]}\Big(\mathbf{y}_{[t-24\mathrm{h},t]} - \mathbf{H}_{[t-24\mathrm{h},t]}\mathbf{x}_{b,[t-24\mathrm{h},t]}\Big) \tag{2.17}$$

$\mathbf{x}_b$ denotes the background soil moisture at the time step $t$; $\mathbf{y}_{[t-24\mathrm{h},t]}$ contains the screen-level and brightness temperature observations from the 24-hour window preceding the analysis, $\mathbf{H}_{[t-24\mathrm{h},t]}\mathbf{x}_{b,[t-24\mathrm{h},t]}$ the corresponding model equivalents; $\mathbf{K}$ is the Kalman gain which performs the weighting of all available information.

The state vector $\mathbf{x}$ contains three elements which are the volumetric moisture values in layer 1, 2, and 3. The bottom soil layer is omitted because it's water content is only very weakly related to the turbulent surface fluxes. The dimension of the observation vector $\mathbf{y}_{[t-24\mathrm{h},t]}$ is flexible and depends on the number of observations. The background vector $\mathbf{x}_b$ results from the forecast based on the preceding analysis, i.e.

$$\mathbf{x}_b(t) = M_{(t-24\mathrm{h})\rightarrow t}\,\mathbf{x}_a(t - 24\mathrm{h}) \tag{2.18}$$

where $M_{(t-24\mathrm{h})\rightarrow t}$ stands for the model which performs the forcast calculations. The forward operator $\mathbf{H}$ includes (a) the parameterisations used to compute the model values of 2-metre temperature and 2-metre relative humidity, and (b) the microwave radiative transfer model which calculates brightness temperatures directly within the regular forecast run. The gain matrix $\mathbf{K}_{[t-24\mathrm{h},t]}$ is calculated

by

$$\mathbf{K}_{[t-24\mathrm{h},t]} = (\mathbf{B}^{-1}(t) + \mathbf{H}^{\mathrm{T}}_{[t-24\mathrm{h},t]}\mathbf{R}^{-1}\mathbf{H}_{[t-24\mathrm{h},t]})^{-1}\mathbf{H}^{\mathrm{T}}_{[t-24\mathrm{h},t]}\mathbf{R}^{-1} \tag{2.19}$$

The size of the quadratic observation error covariance matrix $\mathbf{R}$ depends on the number of observations. For the experiments described in this study, it has been assumed to be constant over time.

For calculating the observation operator matrix $\mathbf{H}_{[t-24\mathrm{h},t]}$, the tangent linear hypothesis (Eq. (2.16)) is applied. $\mathbf{H}_{[t-24\mathrm{h},t]}$ can then be determined from one-side finite differences. This requires one additional perturbed forecast run for each state variable. The resulting matrix elements of $\mathbf{H}_{[t-24\mathrm{h},t]}$ are

$$h_{ij} = \frac{(H\mathbf{x}_p)(t(i),j) - (H\mathbf{x}_b)(t(i))}{x_p\,(t(i),j) - x_b\,(t(i),j)} \tag{2.20}$$

where $H\mathbf{x}$ denotes the model equivalents of the observation vector, and $\mathbf{x}$ the state vector to be analysed. The indices $p$ and $b$ stand for the perturbation and background run, respectively. The index $i$ indicates the observation number within the observation vector $\mathbf{y} = (y_1, ..., y_i, ..., y_n)$. The index $j$ denotes the number of the soil layer within the state vector $\mathbf{x} = (x_1, x_2, x_3)$ and, at the same time, the number of the perturbation run, since only layer 1 is perturbed in the first additional forecast run, only layer two in the second run, etc. Accordingly, the linearised observation operator $\mathbf{H}_{[t-24\mathrm{h},t]}$ is a $n \times 3$-matrix. Finally, $t(i)$ is the time of the observation $y_i$ and the model equivalent $(H\mathbf{x})(i)$.

The background error covariance matrix $B$ temporarily evolves by

$$\mathbf{B}(t) = \mathbf{M}\mathbf{A}(t - 24\mathrm{h})\mathbf{M}^{\mathrm{T}} + \mathbf{Q}(t - 24\mathrm{h}) \tag{2.21}$$

where $\mathbf{A}$ denotes the analysis error covariance matrix, $\mathbf{M}$ the linearised model operator and $\mathbf{Q}$ the model error covariance matrix. $\mathbf{A}$ is recalculated at every analysis time step according to

$$\mathbf{A}(t) = (\mathbf{B}^{-1}(t) + \mathbf{H}^{\mathrm{T}}_{[t-24\mathrm{h},t]}\mathbf{R}^{-1}\mathbf{H}_{[t-24\mathrm{h},t]})^{-1} \tag{2.22}$$

The linearised model operator $\mathbf{M}$ can be derived similarly to the observation operator $\mathbf{H}$ by assuming that small perturbations of the initial state $\mathbf{x}_a$ result in only linear changes of the forecast:

$$M\mathbf{x}(t) - M\mathbf{x}_a(t) = \mathbf{M}(\mathbf{x}(t) - \mathbf{x}_a(t)) \tag{2.23}$$

After calculating one-side finite differences, the matrix elements of $\mathbf{M}$ are assessed

by

$$m_{ij} = \frac{(M\mathbf{x}_p)(i,j) - (M\mathbf{x}_a)(j)}{x_p(i) - x_a(i)} \tag{2.24}$$

where $x_p(i)$ is the perturbed soil moisture of layer $i$ at the beginning of the 24-hour time-frame and $x_a(i)$ the equivalent unperturbed value (determined by the preceding analysis). $(M\mathbf{x}_p)(i,j)$ stands for the soil moisture of layer $j$ simulated at the end of the 24-hour window resulting from the forecast run where the initial soil moisture of layer $i$ is perturbed. $(M\mathbf{x}_a)(j)$ denotes the corresponding background soil moisture. The indices $i$ and $j$ are determined by the number of the root zone soil layers for which the soil moisture analysis is performed. Consequently, $\mathbf{M}$ is a quadratic matrix of dimension $3 \times 3$.

The model error covariance matrix $\mathbf{Q}$ in Eq. (2.21) covers random errors of the forecast that can be attributed to shortcomings in the model. Systematic errors are not included and should have been minimised before the Kalman filter is applied. The quantification of $\mathbf{Q}$ is subject of a separate discussion (Sec. 4.1).

Equations 2.17 – 2.22 and 2.24 are the basis for the ELDAS soil moisture analysis system applied in this study. At the beginning of a forecast cycle, the analysis system requires the initialisation of the state vector $\mathbf{x}_a(t = 0)$ and its error covariance matrix $\mathbf{A}(t = 0)$. Furthermore, the error covariances of the model and of the observations have to be specified. Settings for input parameters and initialisation values are described in detail in section 3.3. An advantage of the extended Kalman filter (EKF) is that the background error covariance matrix is recalculated every analysis time step depending on the meteorological situation. In contrast to 4D-Var (Bouttier and Courtier, 1999), where a perfect model is assumed, the model errors are taken into account. In doing so, the calculation efforts and the storage demands noticeably increase. However, this disadvantage is of minor importance here since the soil moisture analysis is applied on a three-element state vector only.

# Chapter 3

# Data and reference assimilation experiments

The work presented in this thesis is mainly based on observations from the two Southern Great Plains Hydrology Experiments carried out in 1997 and 1999 (denoted by SGP97 and SGP99) over parts of the U.S. state Oklahoma. Required meteorological and hydrological variables that were not provided by the field experiments have been taken from ECMWF's 40-year global reanalyses. Seuffert et al. (2004) also used these datasets to test the feasibility and the potential benefit of the new ELDAS data assimilation system. Their assimilation experiments are the basis for the error analyses presented in this thesis and are summarised in section 3.3.

## 3.1 Southern Great Plains Hydrology Experiments

### 3.1.1 SGP97

The SGP97 field experiment was carried out from 18 June to 17 July, 1997. The observed region is defined by a 40 km by 280 km area ranging from 34.5°N to 37.0°N centered at approximately 97.8°W (see Fig. 3.1(a)). On selected days, an aircraft equipped with the passive microwave Electronically Scanned Thinned Array Radiometer (ESTAR) overflew the area during the first half of the day on predefined flight lines at 7.5 km height. ESTAR provided brightness temperature observations at 1.4 GHz which were normalised to zenith viewing angle and mapped to a horizontal resolution of about 800 m (Jackson et al., 1999). Fig. 3.1(b) shows an example of such a map. ESTAR data is available for 18 of

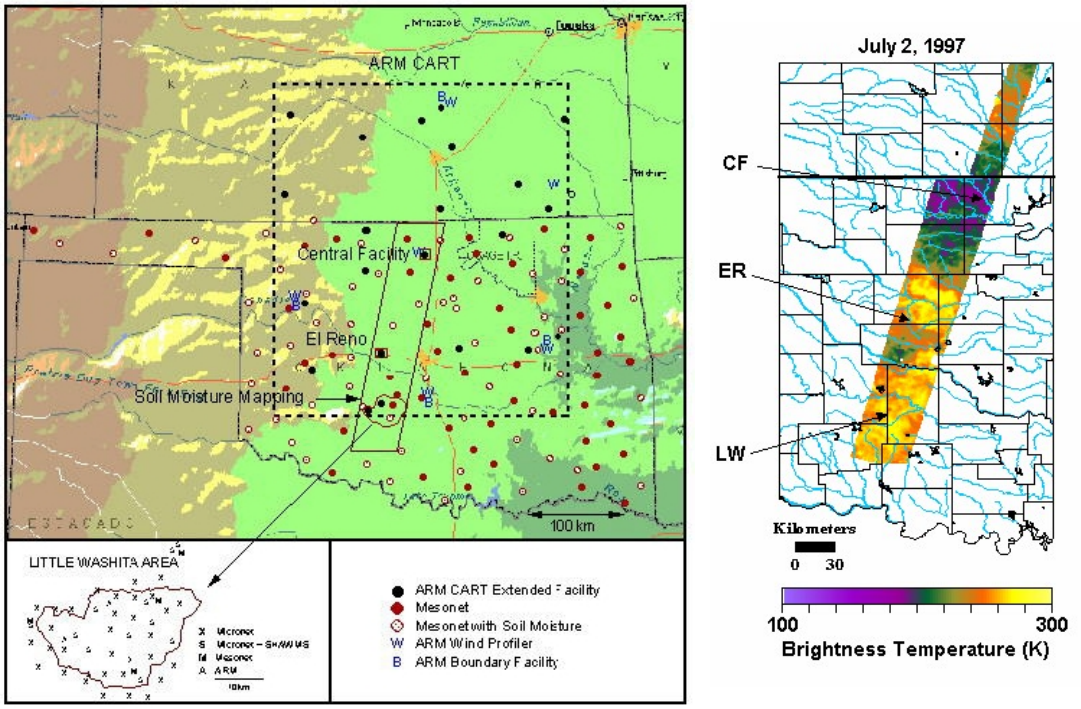


(a) (b)

Figure 3.1: (a) Outline map of observation facilities in Oklahoma and southern Kansas (SGP97 Experiment Plan, 1997). The SGP97 area is indicated by the parallelogram. (b) Example of an SGP97 brightness temperature map (`http://disc.gsfc.nasa.gov/fieldexp/SGP97/estar.html`).

the 30 experiment days (June 18 – 20, 25 – 27, June 29 – July 3, and July 11 – 17). A time series of observed brightness temperatures is shown in Fig. 3.2 for the field site LW02, which is the location for which the assimilation experiments of this study were performed. At this site, ESTAR data was also not available on July 15 and 17. The lacking measurements could have been substituted by artificially generated data. However, this study was intended to exclusively deal with observations facing all the problems potentially occurring under operational circumstances. Furthermore, Calvet et al. (1998) showed that assimilating surface soil moisture information every third day is sufficient for analysing root zone soil moisture when atmospheric forcing and precipitation are known. Site LW02 was chosen because of the comprehensive pool of auxiliary data available for that site (see below).

Simultaneous to the brightness temperature measurements, gravimetric soil moisture samples were collected at three main observation areas (see Fig. 3.1): (a) the Central Facility (CF) of the Atmospheric Radiation Measurement (ARM) Cloud and Radiation Testbed (CART) operated by the United States Depart-

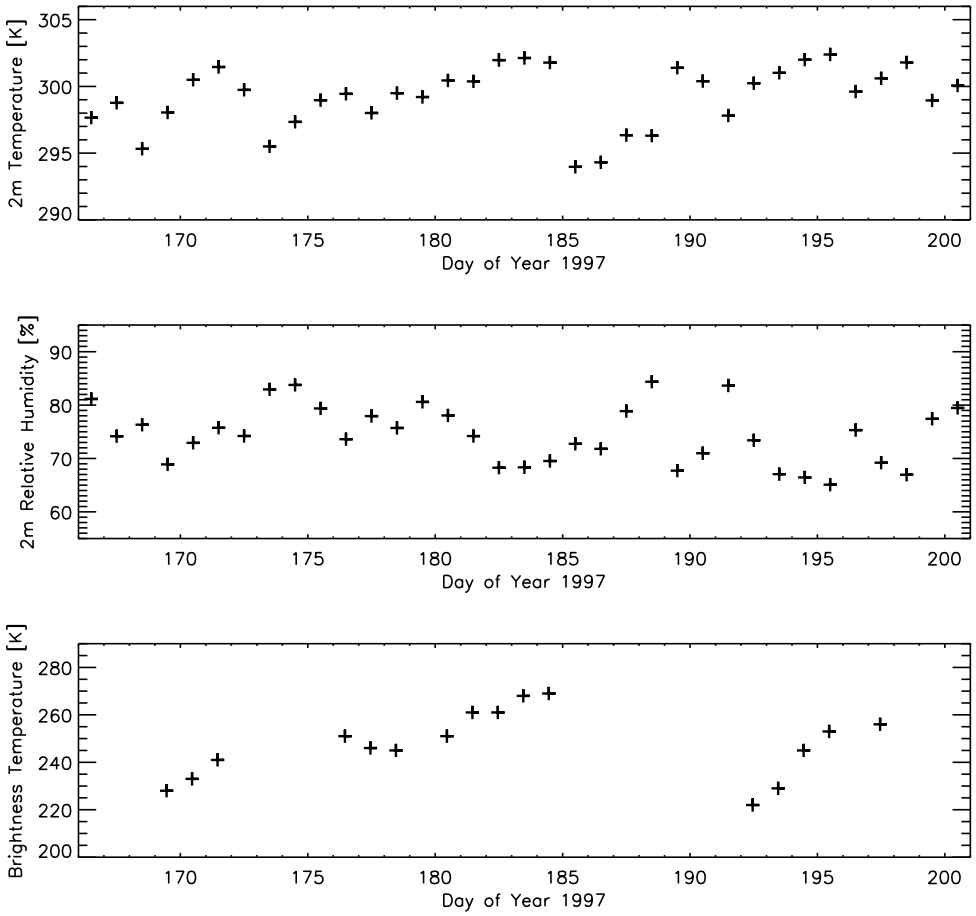


Figure 3.2: NOAA/ATDD 2-metre air temperature and 2-metre relative humdity observations (daily means) and ESTAR brightness temperature measurements (from around 11 LST) at SGP97 site LW02.

ment of Energy, (b) the Grazinglands Research Lab at El Reno (ER) operated by the Agricultural Research Service (ARS) of the United States Department of Agriculture (USDA), and (c) the USDA ARS Little Washita watershed (LW) in the south of the SGP97 region. A number of fields (LW: 23, ER: 16, CF: 9) have been defined in each observation area for which, besides gravimetric soil moisture, several auxiliary soil and vegetation characteristics have been determined, e.g. soil temperature, vegetation type, vegetation water content, soil surface roughness, soil bulk density, and soil texture. The gravimetric soil moisture data is provided as daily area means for each field together with daily standard deviations. The area means and standard deviations result from 14 samples extracted from the top 5 cm of the soil at each field each day whenever possible (field size: 800 m $\times$ 800 m). With the corresponding soil bulk density, the gravimetric val-

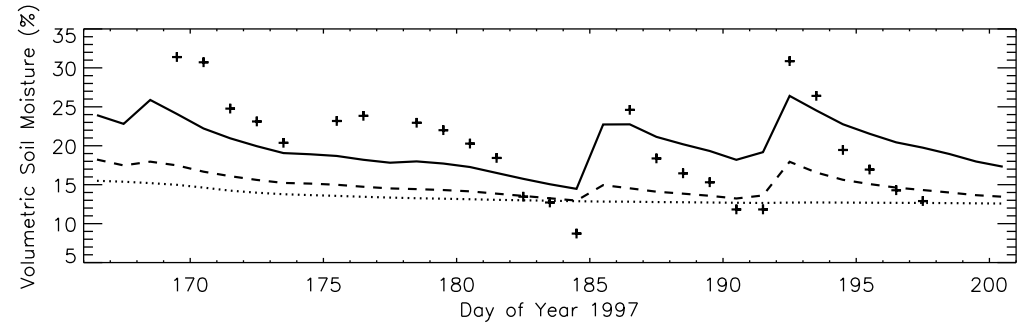


(a)

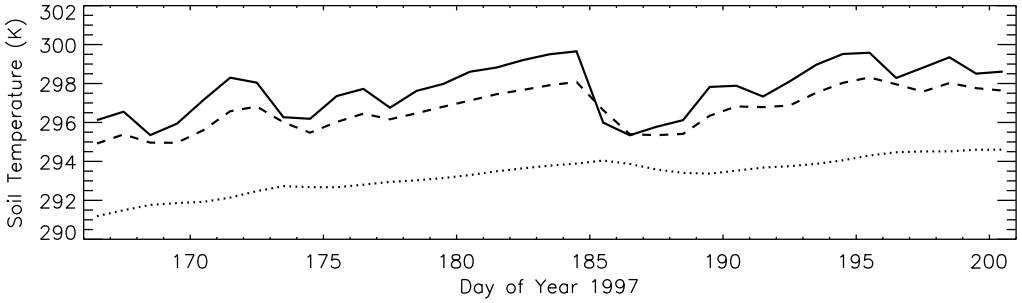


(b)

Figure 3.3: (a) Volumetric soil moisture at site LW02 during SGP97. The plus signs were derived from surface gravimetric samples (0 - 5 cm depth) taken once a day. A soil bulk density of 1.22 g/cm$^3$ was used for conversion as derived from samples of the soil's top 5 cm. The lines represent soil moisture values determined from hourly matric potential observations according to van Genuchten (1980), averaged to daily means (solid line = 5 cm depth, dashed line = average of 10, 15, 20, and 25 cm depth, and dotted line = 60 cm depth). (b) Daily means of measured soil temperatures at the NOAA/ATDD flux-monitoring station during SGP97. The solid line is an average of measurements at 2 and 4 cm depth, the dashed line shows the recordings from a depth of 16 cm, the dotted one from 60 cm.

ues can be converted into volumetric water contents. Fig. 3.3 shows the available surface soil moisture observations for site LW02 (plus signs).

Land use and the type of vegetation in the SGP area are subdivided into 13 classes based on satellite observations and on-site surveys. The vegetation water content, the bulk density, and the surface roughness parameter $h$ (see page 19) are set constant for each of these classes based on sample measurements. Only for three vegetation types the water content is calculated as a function of a contemporary measured normalised difference vegetation index (NDVI). Finally, the soil texture is based on sample measurements and the state soil geographic


Figure 3.4: (a) Aerial photo showing land cover near the NOAA/ATDD site (SGP97 Experiment Plan, 1997).

database (STATSGO). A more detailed description of the data available for all fields can be found in (Jackson et al., 1999).

At some fields, additional data is available due to special measuring campaigns or regularly operating observing systems. This is the case for the SGP97 site LW02 located in the North-East of the Little Washita watershed south-west of the city of Chickasha (34°58'N, 97°57'W). This region is mainly covered with grass and patchy forests (Fig. 3.4). At site LW02, the Atmospheric Turbulence and Diffusion Division (ATDD) of the U.S. National Oceanic and Atmospheric Administration (NOAA) operated a flux-monitoring site (Meyers, 2001). The station provided half-hourly observations of wind speed, wind direction, 2-metre air temperature, 2-metre relative humidity, surface pressure, precipitation, incoming shortwave radiation, surface net radiation, skin temperature, soil temperature at six depths between 2 and 64 cm, sensible heat flux, latent heat flux, ground heat flux, and, since June 1997, volumetric soil moisture for the top 10 cm zone. Time series of the daily means of the 2-metre temperature and relative humidity, which are two of the three variables that are assimilated for the soil moisture analysis, are shown in Fig. 3.2. The humidity values presented are 7 % lower than the values originally recorded due to a measuring bias (Seuffert et al., 2004). The temporal evolution of selected soil temperature measurements as they are used to represent the three root zone layers of the soil model TESSEL is shown in Fig. 3.3.

Another data source at LW02 are soil matric potential observations provided by the USDA ARS as part of the Soil Heat and Water Measurement System

(SHAWMS). The matric potential characterises the ability of the soil to bind water, which in turn depends on the soil's water content, and can be determined with heat dissipation sensors (Reece, 1996). The available data consists of hourly matric potential values at depths of 5, 10, 15, 20, 25, and 60 cm for the complete SGP97 period and therefore supplements the gravimetric measurements of surface soil moisture with profile information. The conversion of the matric potentials to volumetric soil moisture values was done following van Genuchten (1980). Time series of daily means of these soil moisture retrievals interpolated to the three root zone layer depths of TESSEL are shown in Fig. 3.3 together with the values derived from the gravimetric measurements. The amplitude of surface soil moisture derived from the matric potential observations for the model's top layer (solid black line) is significantly smaller than that derived from the gravimetric measurements (plus signs). This results from the different sampling depths of the two datasets. While the gravimetric probes represent the water content of the top 5 cm of the soil, the matric potential closest to the surface has been measured *at* a depth of 5 cm where the fluctuations of soil moisture are generally smaller than in the layer above. However, Fig. 3.3 shows that soil moisture gradients at the soil surface can be quite large, confirming the need of investigating the effects of the surface soil moisture profile in an assimilation setup that uses microwave brightness temperatures (section 4.3).

### 3.1.2 SGP99

The SGP99 experiment covered the period from July 8 to July 20, 1999. The campaign was designed to further evaluate the feasibility of deriving soil moisture from satellite observations (SGP99 Experiment Plan, 1999). Many of the SGP99 datasets resemble the ones described in the SGP97 section, e.g. again ESTAR observations and gravimetric soil moisture measurements have been provided for more than thirty sites. A comprehensive description can be found under `http://hydrolab.arsusda.gov/sgp99/sgp99b.htm`.

One major rainfall event during the night of July 9 and the early morning of July 10 caused a significant increase in soil moisture in the entire SGP region, followed by a dry down period until the end of the experiment. The amounts of rainfall varied from up to 107 mm at the very centre of the storm located in the El Reno (ER) area, about 40 mm in the northern experiment area around the Central Facility (CF) to 10-40 mm in the Little Washita (LW) area in the south (Drusch et al., 2004). Simultaneous to the ESTAR flights, which took place mainly in the morning hours, gravimetric soil moisture estimates were sampled (22 fields in the LW area, 6 at ER, and 5 at CF). Again, fourteen samples were

taken on each field to capture the spatial variability, but different from SGP97, soil moisture was determined for the top 0 to 2.5 and 2.5 to 5 cm separately.

At 10 observation sites in the Little Washita watershed (LW numbers 02 – 06, 09, 12 –14, and 21), soil temperature measurements for the surface and depths of 1, 5, and 10 cm were performed. The data was mainly collected during the morning hours between 8 and 11 local time.

## 3.2 ECMWF's ERA-40 reanalysis

Required data not available from SGP observations has been extracted from ECMWF's ERA-40 archive which is a reanalysis of the meterorological state of the atmosphere from September 1957 to August 2002 (Uppala et al., 2005). The archive provides global data every six hours with a spatial resolution of 125 km. The grid point which coincides best with the location of the NOAA/ATDD site has been chosen as the source for remaining data needs, which are downwelling surface longwave radiation, vertical velocity, geostrophic wind components, advection values of temperature, specific humidity and horizontal wind, cloud fraction, and specific cloud liquid and ice water content.

## 3.3 Reference data assimilation experiments

Seuffert et al. (2004) tested the ELDAS data assimilation system using measurements from the SGP97 site LW02 and the NOAA/ATDD flux monitoring site. Selected model parameter settings, derived from observations and vegetation characteristics, and the LSMEM parameterisations they used are summarised in Tab. 3.1. These specifications have been adopted for this study. The only changes that have been carried out are (a) a necessary transfer to another hard- and software environment (from ECMWF's IBM server to a Linux-PC including a compiler change) and (b) a revised initialisation of soil and skin temperatures (NOAA/ATDD site observations are used instead of values from the ERA-40 reanalysis). Mainly the second point causes small changes in the resulting error statistics. However, they do not affect the conclusions obtained from the reference assimilation experiments.

Model simulations started on 15 July 1997 with soil moisture values derived from the SHAWMS profile measurements. At every 20 minute time step the single-column model was forced with surface observations of precipitation and downward shortwave radiation recorded at the NOAA/ATDD station. The atmospheric conditions were re-initialised every 24 hours at local midnight with

| TESSEL | |
|---|---|
| High vegetation type (area fraction) | Interrupted forest (3 %) |
| Low vegetation type (area fraction) | Tall grass (97 %) |
| Wilting point | 0.26 $m^3/m^3$ |
| Field capacity | 0.11 $m^3/m^3$ |
| **LSMEM** | |
| Fractions of sand/clay/silt | 35/20/45 % |
| Surface roughness | 0.5 cm |
| Vegetation coverage | 0.8 |
| Vegetation water content | 0.34 $kg/m^2$ |
| Single-scattering albedo | 0.1 |
| Vegetation structure coefficient | 0.003 |
| Dielectric mixing model | Dobson et al. (1985) |
| Smooth surface reflectivity | Fresnel equations |
| Rough surface reflectivity | Wang and Choudhury (1981) |
| Vegetation opacity | Kirdyashev et al. (1979) |
| Atmosphere | Liebe (1989) |

Table 3.1: TESSEL/LSMEM parameter settings and parameterisations used in the LW02 reference assimilation experiments (Seuffert et al., 2004, for parameterisation details see Sec. 2.1.3).

data from ECMWF's ERA-40 reanalysis. The soil moisture analysis was performed once per day, also at local midnight, provided that screen-level and/or microwave brightness temperature observations are available within the 24 hours before. 2-metre temperature and relative humidity observations were assimilated at 09, 12, and 15 local standard time (LST), since the coupling of the atmospheric boundary layer to the soil is in general strongest around noon (e.g. Garratt, 1992). ESTAR brightness temperatures were applied at 11 LST whenever available. The uncertainties of the observations were set to 2 K for the 2-metre temperature and the brightness temperature, and to 10 % for the relative humidity. The main diagonal of the observation error covariance matrix $\mathbf{R}$ was therefore defined by 4 $K^2$ and 100 $\%^2$, respectively. Since the errors of the observation types were assumed to be uncorrelated, the covariances are zero, i.e.

$$\mathbf{R} = \begin{pmatrix} 4\,\mathrm{K}^2 & 0 & 0 \\ 0 & 100\,\%^2 & 0 \\ 0 & 0 & 4\,\mathrm{K}^2 \end{pmatrix} \tag{3.1}$$

Four different model runs with varying usage of observation types were carried out for the SGP97 period. The control run (CTRL) was performed without any soil moisture analysis. The three data assimilation runs used (1) screen-level variables alone (KTR), (2) brightness temperatures alone (KB), and (3) all three observations together (KTRB). For each of these assimilation setups, three additional forecast runs were performed every 24 hours in which the initial soil moisture of the first, second, and third root zone layer was slightly perturbed by a factor of 0.00001, respectively, i.e.

$$\Theta_{i,pert} = \Theta_{i,back} \pm \Theta_{i,back} \cdot 0.00001 \tag{3.2}$$

where $\Theta_{i,back}$ denotes the background soil moisture of the $i$-th root zone layer and $\Theta_{i,pert}$ the perturbed value. The direction of the soil moisture perturbation (i.e plus or minus) depends on the deviation of the modelled background of the assimilation variables from the corresponding observations. The finite difference method outlined in section 2.2 can then be applied. The observation and model operators $\mathbf{H}$ and $\mathbf{M}$ are given by Eqs. 2.20 and 2.24, respectively. The model error covariance matrix was set to (more details in section 4.1)

$$\mathbf{Q} = \begin{pmatrix} 0.005\,\mathrm{m}^3/\mathrm{m}^3 & 0 & 0 \\ 0 & 0.005\,\mathrm{m}^3/\mathrm{m}^3 & 0 \\ 0 & 0 & 0.005\,\mathrm{m}^3/\mathrm{m}^3 \end{pmatrix} \tag{3.3}$$

Modelled turbulent fluxes and analysed soil moisture for the three top model layers from the different assimilation runs have been compared against observations from the NOAA/ATDD site. The main results of the reference runs can be summarised as follows (also see Figs. 3.5, 3.6, 3.7 and (Seuffert et al., 2004)): (1) If the initial soil moisture conditions are well known and the forcings are of high accuracy, the land surface model is able to reproduce root zone soil moisture very well. (2) The assimilation of screen-level variables alone improves the modelled turbulent surface fluxes but significantly degrades the accuracy of the resulting analysed root zone soil moisture. (3) Assimilating brightness temperatures alone leads to a smaller improvement in predicted fluxes but deteriorates the analysed root zone soil moisture to a much lesser degree than the assimilation of screen-level variables alone. (4) The combined assimilation of screen-level variables and brightness temperatures leads to the best results for both the turbulent fluxes and the water content in the soil model's top layer. At the same time, however, the model soil moisture drifts away from reality in the deeper root zone layers. (5) It was not possible to improve the accuracy of both root zone soil moisture and turbulent heat fluxes at the same time for the entire period. The KTRB runs

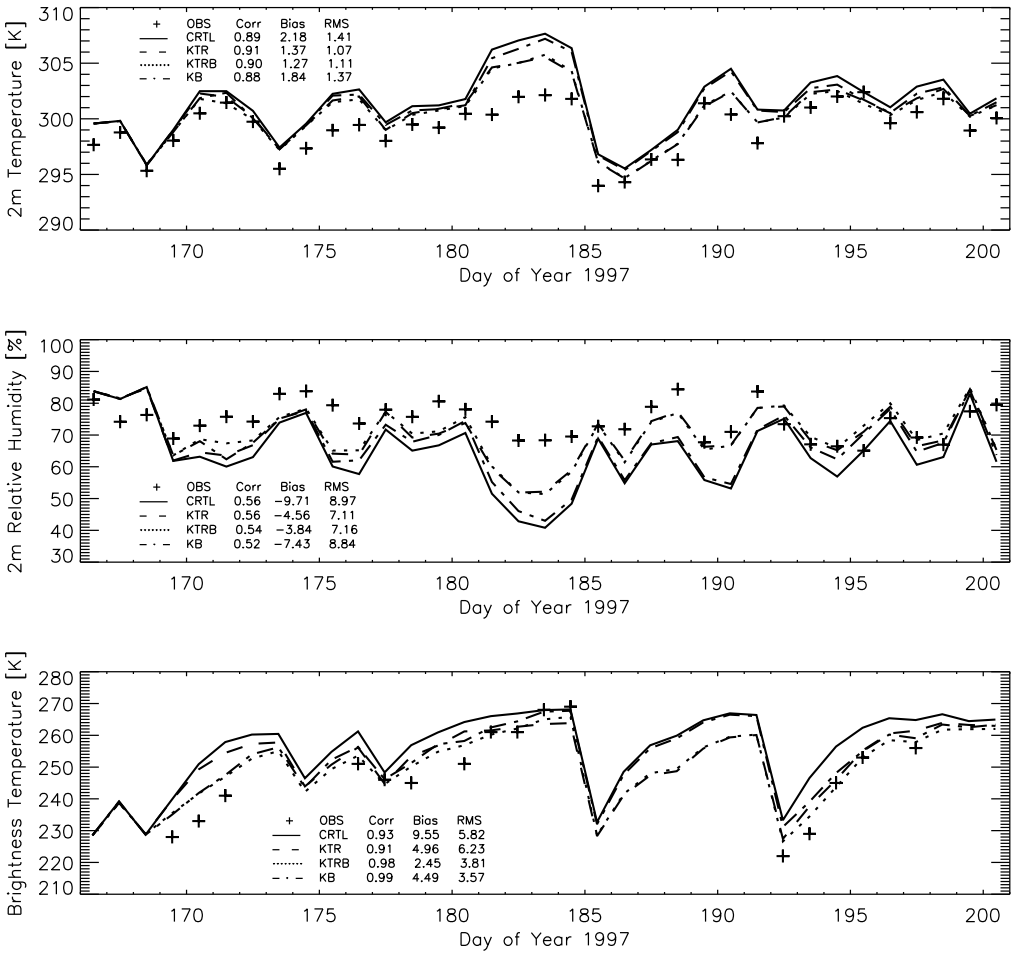


Figure 3.5: Daily means of observed and modelled 2m temperature, relative humidity and microwave brightness temperature from 15 June to 20 July 1997 in the reference data assimilation experiments. The plus signs stand for observations [OBS] (brightness temperature observations are from around 11 LST only); lines denote results from model runs (solid = no assimilation [CTRL], dashed = assimilation of 2m temperature and relative humidity alone [KTR], dash-dotted = assimilation of brightness temperature alone [KB], dotted = assimilation of all observation types together [KTRB]). Specified statistic quantities are correlation coefficient [Corr], bias [Bias] and bias-corrected root-mean-square error [RMS] of the modelled variables in comparison to the observed values.

.

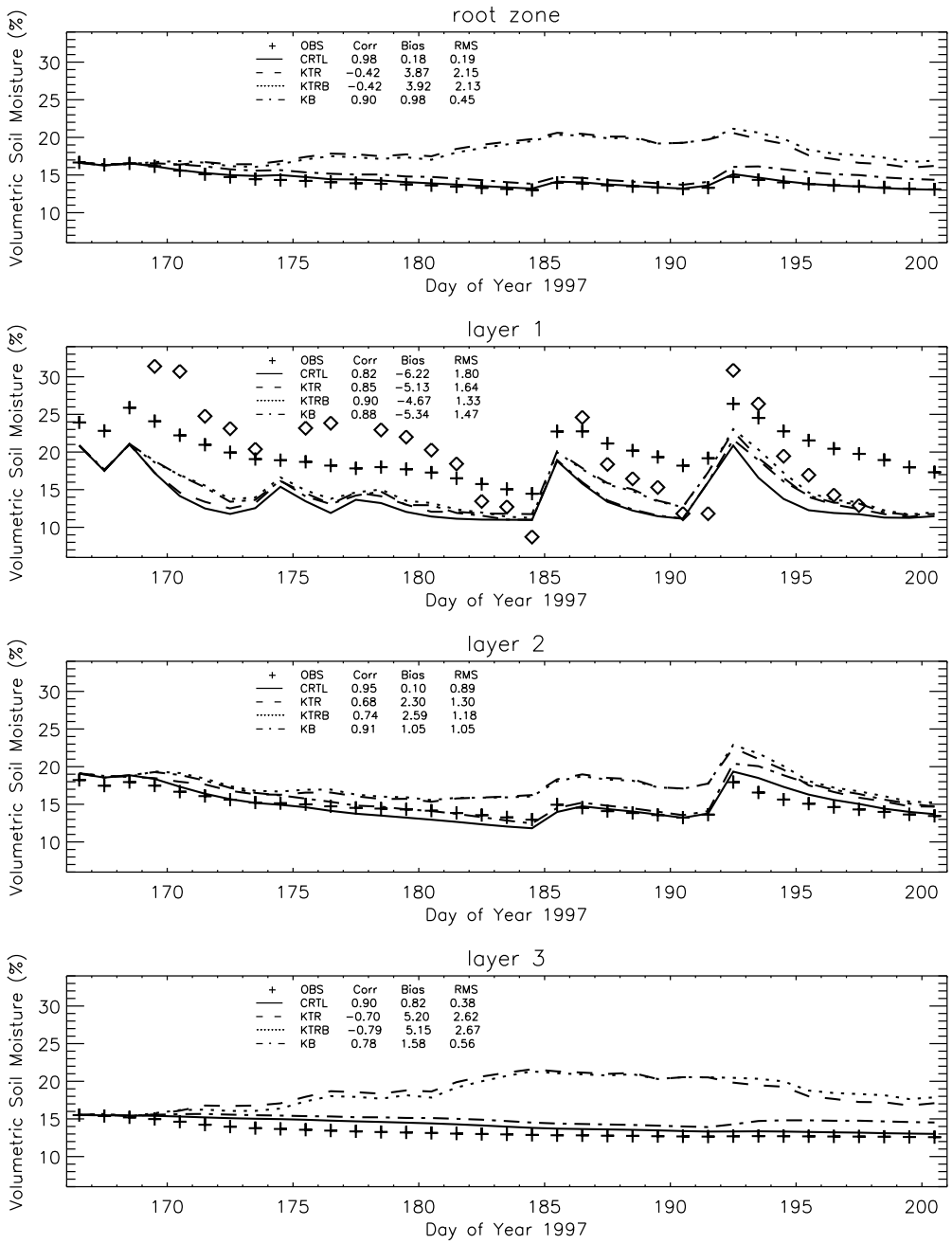


Figure 3.6: Daily means of observed and modelled soil moisture in the three top model layers and the resulting root zone soil moisture from 15 June to 20 July 1997 in the reference data assimilation runs. Plus signs denote SHAWMS observations: values from a depth of 5 cm are chosen to represent model layer 1; the mean from 10, 15, 20 and 25 cm corresponds to layer 2; the 60-cm measurement stands for layer 3. The diamonds represent water contents derived from the gravimetric probes whenever available (not used for calculation of error statistics). For the meaning of the lines and the statistic data see Fig. 3.5.

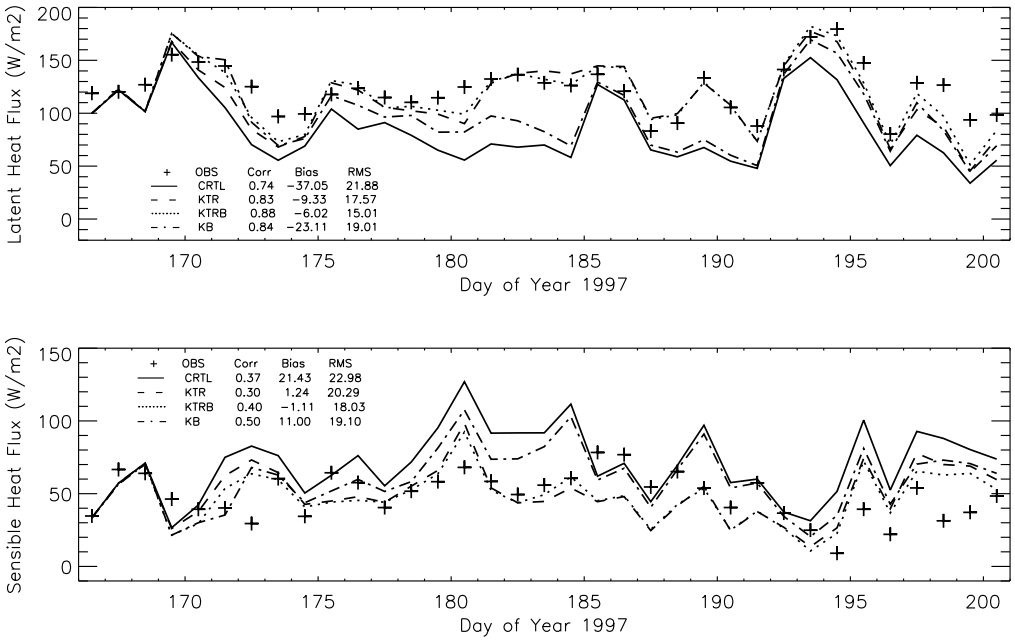


Figure 3.7: Daily means of surface latent and sensible heat fluxes from 15 June to 20 July 1997 in the reference data assimilation runs (further denotations see Fig. 3.5).

served best in simulating the fluxes, whereas root zone soil moisture deteriorates least from observations when assimilating only the brightness temperature. Some of these findings will be discussed further in section 4.4 in light of the following error analyses.

# Chapter 4

# Assimilation studies and error analyses

First results from the single-column tests with the ELDAS data assimilation system (Chap. 2) have been published by Seuffert et al. (2003, 2004). They proved the applicability and the potential benefits of passive microwave remote sensing information in the ECMWF weather prediction model. Based on these assimilation experiments, which are in part recapitulated in chapter 3.3, we address in more detail a set of errors affecting the soil moisture analysis. A revised quantification of the random model error is presented in chapter 4.1. Chapter 4.2 concentrates on biases caused by the model background, observations and forward operators and how to take them into account in an operational data assimilation setup. Chapter 4.3 finally addresses the systematic errors caused by the insufficient vertical near-surface resolution of the soil model.

## 4.1 Quantification of the model error covariance matrix

The background error covariance matrix evolves in time as a function of the analysis errors, the forecast operator (i.e. the model), and the model error covariance matrix (Eq. 2.21). The model error $\varepsilon_{mod}$ at an arbitrary analysis time step $i$ is defined as the deviation of the forecast from the true model state vector $\mathbf{x}_t$:

$$\varepsilon_{mod}(i) = M_{i-24\mathrm{h}\rightarrow i}\,\mathbf{x}_t(i-24\mathrm{h}) - \mathbf{x}_t(i) \tag{4.1}$$

$M_{i-24\mathrm{h}\rightarrow i}$ denotes the model or forecast operator applied to the model state vector. Model errors can originate from imperfect parameterisations or inevitable

discretizations in time and space. They also include forecast errors arising from uncertainties in the model's forcing data.

The model error covariance matrix is defined by

$$\mathbf{Q} = \overline{(\varepsilon_{mod} - \overline{\varepsilon_{mod}})(\varepsilon_{mod} - \overline{\varepsilon_{mod}})^{\mathrm{T}}} \tag{4.2}$$

where the overbars denote the expectation values and T marks the transpose. The Kalman filter assumes that the forecast model is free of biases so that the mean error in Eq. (4.2) becomes zero. Since $\mathbf{x}$ represents the soil moisture of the three model root zone layers in the assimilation system used here, $\varepsilon_{mod}$ is a three-element vector at each analysis time step. The model error covariance matrix $\mathbf{Q}$ for the ELDAS soil moisture analysis system is therefore given by

$$\mathbf{Q} = \begin{pmatrix} \overline{\varepsilon_{mod,1}^2} & \overline{(\varepsilon_{mod,1} \cdot \varepsilon_{mod,2})} & \overline{(\varepsilon_{mod,1} \cdot \varepsilon_{mod,3})} \\ \overline{(\varepsilon_{mod,2} \cdot \varepsilon_{mod,1})} & \overline{\varepsilon_{mod,2}^2} & \overline{(\varepsilon_{mod,2} \cdot \varepsilon_{mod,3})} \\ \overline{(\varepsilon_{mod,3} \cdot \varepsilon_{mod,1})} & \overline{(\varepsilon_{mod,3} \cdot \varepsilon_{mod,2})} & \overline{\varepsilon_{mod,3}^2} \end{pmatrix} \tag{4.3}$$

where $\varepsilon_{mod,1}$, $\varepsilon_{mod,2}$, and $\varepsilon_{mod,3}$ represent the soil moisture model errors of the top, middle and lowest root zone layer, respectively.

In practice, the determination of the model error covariance matrix is difficult because theoretically all single model errors, i.e. magnitudes and interdependencies, have to be known. Seuffert et al. (2004) applied an indirect method. They searched for a $\mathbf{Q}$ with which an optimal combination of observational and background information is achieved by checking the compliance with

$$\overline{(\mathbf{y} - \mathbf{H}\mathbf{x}_t)(\mathbf{y} - \mathbf{H}\mathbf{x}_t)^{\mathrm{T}}} - \overline{(\mathbf{y} - \mathbf{H}\mathbf{x}_a)(\mathbf{y} - \mathbf{H}\mathbf{x}_b)^{\mathrm{T}}} = \mathbf{0} \tag{4.4}$$

where $\mathbf{y}$ denotes the observation vector, $\mathbf{H}$ the linearised forward operator, and $\mathbf{x}_t$, $\mathbf{x}_b$ and $\mathbf{x}_a$ the true, background and analysed soil moisture state vector, respectively. The first term on the left side is the observation error covariance matrix $\mathbf{R}$ (also see Sec. 2.2). The second term resembles the first one, but additionally accounts for errors caused by the model (via $\mathbf{x}_b$) and the analysis (via $\mathbf{x}_a$). In case of an optimal analysis, $\mathbf{x}_b$ and $\mathbf{x}_a$ would, on average, be equal to the true state so that the second term converts to the observation error covariance matrix and Eq. (4.4) is fulfilled (provided that systematic model errors have been eliminated and the assumption of a linearised forward operator holds). In a suboptimal analysis which tends to stay too close to the observations, the absolute values of the deviations $\mathbf{y} - \mathbf{H}\mathbf{x}_a$ and $\mathbf{y} - \mathbf{H}\mathbf{x}_b$ would, on average, be smaller than $\mathbf{y} - \mathbf{H}\mathbf{x}_t$ so that Eq. (4.4) becomes positive. Accordingly, if the background field is weighted too much, it would become negative. Therefore,

Eq. (4.4) provides an opportunity to assess the balance of the analysis.

Seuffert et al. (2004) performed a number of case studies with varied model error covariance matrices. For the observation error covariance matrix, they used variances of $(2\ \mathrm{K})^2$ for 2-metre temperature and brightness temperature and $(10\ \%)^2$ for relative humidity to allocate the diagonal; covariances were set to zero (these settings have been adopted in this thesis). By assuming $\mathbf{Q}$ to be diagonal and constant in time, too, they found that a model error covariance matrix with $\varepsilon_{mod} = 0.005\ \mathrm{m}^3/\mathrm{m}^3$ for all three root zone layers best matches Eq. (4.4).

However, two types of observations are used in the ELDAS assimilation system which mainly depend on the soil water storage in different depths: Screen-level variables are closely linked to the available water in the entire root zone, while the microwave brightness temperature mainly represents the soil moisture content of the surface layer. Consequently, it is likely to achieve an improved soil moisture analysis when the vertical distribution of the model error is resolved more accurately.

### 4.1.1 Error propagation experiment with perturbed precipitation

As mentioned above, the forcing data for the land surface model is one potential major error source contributing to $\mathbf{Q}$. It is possible to estimate this contribution from an ensemble of model runs with artificially perturbed forcing data. Precipitation was chosen because of its direct impact on the soil water budget: a rain event can cause a significant wetness increase in the root zone within hours while the effects of radiation and wind are much smoother.

Forcing errors from precipitation can be quite large because current atmospheric models still have difficulties to accurately forecast the movement and intensity of low-pressure systems and are hardly able to simulate the development of single showers and thunderstorms. Therefore, we decided to perturb the measured amount of rainfall randomly by a value of up to 100 % each day, i.e. we assumed that in the worst case the model simulates no precipitation or the double amount of what really occurs. Since the probability of correctly forecasting the weather situation "dry" or "not dry" is much higher than the probability of forecasting the correct rain amount, days without precipitation have not been perturbed. Based on 10 perturbed rainfall time series for site LW02, the same number of model runs without any data assimilation were performed. Fig. 4.1 shows the perturbed precipitation amounts and the resulting soil water contents of the model's root zone layers. The soil moisture values of each run with perturbed precipitation were then compared to the corresponding values of

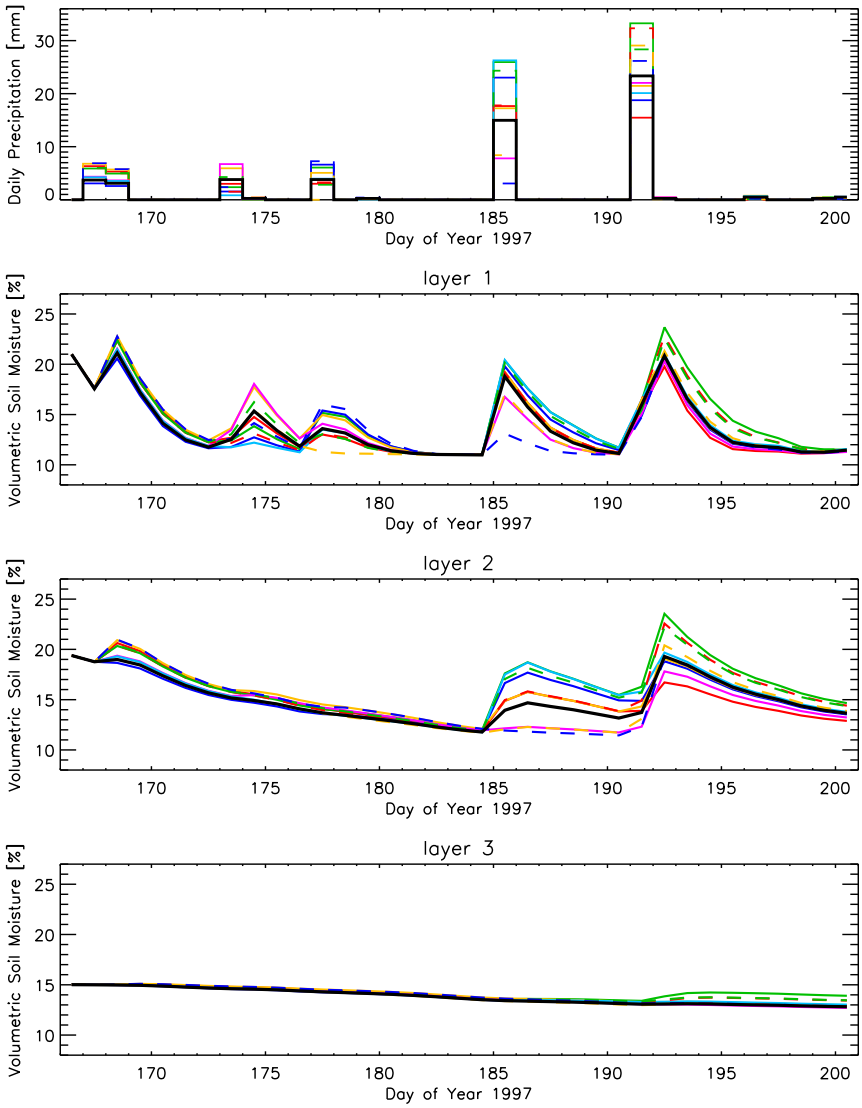


Figure 4.1: Daily observed (black) and perturbed (colored) precipitation amounts and resulting soil moisture values in the model's root zone layers at SGP97 site LW02.

the unperturbed control run and the respective bias-corrected root-mean-square deviations (representing the random forcing errors) were calculated. This procedure yields a mean rms error of 0.0045 $\pm$ 0.0004 $m^3/m^3$ for the root zone soil moisture.

The analysis of the single soil layers reveals that perturbing precipitation does not have the same effect in all model layers. For the surface layer, a mean rms error of 0.0086 $\pm$ 0.0008 $m^3/m^3$ was found when compared to the soil moisture of the run using observed rain amounts. The soil moisture for layers 2 and 3 are

characterised by values of 0.0096 ± 0.0007 $m^3/m^3$ and 0.0013 ± 0.0004 $m^3/m^3$, respectively. Since the infiltration process smoothes the randomly distributed errors, the value for layer 3 is comparably low. At the same time, it might be surprising that the rms error of the top layer is smaller than that of the second layer since errors in the precipitation forcing are expected to have the strongest impact on the surface. This unexpected behavior can be explained by a comparison of the soil moisture evolutions in layer 1 and 2 resulting from the precipitation perturbations (second and third plot in Fig. 4.1). The two strong rain events on day 185 and 191 mainly affect the second soil layer because the surface layer already gets very wet both days in the control run. In those perturbation runs with more precipitation than observed the additional water quickly percolates into the layer below, leading to a significant increase in soil moisture which noticeably affects the examined rms errors. To a lesser degree this can also be observed at day 168.

For the following data assimilation experiments it is assumed that precipitation uncertainties result in errors of the same magnitude in model layer 1 and 2. Model error variances of $(0.010\ m^3/m^3)^2$ and $(0.0015\ m^3/m^3)^2$ have been used for the two upper layers and the bottom root zone layer, respectively. These values are slightly higher than the ones found above. However, by this adjustment the difference between the root zone means of the model error resulting from the error propagation experiment (0.0045 $m^3/m^3$) and found by Seuffert et al. (2004, 0.0050 $m^3/m^3$) is reduced. The approximately identical mean errors allow for a comparison of the different analysis setups which only takes the effect of the vertical distribution of the layer-specific model errors into account.

It has to be noted that the outcome of this error propagation experiment strongly depends on the chosen perturbations. If, for instance, the temporal evolution of the rainfall events (i.e. the days of their occurence) was additionally changed or the actual amount of precipitation was perturbed with larger increments, the model errors integrated in $\mathbf{Q}$ would be larger as well. Therefore, the choice of the perturbations also affects the weighting of the observational and background information in the soil moisture analysis. As a consequence, the optimal combination of the available information as requested by Eq. (4.4) may no longer be ensured. Therefore, Eq. (4.4) is additionally checked with the new finding of $\mathbf{Q}$ and compared to the corresponding values from the reference experiment with the vertically constant model error. Results are presented for the KTRB run only, because the outcome of the KTR and KB setup is qualitatively the same.

For the reference experiment (REF), the left side of Eq. (4.4) yields (values

are rounded to integer for better readibility)

$$\mathbf{R} - \overline{(\mathbf{y} - \mathbf{H}\mathbf{x}_a)(\mathbf{y} - \mathbf{H}\mathbf{x}_b)^{\mathrm{T}}} = \begin{pmatrix} 0 & -3 & -2 & 7 & 8 & 7 & -1 \\ -3 & 0 & -3 & 6 & 13 & 14 & 0 \\ -2 & -3 & -1 & 7 & 12 & 22 & 0 \\ 7 & 7 & 7 & 44 & -58 & -58 & 10 \\ 8 & 13 & 12 & -56 & 15 & -87 & 3 \\ 6 & 14 & 22 & -55 & -87 & -45 & -1 \\ 0 & 1 & 0 & 5 & 0 & -3 & -9 \end{pmatrix} \tag{4.5}$$

while using the new $\mathbf{Q}$ setting results in

$$\mathbf{R} - \overline{(\mathbf{y} - \mathbf{H}\mathbf{x}_a)(\mathbf{y} - \mathbf{H}\mathbf{x}_b)^{\mathrm{T}}} = \begin{pmatrix} 0 & -2 & -2 & 6 & 7 & 6 & 1 \\ -2 & 0 & -3 & 5 & 13 & 12 & 2 \\ -2 & -3 & -1 & 6 & 11 & 19 & 1 \\ 6 & 6 & 6 & 49 & -52 & -49 & 4 \\ 7 & 13 & 11 & -50 & 17 & -80 & -3 \\ 5 & 12 & 18 & -45 & -79 & -21 & -8 \\ 1 & 2 & 2 & -3 & -9 & -13 & -6 \end{pmatrix} \tag{4.6}$$

At first sight, the matrices look quite similar. For an easier interpretation, the values of the main diagonal have been normalised by the observation variances (which are (2 K)$^2$ for air and brightness temperature and (10 %)$^2$ for relative humidity). This normalisation results in

$$\begin{pmatrix} 0.08 & \cdots & \cdots & \cdots & \cdots & \cdots & \cdots \\ \cdots & -0.06 & \cdots & \cdots & \cdots & \cdots & \cdots \\ \cdots & \cdots & -0.34 & \cdots & \cdots & \cdots & \cdots \\ \cdots & \cdots & \cdots & 0.44 & \cdots & \cdots & \cdots \\ \cdots & \cdots & \cdots & \cdots & 0.15 & \cdots & \cdots \\ \cdots & \cdots & \cdots & \cdots & \cdots & -0.45 & \cdots \\ \cdots & \cdots & \cdots & \cdots & \cdots & \cdots & -2.13 \end{pmatrix}_{\mathrm{REF}} \tag{4.7}$$

and

$$\begin{pmatrix} 0.10 & \cdots & \cdots & \cdots & \cdots & \cdots & \cdots \\ \cdots & -0.11 & \cdots & \cdots & \cdots & \cdots & \cdots \\ \cdots & \cdots & -0.19 & \cdots & \cdots & \cdots & \cdots \\ \cdots & \cdots & \cdots & 0.49 & \cdots & \cdots & \cdots \\ \cdots & \cdots & \cdots & \cdots & 0.17 & \cdots & \cdots \\ \cdots & \cdots & \cdots & \cdots & \cdots & -0.21 & \cdots \\ \cdots & \cdots & \cdots & \cdots & \cdots & \cdots & -1.44 \end{pmatrix}_{\mathrm{Q}} \tag{4.8}$$

Matrix (4.7) stands for the reference experiment and matrix (4.8) for the run with the new **Q**. Beginning at the top left, the single elements represent air temperature at 9, 12, and 15 LST, relative humidity at the same times, and brightness temperature, respectively, similarly to the order in the observation vector **y**. As written above, a negative value indicates an analysis which tends to stick too close to the background. A positive sign represents an analysis which overweights the observations, and a value of zero stands for an optimal analysis.

The new setting of **Q** noticeably improves the analysis, in terms of a more balanced processing of observations and background, for the air temperature and relative humidity data at 15 LST and the brightness temperatures (compare 3rd, 6th, and 7th element of the diagonal). The other values hardly change. The new model error covariance matrix therefore seems to be a reasonable estimate. However, the check of the analysis balance reveals that for the brightness temperature the background might be weighted too much in comparison to the observations. The easiest way to level this out would be to reduce the brightness temperature observation error. Nevertheless, for a consistent comparison of the runs with different **Q**, this adjustment has not been done in this study. A revised brightness temperature observation error will be tested and potentially incorporated in a subsequent one-year assimilation study (see Sec. 5)

### 4.1.2 Application of a revised model error covariance matrix

The revised setting of the model error covariance matrix has been applied in an assimilation experiment at SGP97 site LW02. Two different setups concerning precipitation have been chosen: (a) observed, quality-controlled precipitation (solid line in the top plot of Fig. 4.1), and (b) rain amounts set to zero so that the response of the analysis system to false precipitation forcing data can also be assessed. In both precipitation setups and analogous to the reference experiment, model runs have been performed without assimilation (CTRL), with the assimilation of screen-level variables alone (KTR), with the assimilation of brightness temperatures alone (KB), and with the assimilation of all observations together (KTRB). The results in terms of the bias-corrected rms deviation of modelled soil moisture and fluxes from the corresponding observations are summarised in Tab. 4.1(a) (observed precipitation) and 4.1(b) (precipitation set to zero).

The change of **Q** significantly modifies the rms errors in the KTR and KTRB runs. The model drift away from the soil moisture measurements within layer 3 caused by the reference assimilation setup is clearly reduced when the revised model errors are used (also shown in Fig. 4.2 for the KTRB run). This improve-

(a)

| | | Root zone soil moisture (vol. %) | Layer 1 soil moisture (vol. %) | Layer 2 soil moisture (vol. %) | Layer 3 soil moisture (vol. %) | Latent heat flux ($W/m^2$) | Sensible heat flux ($W/m^2$) |
|---|---|---|---|---|---|---|---|
| CTRL | | 0.19 | 1.80 | 0.89 | 0.38 | 21.9 | 23.0 |
| KTR | REF | 2.15 | 1.64 | 1.30 | 2.62 | 17.6 | 20.3 |
| | Q | 1.14 | 2.15 | 1.56 | 1.14 | 20.8 | 22.5 |
| KTRB | REF | 2.13 | 1.33 | 1.18 | 2.67 | 15.0 | 18.0 |
| | Q | 1.16 | 1.61 | 1.54 | 1.25 | 18.1 | 18.9 |
| KB | REF | 0.45 | 1.47 | 1.05 | 0.56 | 19.0 | 19.1 |
| | Q | 0.40 | 1.50 | 1.11 | 0.45 | 18.9 | 18.6 |

(b)

| | | Root zone soil moisture (vol. %) | Layer 1 soil moisture (vol. %) | Layer 2 soil moisture (vol. %) | Layer 3 soil moisture (vol. %) | Latent heat flux ($W/m^2$) | Sensible heat flux ($W/m^2$) |
|---|---|---|---|---|---|---|---|
| CTRL | | 0.67 | 2.77 | 1.59 | 0.45 | 30.4 | 28.5 |
| KTR | REF | 1.72 | 2.78 | 1.04 | 2.33 | 19.8 | 20.5 |
| | Q | 1.12 | 3.05 | 1.83 | 1.18 | 26.6 | 24.7 |
| KTRB | REF | 2.14 | 2.19 | 1.03 | 2.85 | 17.4 | 17.7 |
| | Q | 1.14 | 2.17 | 2.22 | 1.18 | 21.7 | 21.3 |
| KB | REF | 0.61 | 2.26 | 1.79 | 0.51 | 24.4 | 21.0 |
| | Q | 0.61 | 2.36 | 1.50 | 0.46 | 25.0 | 19.8 |

Table 4.1: (a) Bias-corrected rms errors of model soil moisture and surface fluxes (compared to observations) resulting from the assimilation experiments with applying the vertically constant model error according to Seuffert et al. (2004, REF) or with applying the revised depth-varying model error according to the precipitation sensitivity study (Q) [all runs use *observed* precipitation; CTRL = no soil moisture analysis applied; KTR = assimilating screen-level variables alone; KTRB = assimilating screen-level variables and brightness temperature together; KB = assimilating brightness temperature alone]. (b) Same as (a), but using precipitation set to zero.

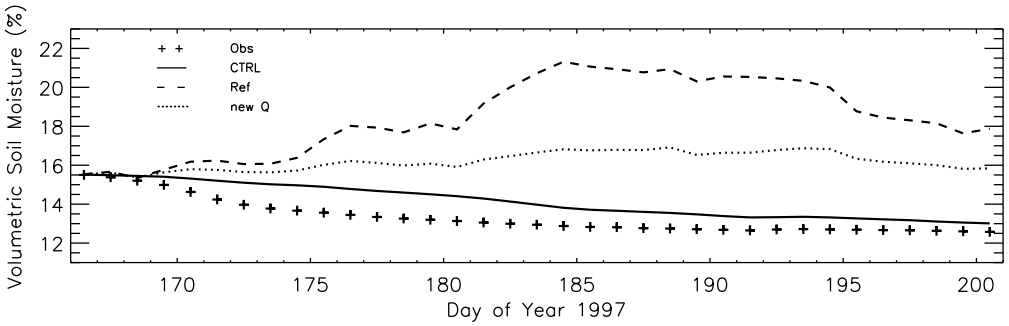


Figure 4.2: Soil moisture in the third soil model layer simulated without any assimilation (solid line), with using the model error setting of Seuffert et al. (2004) (dashed line) in the KTRB assimilation run, and with applying the revised model error according to the rainfall sensitivity study (dotted line, also KTRB). The plus signs denote observations.

ment is achieved by the smaller model error setting for layer 3. It gives more weight to the background soil moisture which is closer to the observations than the model values resulting from the reference assimilation runs (CTRL vs. REF). At the same time, however, the KTR and KTRB simulations for layer 1 and 2 become worse by the revised model errors (except for layer 1 soil moisture in the KTRB run with no precipitation). Nevertheless, since layer 3 contributes most to the root zone, analysed root zone soil moisture in the Q runs fits substantially better to the observations than in the reference.

In contrast to root zone soil moisture, the simulation of the surface turbulent heat fluxes does not benefit from the new estimate of the model error. The rms deviation between model values and observations increases in all KTR and KTRB runs. This opposing behavior of root zone soil moisture and turbulent fluxes in the soil moisture data assimilation system has also been observed by Seuffert et al. (2004) and Drusch and Viterbo (2006). Obviously, the deterioration of layer 1 and 2 soil moisture simulations has a larger effect on the surface fluxes than the improved modelling of layer 3 soil moisture due to the predominantly shallow roots of the main vegetation type grass. However, the improvement in root zone soil moisture calculations (the rms error decreases by 45 % in the KTRB run with observed precipitation) is larger than the loss of performance in sensible and latent heat fluxes (rms error increase of 5 and 21 %, respectively).

Different from the KTR and KTRB outcome, the assimilation of brightness temperature alone provides reduced rms errors for the root zone soil moisture as well as for the surface heat fluxes in the case of using observed precipitation. This result might indicate that the depth-varying model error setting is preferable

when using passive microwave data. However, the improvements found are small and do not consistently occur in the zero-precipitation setup.

The exercise presented in this section shows that a vertically varying model error is able to improve the performance of the root zone soil moisture analysis in comparison to a vertically constant model error. However, this improvement was found to be either small (KB setup) or to come along with worse surface heat flux simulations (KTR and KTRB setups) which are not desirable for atmospheric modelling applications. Thus, a definite conclusion on the preferable setting of the model error covariance matrix can not be given yet. Furthermore, the determination of $\mathbf{Q}$ as applied in this thesis is based on a single forcing variable only. Ideally, before applying the assimilation system in a future operational forecast environment, a number of variables (e.g. precipitation, radiation, and wind speed) should be examined in similar sensitivity studies and the individual perturbations should be correlated to represent a meteorologically consistent situation. This should further improve the outcome of the soil moisture analysis. Finally, contributions from model errors caused e.g. by discretization procedures and imperfect parameterisations have to be assessed. However, it becomes clear from this study that the specification of the model error covariance matrix can be of essential importance for the performance of the extended Kalman filter soil moisture analysis and therefore requires thorough calibration efforts.

## 4.2 Correcting for background, observation and forward operator biases

### 4.2.1 Approach

Prerequisites for an accurate setup of a data assimilation system based on the least-squares estimation are that the background state vector $\mathbf{x}_b$ is unbiased and that no systematic deviation exists between the observations $\mathbf{y}$ and the model equivalents $H\mathbf{x}_t$ calculated from the true state vector $\mathbf{x}_t$ via the forward operator $H$ (Bouttier and Courtier, 1999), i.e.

$$\overline{\mathbf{x}_b - \mathbf{x}_t} = 0 \tag{4.9}$$

$$\overline{\mathbf{y} - H\mathbf{x}_t} = 0 \tag{4.10}$$

In the data assimilation system of this study, $\mathbf{x}_b$ contains the model soil moisture of the three root zone layers. Observed assimilation variables denoted by

$\mathbf{y}$ are 2-metre temperature, 2-metre relative humidity and 1.4 GHz brightness temperature. The overbar indicates that the term beneath is time-averaged.

Deviations from Eqs. (4.9) and (4.10) degrade the quality (optimality) of the soil moisture analysis and should be minimised. Causes for a model soil moisture bias can be, for instance, imperfect parameterisations, incorrect settings of soil and vegetation characteristics and biased forcing data (see Sec. 1.2). Non-compliance with Eq. (4.10) can originate from biased observations and from a non-perfect forward operator. Only when the systematic errors induced by the observations and the forward operator are equal in magnitude and sign, Eq. (4.10) would still be fulfilled.

In practice, a verification of the prerequisites (4.9) and (4.10) is difficult because the true soil moisture state vector $\mathbf{x}_t$ is not known. However, when assuming a quasi-linear forward operator $\mathbf{H}$ (see Eq. 2.16), a consequence of Eqs. (4.9) and (4.10) is that the mean difference between the observed assimilation variables $\mathbf{y}$ and the model equivalents $H\mathbf{x}_b$ calculated from the background soil moisture state $\mathbf{x}_b$ becomes zero (e.g. Dee and da Silva, 1998):

$$\overline{\mathbf{y} - H\mathbf{x}_b} \approx \overline{\mathbf{y} - \mathbf{H}\mathbf{x}_b} = 0 \tag{4.11}$$

The differences between the elements of $\mathbf{y}$ and $H\mathbf{x}_b$ are called innovations (Bouttier and Courtier, 1999) or observed-minus-forecast residuals (Dee and da Silva, 1998). Equation (4.11) describes a prerequisite for an optimally set up soil moisture analysis which can be checked easily in an operational data assimilation system. Existing innovation biases can then be accounted for by adjusting the observations before they are assimilated into the model.

### 4.2.2 Bias analysis for the SGP97 assimilation experiment

In the reference assimilation experiment, mean innovations of +2.18 K for the 2-metre temperature, -9.71 % for the 2-metre relative humidity, and +9.55 K for the brightness temperature were found (Fig. 3.5). Possible sources for these biases are the observations, the forward operators and the background soil moisture. In general, it is difficult to quantify the single bias contributions. However, some qualitative assumptions can be made for the assimilation system used in this study:

- The contribution of the observations to the innovation biases is expected to be small since these datasets have been subject to quality checks (Jackson

et al., 1999; Meyers, 2001; Seuffert et al., 2004). A bias of 7 % occurring in the relative humidity measurements has already been substracted.

- The forward operators for the screen-level variables (2m air temperature and relative humidity) are also expected to cause negligible biases because these parameterisations (see ECMWF, 2001, for details) have already extensively been tested and used in ECMWF's operational weather forecast system.

- The forward operator for calculating the model equivalents of the brightness temperature observations is, in this thesis, represented by the microwave radiative transfer model LSMEM (Sec. 2.1.3). This model has already widely been used in studies combining hydrological and remote sensing aspects (e.g. Drusch, 1998; Drusch et al., 2001; Gao et al., 2004). In the reference assimilation experiments, the settings of parameterisation options and static input variables have been set according to previous studies and measurements available from the SGP field experiments (see Sec. 3.3 and Seuffert et al. (2004)). However, the surface roughness and the vegetation structure coefficient, which significantly influence the brightness temperature calculations, are only estimates, and the parameterisations used in the model cannot completely reproduce reality. Consequently, the LSMEM may be a source for a serious innovation bias.

- A large contribution to the innovation bias can also be expected from the model's surface soil moisture, which is significantly lower than the observations throughout the SGP97 period (Fig. 3.6).

Assuming that the SGP97 soil moisture retrievals derived from the SHAWMS matric potential observations and the soil temperature measurements are a reasonable approximation of the true soil state, the contribution of the background to the innovation biases can be assessed by comparing two different control runs (i.e. no soil moisture analysis is performed): (a) model soil moisture and temperature are re-initialised by the observations (representing the truth) at every model time step; (b) model soil moisture and temperature are freely run as in the reference control run. The differences of the resulting innovation biases can be attributed to the model background.

For setup (a), the soil moisture observations for the top soil layer in model space are represented by the mean of the three SHAWMS measurements from a depth of 5 cm. The second layer (7 – 28 cm) soil moisture was provided by the mean of the observations from depths of 10, 15, 20, and 25 cm, and the third layer (28 – 100 cm) value was taken from the 60-cm measurement. The model's

soil temperature was set equal to the observations determined from depths of 2 and 4 cm for the top layer, 16 cm for the second and 64 cm for the third layer. In the control run regularly re-initialised with these soil moisture and soil temperature observations (MP run), the innovation biases of the modelled 2-metre temperature and 2-metre relative humidity are significantly reduced from 2.18 K to 0.56 K and from -9.71 % to -0.27 %, respectively (Fig. 4.3). This distinct convergence of the model values towards the observations confirms the expectation of basically unbiased screen-level observations and forward operators as stated above. In contrast to the screen-level variables, the brightness temperature innovation bias resulting from the revised control run is quite large (-12.88 K). This bias can probably be traced back to the microwave forward operator, i.e. the LSMEM, as described above.

However, it can be doubted that the SHAWMS soil moisture values from a depth of 5 cm are representative for the surface layer since the comparison with the gravimetric probes shows that the fluctuations at 5 cm are much smaller than within the top 5 cm. Therefore, the control run using observations was repeated with a modified determination of the "real" soil moisture in the surface layer by using a depth-weighted average of gravimetric and matric potential retrievals, filling gaps in the gravimetric data with interpolated values (Fig. 4.3, GVMP run in the bottom plot). As expected, these settings lead to a larger amplitude in the resulting brightness temperatures (Fig. 4.3). The overall bias, however, does not change substantially (-12.88 K vs. -13.88 K).

Despite of the potential deficiencies of the soil moisture measurements, the outcome of the modified control runs strongly indicate that the main contributions to the innovation biases result from the systematically too dry model soil moisture and the microwave forward operator. These biases could be minimised for every observation site separately by adjusting e.g. the surface roughness or the vegetation structure coefficient in the LSMEM or predefined soil properties like the hydraulic conductivity in TESSEL. However, in an operational application, a bias correction as described in Sec. 4.2.1 would be the most feasible way to achieve compliance with Eq. (4.11). The effects of such a correction on the analysed model soil moisture and on the simulation of the surface fluxes of sensible and latent heat is examined next.

### 4.2.3 Application of a bias correction

In order to fulfill prerequisite (4.11), the observations were corrected by the corresponding innovation biases found from the reference control run (2-metre temperature: +2.18 K, relative humidity: -9.71 %, and brightness temperature:

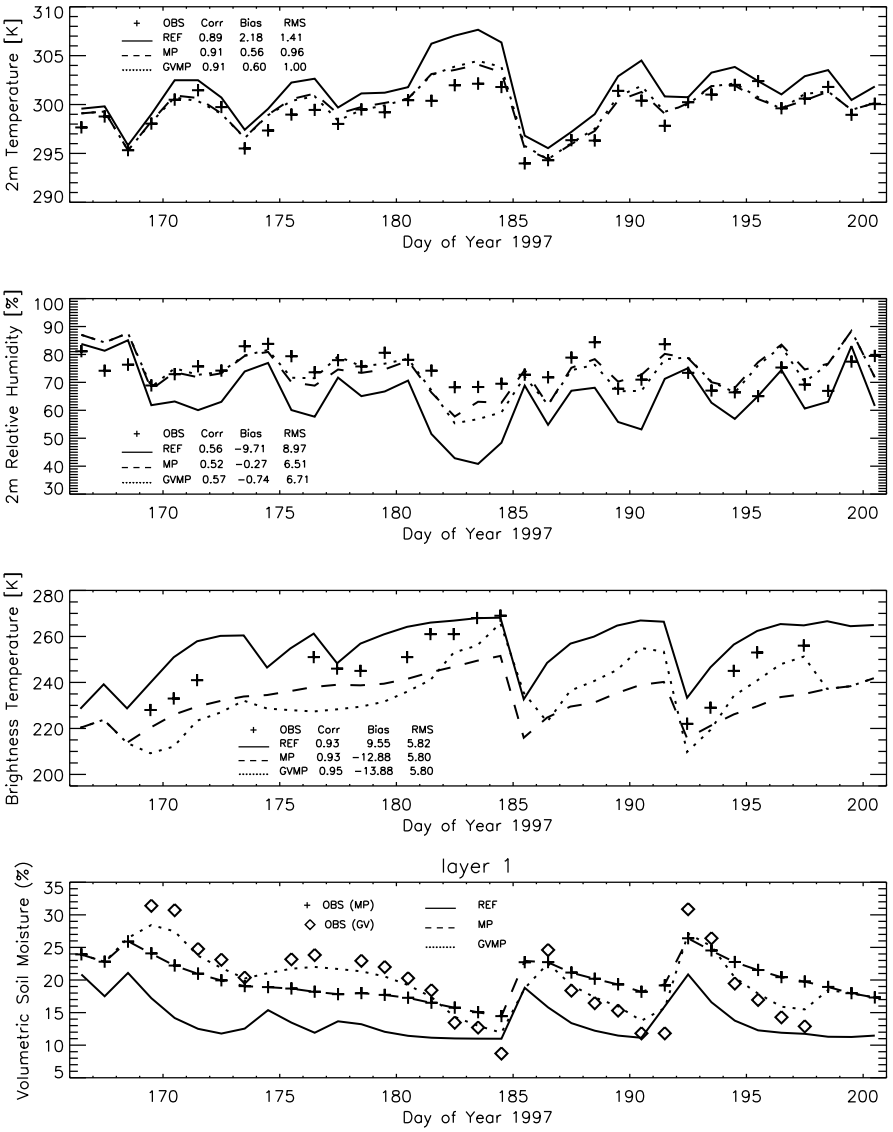


Figure 4.3: Model evolution of 2m temperature, relative humidity, brightness temperature, and top layer soil moisture during SGP97 based on different soil moisture and soil temperature settings. In the REF run (solid line), model soil moisture and temperature evolve freely. The MP run (dashed line) is initialised every model time step with soil moisture values derived from the SHAWMS matric potential observations and soil temperature measurements taken at the NOAA/ATDD station (see text for details). The GVMP run (dotted line) resembles the MP run, only the soil moisture of the first model layer is replaced by a depth-weighted average of matric potential and gravimetric retrievals. Plus signs denote observations. In case of soil moisture (bottom plot), the plus signs and diamonds stand for the soil moisture retrievals from the 5 cm matric potential and from the 0 - 5 cm gravimetric measurements, respectively.

+9.55 K, see Fig. 3.5) before they are assimilated into the single-column model. All assimilation setups (KTR = using screen-level variables alone, KB = brightness temperature alone, and KTRB = all observations together) have then been re-run. The evolution of the corrected observations and the corresponding model simulations are shown in Figure 4.4, the resulting moisture increments applied by the soil moisture analysis in Fig. 4.5. Consistent with the physical dependencies — the brightness temperature signal mainly originates from the top few centimetres of the soil while 2-metre temperature and humidity rely on the soil moisture distribution in the whole root zone — significant moisture increments in the KB run are predominantly applied in model layer 1 (red lines in Fig. 4.5) whereas the soil moisture analysis based on screen-level variables affects all three root zone layers (black lines), with slightly increasing increments from the top layer to layer 3.

The most significant deviations of modelled values from the bias-corrected observations occur from day 181 to day 184 (Fig. 4.4). The modelled 2-metre temperature is higher, the relative humidity lower than the observations, suggesting a too dry soil in the model. Consequently, the soil moisture analysis aims to increase the soil water content during these days (solid black line in Fig. 4.5). At the same time, the modelled brightness temperatures are lower than the bias-corrected observations. Thus, in contrast to the calculated increments based on the screen-level variables, the analysis tries to remove water especially from the top soil layer (solid red line in Fig. 4.5). This opposite behavior can also be observed on day 178, 180, 192, and 193.

The effects of these different soil moisture adjustments on the model performance during SGP97 at site LW02 are shown in Fig. 4.6 for the soil moisture of all root zone layers (for a similar plot for fluxes, see Appendix B). The bias-corrected root-mean-square deviations of modelled soil moisture and fluxes from the independent observations (they are not used in the assimilation procedure) again serve as a measure of the quality of the analysis. These rms errors are summarised in Tab. 4.2.

When using observations corrected by the innovation bias, the assimilation of brightness temperatures alone performs best for the soil moisture of the top model layer (bias-corrected rms errors of volumetric soil moisture: CTRL 1.80 %, KB 1.68 %, KTR 1.98 %, KTRB 1.73 %). For layer 2, the best results are obtained from the assimilation of the screen-level variables alone whereas layer 3 soil moisture does not benefit from the assimilation procedures at all. The rms error of the root zone soil moisture also gets worse for all assimilation runs, especially for the KTR and KTRB run.

In comparison to the reference runs, however, the bias correction of the obser-

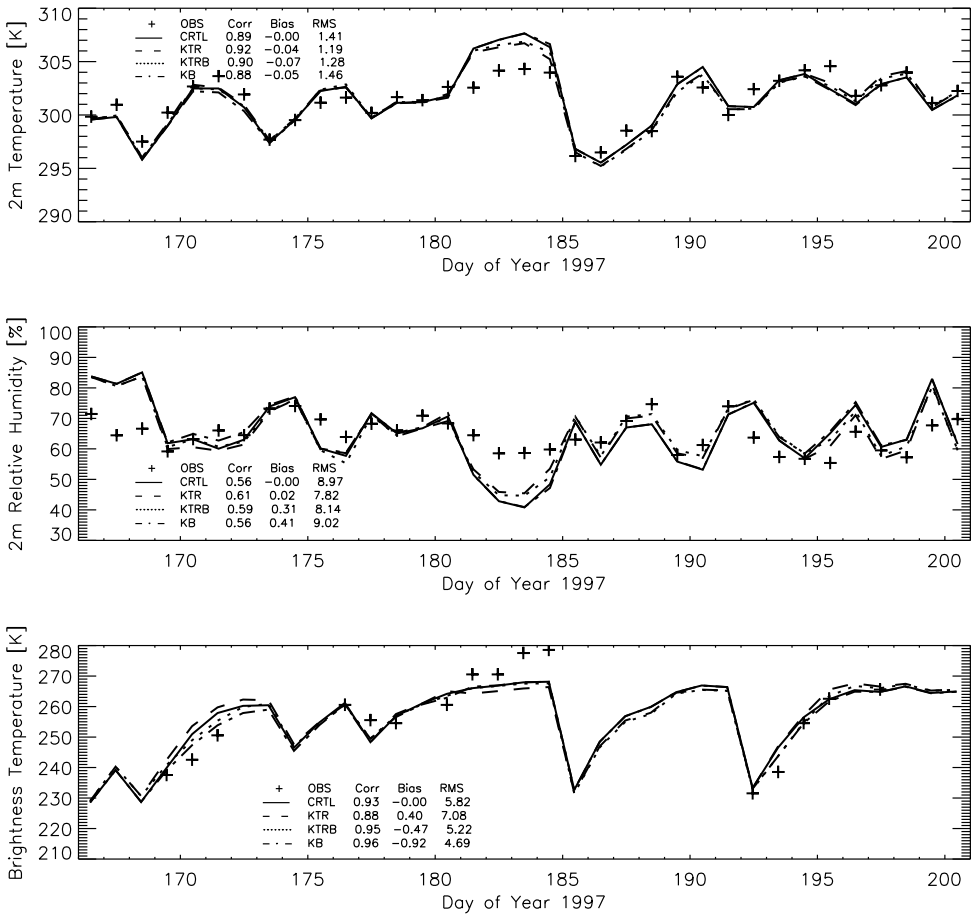


Figure 4.4: SGP97 daily means of observed and modelled 2m temperature, relative humidity and microwave brightness temperature in the assimilation runs using observations corrected by the innovation biases. The plus signs stand for bias-corrected observations [OBS] (brightness temperature observations are from around 11 LST only); lines denote results from model runs (solid = no assimilation [CTRL], dashed = assimilation of 2m temperature and relative humidity alone [KTR], dash-dotted = assimilation of brightness temperature alone [KB], dotted = assimilation of all observation types together [KTRB]). Specified statistic quantities are correlation coefficient [Corr], bias [Bias] and bias-corrected root-mean-square error [RMS] of the modelled variables in comparison to the bias-corrected observed values.

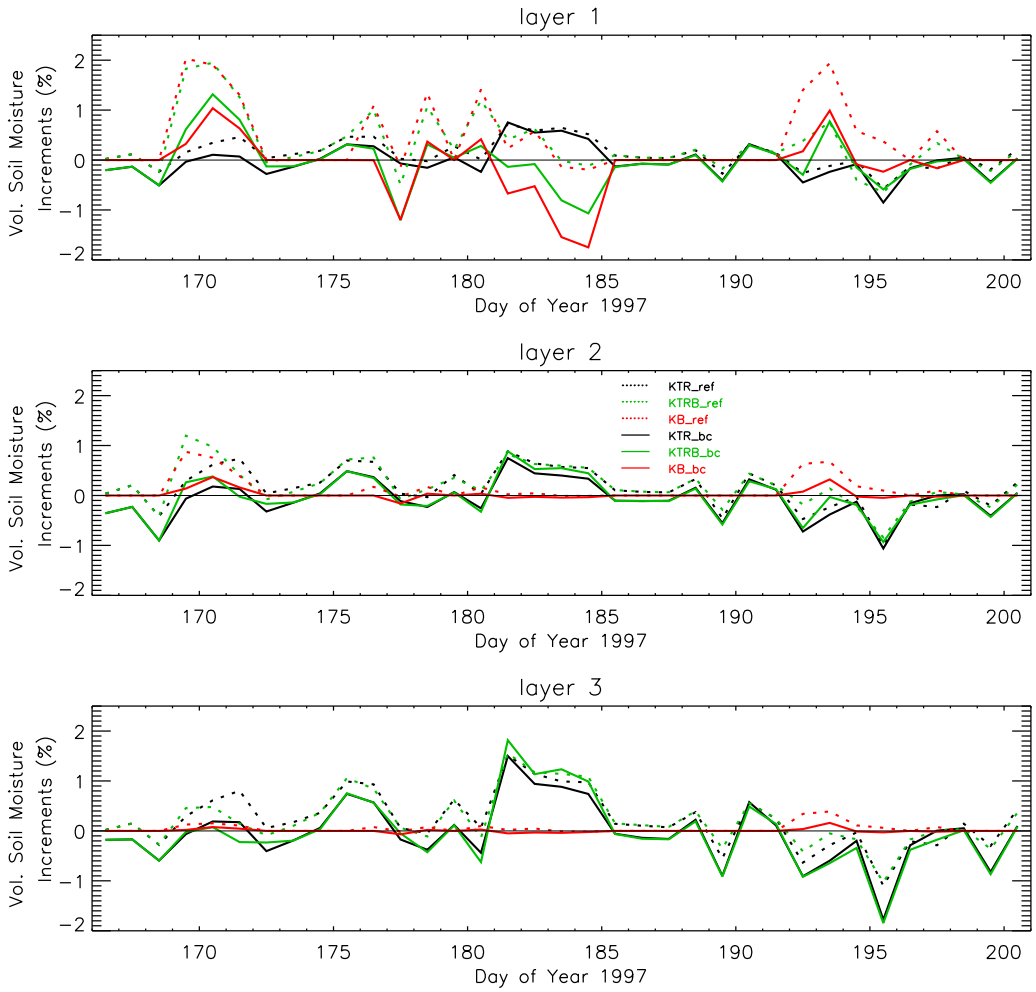


Figure 4.5: Soil moisture increments applied by the analysis in the reference assimilation experiments (dotted lines) and in the assimilation runs using biased-corrected observations (solid lines).

vations significantly improves the performance of the soil moisture simulations for the root zone. This improvement relies on the model's soil moisture evolution in layer 2 and 3 which is in better agreement with the observations when the bias correction is applied, whereas the rms error for the soil moisture of the top soil model layer increases in comparison to the reference run. However, the rms error values for layer 1 should be taken with care since the soil moisture retrievals from the matric potential measurements can probably not fully represent the amplitude of the real soil moisture evolution within the top 7 cm of the soil, as the gravimetric measurements indicate. Secondly, the top layer model soil moisture has already reached its minimum (the predefined wilting point) from day 182 to 184 (Fig. 4.6). The removement of water, as calculated by the soil moisture

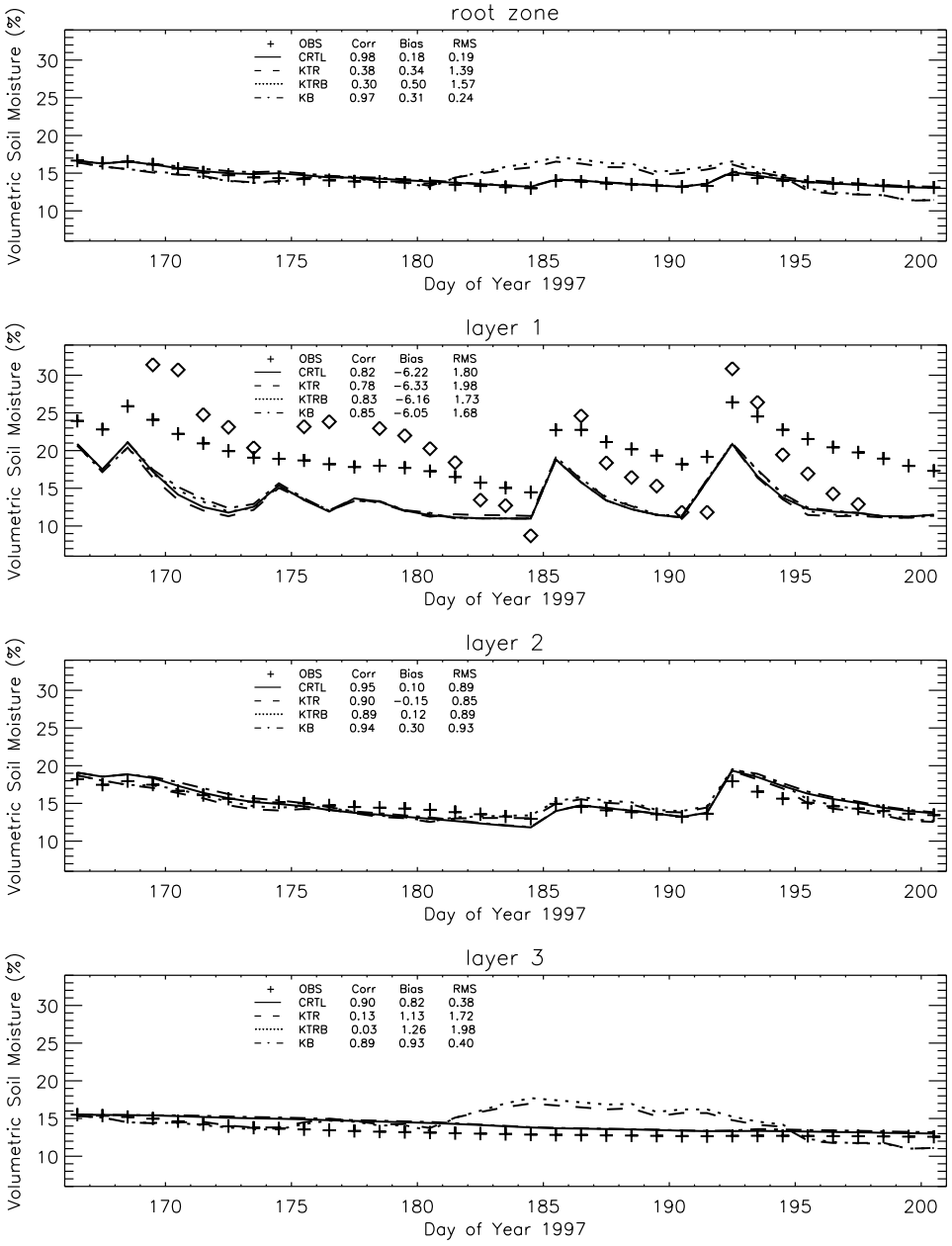


Figure 4.6: SGP97 daily means of observed and modelled soil moisture in the three top model layers and the resulting root zone soil moisture in the assimilation runs using observations corrected by the innovation biases (lines, symbols, and statistic data as in Fig. 3.5 and 3.6).

| | | Root zone soil moisture (vol. %) | Layer 1 soil moisture (vol. %) | Layer 2 soil moisture (vol. %) | Layer 3 soil moisture (vol. %) | Latent heat flux ($W/m^2$) | Sensible heat flux ($W/m^2$) |
|---|---|---|---|---|---|---|---|
| CTRL | | 0.19 | 1.80 | 0.89 | 0.38 | 21.9 | 23.0 |
| KTR | REF | 2.15 | 1.64 | 1.30 | 2.62 | 17.6 | 20.3 |
| | BCO | 1.39 | 1.98 | 0.85 | 1.72 | 24.1 | 26.2 |
| KTRB | REF | 2.13 | 1.33 | 1.18 | 2.67 | 15.0 | 18.0 |
| | BCO | 1.57 | 1.73 | 0.89 | 1.98 | 23.4 | 25.3 |
| KB | REF | 0.45 | 1.47 | 1.05 | 0.56 | 19.0 | 19.1 |
| | BCO | 0.24 | 1.68 | 0.93 | 0.40 | 21.9 | 22.4 |

Table 4.2: Bias-corrected rms errors of model soil moisture and surface fluxes (compared to observations) in the reference assimilation experiments (REF) and in the assimilation runs using observations corrected by the innovations biases (BCO). The different assimilation settings: assimilating screen-level variables and brightness temperature together (KTRB), screen-level variables alone (KTR), brightness temperature alone (KB), and applying no soil moisture analysis (CTRL).

analysis in the KTRB and KB runs (see Fig. 4.5), could therefore not be applied for these days.

Despite of the reduced rms errors of the root zone soil moisture in the bias-corrected assimilation runs in comparison to the reference experiment, the rms error of the fluxes increases in all assimilation runs (see Tab. 4.2). This opposite behavior was already described in Sec. 4.1.2. The soil moisture analysis based on the soil scheme TESSEL is apparently not able to improve both root zone soil moisture and turbulent surface heat fluxes at the same time. However, when looking at the different observation types, the best overall performance during SGP97 seems to be obtained from using brightness temperatures alone.

The study presented in this section shows that, in comparison to the reference assimilation runs, the observation correction based on the innovation biases is able to significantly improve the quality of the soil moisture analysis for the root zone. It has to be emphasised that this improvement solely affects the bias-corrrected rms deviation of the modelled soil moisture from the observations; the extended Kalman filter, like other assimilation systems based on the least square estimation, is not designed to reduce model state vector biases as they

occur during SGP97 (systematically too dry near-surface soil moisture in the model). Such biases need to be minimised by other means: accurate calibration of the soil model for different soil types (only one is included in TESSEL) could for instance reduce biases in advance; and when screen-level observations and their forward operators can be assumed to be basically bias-free (as indicated for SGP97 in Sec. 4.2.2), monitoring the innovation biases of these observations for days with a strong atmosphere-to-surface coupling can give hints on model soil moisture biases.

In view of the practical application of the bias correction presented here, it has to be noted that this study is based on only 16 brightness temperature observations with larger gaps in between (e.g. from day 185 to 191). This limited dataset is sufficient to qualitatively examine the potential effects of an innovation bias correction on the assimilation performance but can hardly provide an accurate quantitative estimate of the "real" biases occurring during a complete annual cycle. Especially the model's near-surface soil moisture bias which significantly contributes to the innovation bias may be a specific characteristic of the SGP97 period. Since such model soil moisture biases should be corrected separately, in general only the innovation bias caused by the microwave forward operator needs to be corrected (assuming that observations and the screen-level forward operators are free of systematic errors). As a result of SGP97 for instance, observed brightness temperatures would be reduced by -12.88 K (see MP run in Fig. 4.3).

## 4.3 The impact of non-uniform soil moisture and temperature profiles

The main contribution to the microwave radiation measured by an aircraft-borne or satellite-borne sensor originates from the top few centimetres of the soil. Consequently, in order to be able to accurately interpret observed brightness temperatures, not only bulk characteristics of the soil (e.g. texture) have to be known; it is also necessary that the soil model is capable of resolving the vertical near-surface soil moisture distribution. In the case of ECMWF's soil model TESSEL, in which the top layer covers the upper 7 cm, this prerequisite is not fulfilled. The potential effects of this shortcoming are illustrated in Fig. 4.7 for an arbitrary artificial soil moisture profile (black line) as it may occur in reality (e.g. Shutko et al., 1995; Dingman, 2002). This profile is characterised by a vertical mean of 0.2 $m^3/m^3$ (= 20 % volumetric water content) within the top 7 cm. Ideally, exactly this value should be derived for the soil model's first layer from

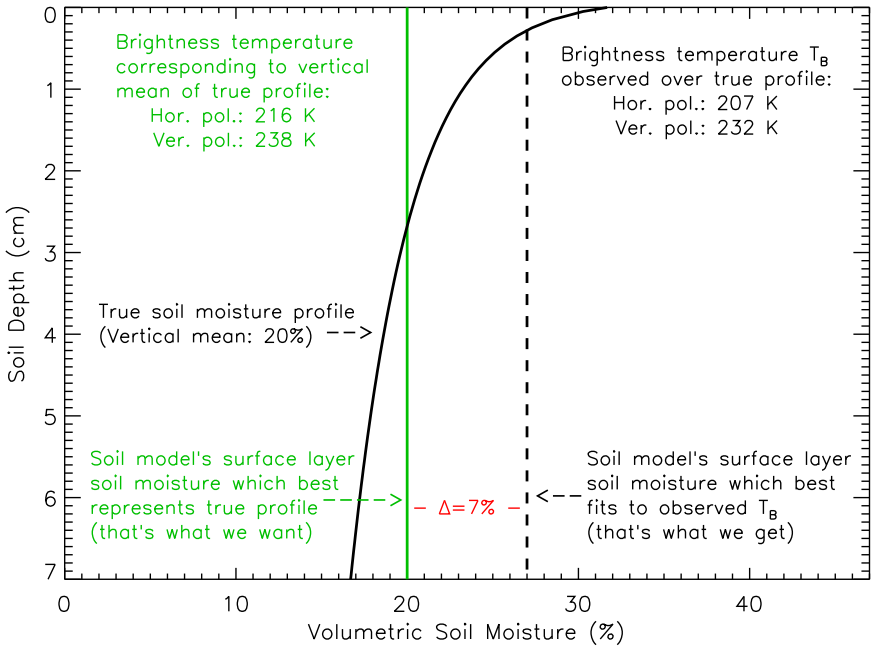


Figure 4.7: Example of a potential misleading interpretation of L-band brightness temperature observations in the ELDAS land data assimilation system due to TESSEL's inadequate resolution of the near-surface soil moisture profile.

corresponding brightness temperature observations. However, a look at the 1.4 GHz brightness temperatures that would be observed over the true profile (calculated with the LSMEM), and those that would result from the uniform profile within the soil model (green line) reveals differences of several Kelvin at horizontal as well as vertical polarisation. The uniform profile that corresponds to the observed brightness temperatures would have a vertically constant value of 27 %. Consequently, the soil water content of the first soil model layer that would be derived from the brightness temperature observations differs by 7 % from the ideal value. The impact of such a systematic error source on a potential operational assimilation system using microwave brightness temperatures is examined in this section.

The upgrade of the soil model with additional near-surface layers would require elaborate re-calibration and validation of the model and in addition increases computing time and memory demands. Easier-to-apply possibilities of accounting for the systematic profile errors in the soil moisture analysis are: (a) parameterising the near-surface soil moisture (e.g. as a function of the model's top layer soil moisture, the time elapsed since the last rain event and the evaporation intensity) for the microwave radiative transfer calculations; (b) adjusting the

brightness temperature observations based on sensitivity studies (also accounting for rain events and drying periods). Since this latter statistical approach can be carried out offline without modifying the model itself and since the adjustment of the brightness temperature observations has to be done anyway when accounting for potential innovation biases (as presented in Sec. 4.2), option (b) was chosen for this study.

The vertical resolution of soil moisture observations from field experiments is usually too low to study its effect on modelled brightness temperatures. However, during SGP99 gravimetric samples were taken from depths of 0 to 2.5 cm and 2.5 to 5 cm. Soil temperatures were measured at depths of 1 cm and 5 cm. Based on these observations, ensembles of 99 artificial soil moisture and temperature profiles have been generated for site LW03 each day. From these ensembles, brightness temperatures have been calculated following the single-layer approach as used in the reference assimilation experiments and the multi-layer radiative transfer model proposed by Wilheit (1978, Sec. 2.1.3) in order to quantify the errors in modelled brightness temperatures which can result from the insufficient vertical resolution of the soil model.

### 4.3.1 Ensembles of artificial profiles

#### Soil moisture

The two-layer gravimetric soil moisture measurements and the observed soil bulk densities from 33 SGP99 sites (LW02–14, LW17, LW18, LW21–27, ER1, ER5, ER17–20, CF01, CF02, CF04, CF05, CF11) have been used to calculate volumetric soil moisture differences between the first layer (0–2.5 cm depth) and the second layer (2.5–5 cm). The distribution of these differences grouped by the days after the rainfall event of July 10 is shown in Fig. 4.8. The spread in differences at individual days is large due to the local differences in the amount of rainfall, soil and vegetation characteristics, and errors of the in-situ measurements. Nevertheless, the daily averages of the layer differences show a clear trend: One day after the rainfall event the upper layer is nearly 3 % wetter than the bottom layer. During the following days the drying of the surface layer due to evaporation and infiltration leads to a decrease and a change of sign of the mean soil moisture difference. The difference remains almost constant at a value of approx. 2 % from day 6 after the rainfall.

Then, artificial soil moisture profiles have been calculated for the layer-resolving radiative transfer model. The mean differences and the corresponding standard deviations resulting from Fig. 4.8 are constraints in the generation process. It has been assumed that the soil moisture profiles are of logarithmic shape

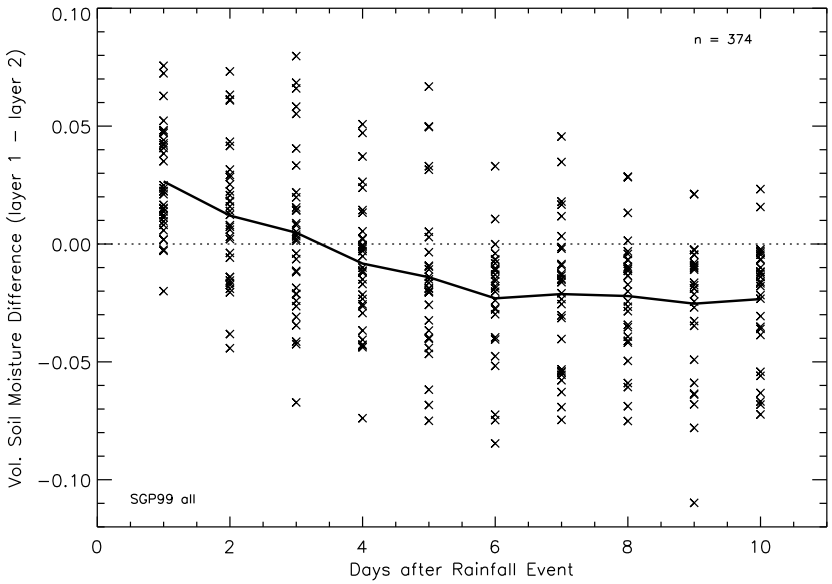


Figure 4.8: Differences between measurements of volumetric soil moisture in layer 1 (0–2.5 cm depth) and layer 2 (2.5–5 cm depth) as a function of the elapsed time since the rainfall event on the 10th of July 1999 for all available SGP99 sites. The line represents the mean.

(this choice is further commented at the end of this subsection) following

$$\theta(z) = a \ln(z + b) + c \tag{4.12}$$

where $\theta$ is the volumetric soil moisture and $z$ the soil depth. The parameters $a$, $b$, and $c$ determine the shape of the profile and are defined by the observation statistics: (1) The vertically integrated soil moisture of the artificial profile shall be equal to the soil moisture value of the uniform profile wich is given by the observed mean from the two different moisture sampling depths, i.e. $\theta_m = (\theta_{0-2.5\mathrm{cm}} + \theta_{2.5-5\mathrm{cm}})/2$. (2) The difference between the profile's soil moisture value $\theta_1$ at a depth of $z_1 = 1.25$ cm (centre of the upper observation layer) and $\theta_2$ at $z_2 = 3.75$ cm (centre of the lower observation layer) is determined by

$$\theta_1 - \theta_2 = \Delta_i + r\ \sigma_{\Delta_i} \tag{4.13}$$

where $\Delta$ is the mean soil moisture layer difference and $\sigma_\Delta$ the corresponding standard deviation for day $i$ as given by Fig. 4.8. $r$ is a random number (with Gaussian distribution) with zero mean and a standard deviation of 1. These

constraints lead to

$$a = (\theta_1 - \theta_2)/(\ln \frac{z_1 + b}{z_2 + b}) \tag{4.14}$$

and

$$c = \theta_m - \overline{a \ln(z + b)} \tag{4.15}$$

where the overbar denotes the vertical mean. The parameter $b$, which determines the magnitude of the vertical gradients in the profile, cannot be unambiguously fixed. In order to obtain soil moisture values in a realistic range, $b$ has been set to random values between 0.1 and 10 calculated by $b = 100^{r_{ed}}/10$ where $r_{ed}$ is a random number equally distributed between 0 and 1.

Figure 4.9 shows the soil moisture profiles generated for site LW03 for the 10 days following the rainfall event. Each of these profiles would match the 5 cm mean of the soil moisture measurements obtained at the particular date. It can be seen that just after the rainfall, profiles with a wet surface are dominating in number as expected, but that the variance illustrated by Fig. 4.9 also allows for profiles which are dryer at the surface than at deeper layers. During the following days without relevant precipitation the profiles on the whole move towards lower water contents, with the surface drying faster than the underlying soil. In the last six plots some artificial profiles with surface soil moisture values lower than zero have been removed. They also have not been included in the subsequent calculations.

It has to be noted that the assumption of a logarithmic-shaped profile most of the time does not match the real soil moisture distribution. Depending on the soil characteristics and on the history of precipitation events and drying periods, the shape of the profile can be very inhomogeneous with strong gradients (see e.g. Shutko et al., 1995; Dingman, 2002; Raju et al., 1995). However, this study does not focus on single events and the model soil moisture always represents a spatial mean of the grid boxex. Therefore, the assumption of logarithmic profiles as applied here is, on average, a reasonable first guess approximation which takes into account that the gradients at the surface are most of the time larger than in deeper layers.

### Soil temperature

Artificial temperature profiles were produced in a similar way (keeping in mind the comments of the preceding paragraph which, when replacing the history of precipitation events and drying periods with the history of heating and cooling conditions, hold for soil temperature profiles, too). The SGP99 temperature observations at depths of 1 cm and 5 cm from the 10 available sites were used as

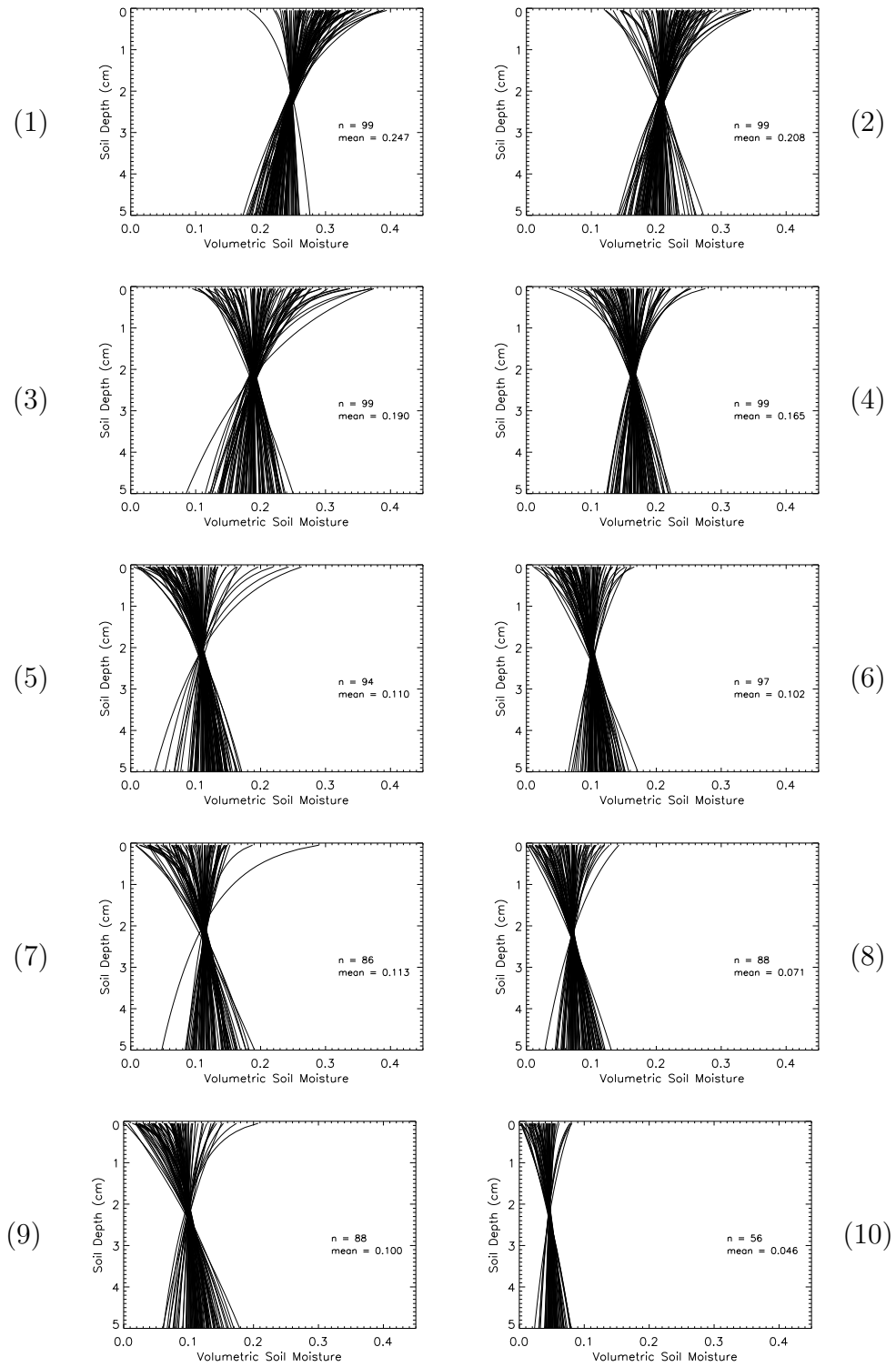


Figure 4.9: Ensembles of artificial near-surface soil moisture profiles generated for site LW03 under the constraints described in the text. (1) One day after rainfall (July 11), (2) two days after rainfall, etc.

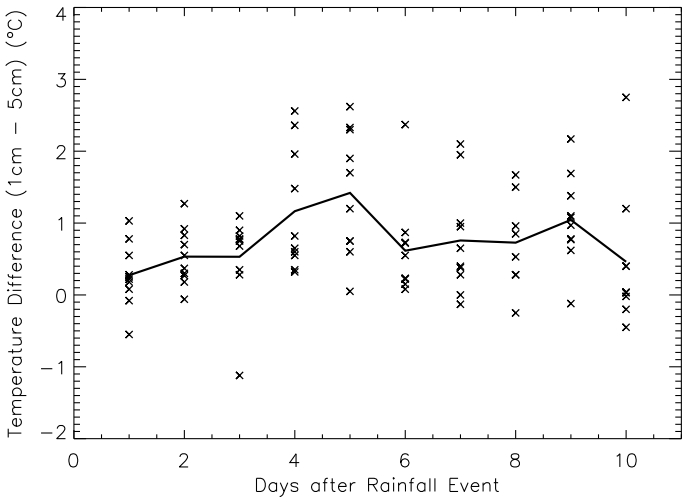


Figure 4.10: Differences between measurements of the soil temperature at 1 cm and 5 cm depth from ten SGP99 sites in the Little Washita watershed (no data from the Central Facility and the El Reno area available). The rainfall event occured at the 10th of July (denoted by 710).

constraints. Since no clear temporal dependency between the vertical gradient and the elapsed time after the rainfall event has been found (Fig. 4.10) and due to the limited number of available measurements, the temperature differences between 1 cm and 5 cm depth have been averaged over all days and sites. This results in a mean difference of 0.79 K; the corresponding standard deviation is 0.86 K. The reason for the positive systematic deviation of the 1 cm temperature from the 5 cm value is that measurements have been carried out in the morning hours when increasing solar insolation heats the surface.

Similar to the soil moisture profile, it has been assumed that the temperature profiles show a logarithmic shape (also see Raju et al., 1995) described by

$$T(z) = a_T \ln(z + b_T) + c_T \tag{4.16}$$

And following the same pattern as above we get

$$T_1 - T_2 = 0.79\,\mathrm{K} + r\ 0.86\,\mathrm{K} \tag{4.17}$$

$$a_T = (T_1 - T_2)/(\ln \frac{z_1 + b_T}{z_2 + b_T}) \tag{4.18}$$

and

$$c_T = T_m - \overline{a_T \ln(z + b_T)} \tag{4.19}$$

where $T_m$ is the mean of the observed temperatures from the depths of 1 cm and 5 cm. It was assumed that this value could best represent the temperature of the uppermost layer of the soil model. The only unknown parameter left is $b_T$. It was randomly set to values between 0.001 and 10 calculated with the formula $10000^{r_{ed}}/1000$ ($r_{ed}$ obtained as described in the previous section).

The resulting soil temperature profiles are presented in Fig. 4.11. In contrast to soil moisture, the ensembles look similar for each day, since the constraints for the profile gradients have been chosen to be independent of the date. Only the mean soil temperature noticeably varies as given by the observations.

### 4.3.2 Effects on modelled brightness temperature

The generated ensembles of soil moisure and temperature profiles have been used to simulate the corresponding L-band brightness temperatures. For the radiative transfer calculations, the top 5 cm of the soil have been represented by 50 layers of 1 mm depth in the LSMEM. This choice is based on sensitivity studies performed by Wilheit (1978) who showed that for soil moisture transition zones with thicknesses from $\lambda/100$ to $10\lambda$ — with $\lambda$ being the microwave wavelength (21.4 cm in this study) — 40 to 80 model layers are in most cases sufficient to achieve a brightness temperature accuracy of better than $\pm 0.5$ K.

Figure 4.12 shows that — based on the artificial profiles — a wide range of brightness temperatures could be observed for a given mean soil moisture value of the top 5 cm. For July 11 for instance, the modelled brightness temperatures range from 216 K to 236 K. After six days of dry-down (July 16), the values vary from 246 K to 274 K. The histograms on the whole clearly move towards higher brightness temperatures during the drying period which can only in part be attributed to the soil temperature (see top 5 cm soil temperatures in Fig. 4.11). The main contribution comes from the soil moisture decrease. It has to be emphasised that, although the effects of the soil moisture profiles on the observed brightness temperatures are significant, the brightness temperature probability density function of the first day after the rain event (July 11) and those of July 16 or later do not overlap. Therefore, the effect of rainfall on soil moisture is at least qualitatively observable with L-band, independent of the actual vertical distribution within the soil.

For each individual day the mean brightness temperature of the artificial ensemble (TBA) has been derived and compared with the corresponding brightness temperature calculated from the mean soil moisture value using the single layer radiative transfer model (TBU). Fig. 4.13 shows the mean differences between TBU and TBA for the experiment period. It can be seen that just after the

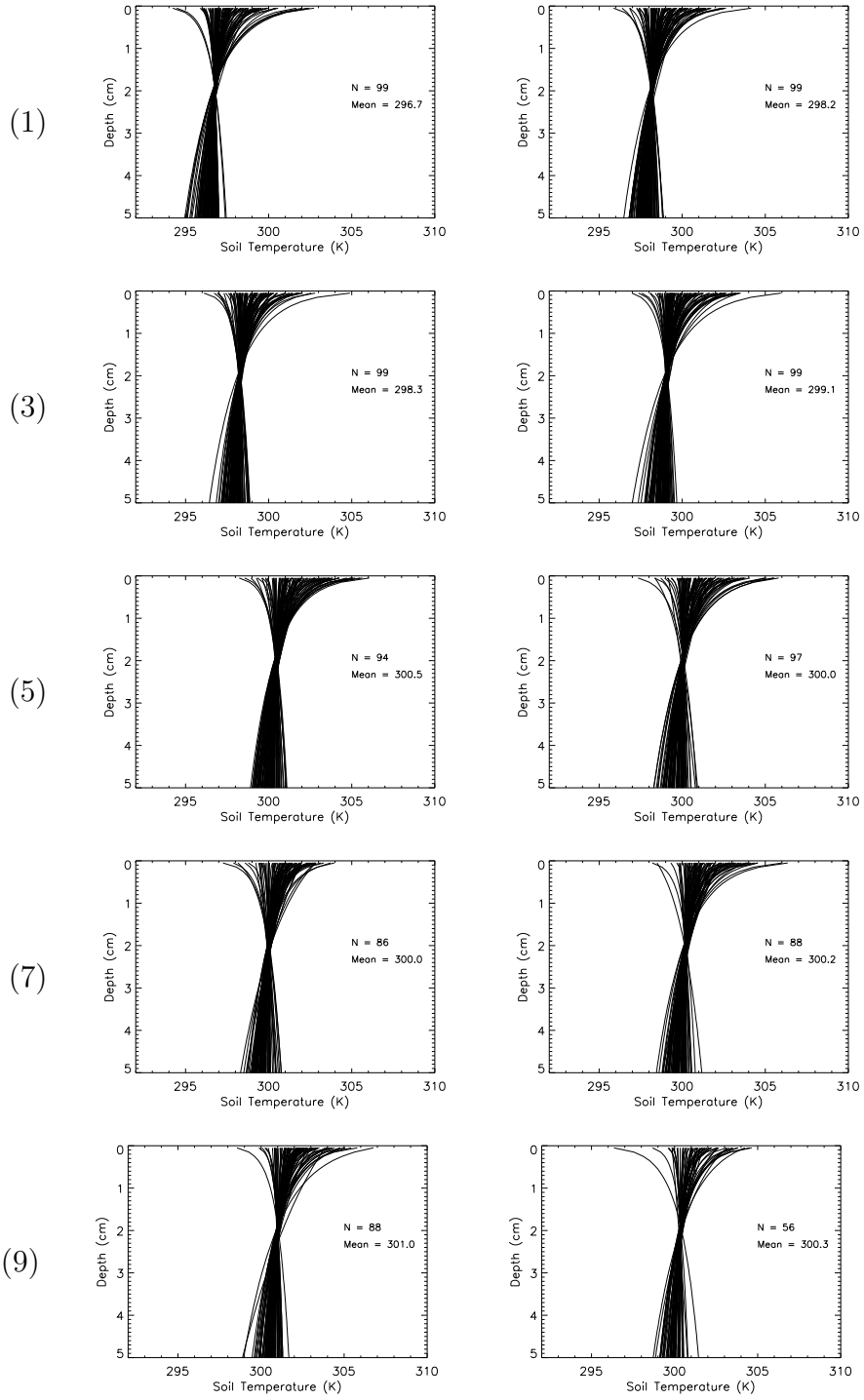


Figure 4.11: Ensembles of artificial near-surface soil temperature profiles generated for site LW03 under the constraints described in the text. (1) One day after rainfall (July 11), (2) two days after rainfall, etc.

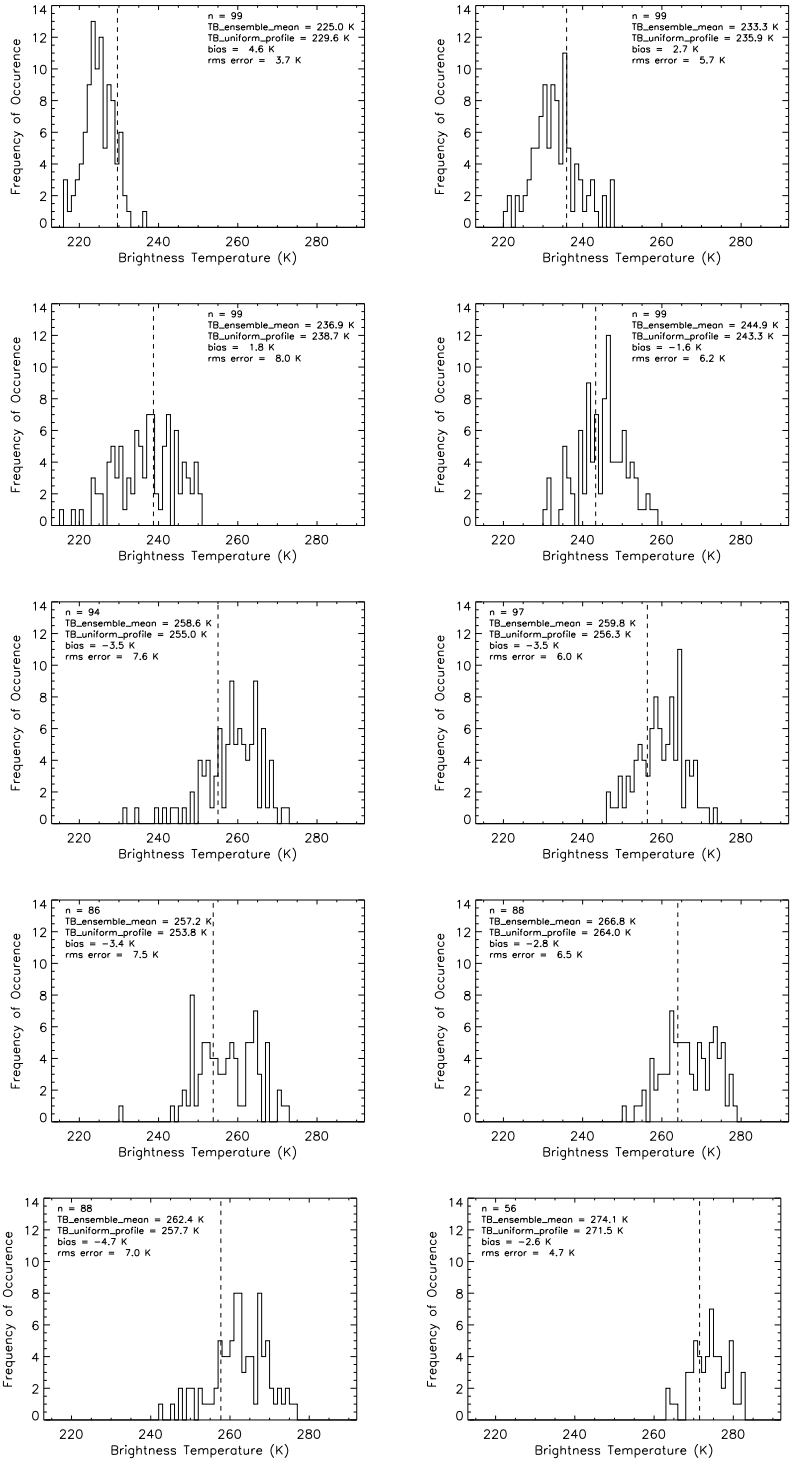


Figure 4.12: Frequency distributions of brightness temperature calculated from the soil moisture and temperature profile ensembles shown in Figs. 4.9 and 4.11. (1) One day after rainfall (July 11), (2) two days after rainfall, etc. The dashed line indicates the brightness temperature resulting from the uniform profile.

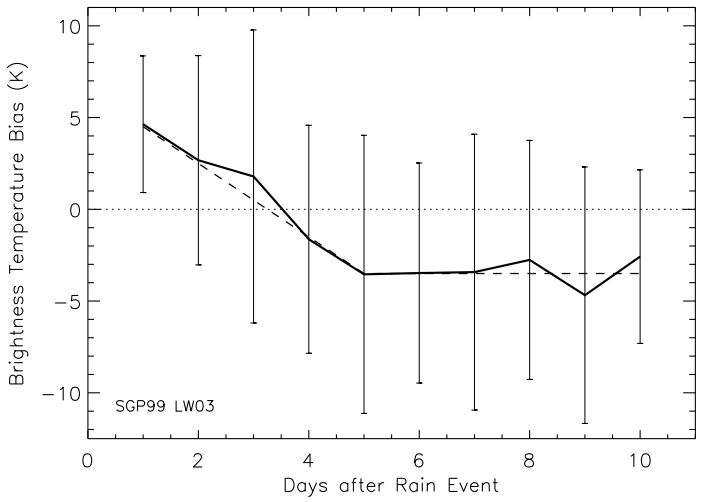


Figure 4.13: Mean difference between brightness temperatures calculated from uniform soil moisture and temperature profiles and brightness temperatures calculated from non-uniform soil moisture and temperature profiles (solid line). The error bars indicate the daily standard deviation of the differences. The dashed line shows the systematic error as it was used in the soil moisture analysis.

rain TBU is almost 5 K higher than TBA. This can be attributed to the fact that most profiles from the ensemble are characterised by wet surfaces (see Fig. 4.9). Therefore, the corresponding brightness temperature is lower than the one modelled with the uniform soil moisture profile. The following days the surface dries quicker than the soil below so that the absolute value of the systematic error between TBU and TBA decreases and becomes negative. After five days of dry down the difference remains nearly constant at values between - 3 and - 5 K. The rms deviation between the two brightness temperature simulation methods shows no significant dependency on the elapsed days after the rain event. Its daily value fluctuates between 3.7 and 8.0 K with an average of 6.3 K (see error bars in Fig. 4.13 or rms errors specified in the daily plots of Fig. 4.12).

At first sight, the relatively large error bars in Fig. 4.13 may lead to doubts about the significance of the relation found between the systematic brightness temperature error and the occurence of raining and drying periods. However, the uncertainties shown are the result of the underlying database which is a collection of sites from a large area with differing soil types and differing amounts of initial rainfall. Therefore, the error bars show the variance within the set of single sites. They would likely be significantly smaller if all sites would have had the same soil and vegetation characteristics and the same forcing. The fact that the relationship shown by Fig. 4.13 occurs despite of the large spatial heterogeneities

| | | Root zone soil moisture (vol. %) | Layer 1 soil moisture (vol. %) | Layer 2 soil moisture (vol. %) | Layer 3 soil moisture (vol. %) | Latent heat flux ($W/m^2$) | Sensible heat flux ($W/m^2$) |
|---|---|---|---|---|---|---|---|
| KTRB | Q | 1.16 | 1.61 | 1.54 | 1.25 | 18.1 | 20.0 |
| | PCB | 1.15 | 1.62 | 1.61 | 1.18 | 18.7 | 20.7 |
| KB | Q | 0.40 | 1.50 | 1.11 | 0.45 | 18.9 | 18.6 |
| | PCB | 0.34 | 1.46 | 1.05 | 0.42 | 17.5 | 18.1 |

Table 4.3: Bias-corrected rms errors of model soil moisture and surface fluxes (compared to observations) resulting from the assimilation experiments with (PCB) and without (Q) applying the systematic error correction of observed brightness temperatures due to the profile sensitivity study (KTRB and KB as supplied before).

rather confirms that a correction of brightness temperatures due to soil model resolution deficiencies is necessary. For that purpose, the curve in Fig. 4.13 has been smoothed as indicated by the dashed line.

### 4.3.3 Application of error corrections

The relationship between the systematic brightness temperature error and the days elapsed after the rain event has been derived from SGP99 data. A correction procedure is now applied for the SGP97 assimilation runs (using the depth-varying model errors determined in section 4.1). The daily precipitation amounts for the SGP97 period at site LW02 are shown in Fig. 4.1 (solid line within the top plot). There were six days with significant rainfall and another six days with minor rainfall which are classified as dry in the correction procedure. The observed brightness temperatures (see Fig. 3.2) have been adjusted according to the six rain events following the fitted curve outlined in Fig. 4.13. June 26 (day 177) was the only day when rain occured and a brightness temperature measurement existed. Since a correction for this case can not be derived from the available data shown in Fig. 4.13 (day equals 0), the observation of that day has not been corrected. The LW02 KTRB and KB assimilation runs have then been repeated applying the systematic error correction. These runs are denoted by PCB in the following, their results in comparison to the Q runs are listed in Tab. 4.3.

In the case of assimilating only brightness temperatures (KB), the systematic error correction leads to an improvement of modelled variables. This improvement is relatively small, but in contrast to previous experiences affects both soil moisture and turbulent fluxes. When using all three observation types (KTRB), there is not such a clear impact: the analysed layer 3 soil moisture tends to be closer to reality in the PCB than in the Q experiments while the accuracy of the modelled fluxes and of the upper two model layers is slightly reduced. It seems that the improved information content of the corrected brightness temperature observations (as indicated by the KB runs) still conflicts with the 2-metre temperature and humdity measurements. However, the results in the KB-runs are promising, and further additions to the simple correction scheme, for example by accounting for precipitation amount and soil type, may further reduce the errors.

## 4.4 Summary of the assimilation experiments

The results of all assimilation studies are summarised in Tab. 4.4 in terms of the bias-corrected rms error of soil moisture and surface fluxes. The table lists the outcome of the revised quantification of the model errors (Q), the pre-assimilation bias correction of observations based on the innovations biases (BCO), and the correction of brightness temperature observations based on the profile sensitivity study (PCB, including the revised model errors).

The overall picture can be described as follows: With quality-controlled forcing data and a close-to-reality model initialisation the SCM is able to reproduce the evolution of root zone soil moisture quite well (as already stated by Seuffert et al. (2004); also see top plot of Fig. 3.6). All assimilation runs — to a varying extent — deteriorate the modelled root zone soil moisture in comparison to the CTRL run while the turbulent surface fluxes are improved in most cases. Only in the BCO-KTR and BCO-KTRB analysis, the rms error of both fluxes and soil moisture increase. The assimilation of screen-level variables was expected to reduce the rms error of modelled fluxes since 2-metre temperature and humidity are in general directly linked to the sensible and latent heat transports under summer conditions like during the SGP experiments. However, also the use of microwave brightness temperatures has a positive effect on the simulated fluxes. In the reference setup, the KB run leads to flux improvements comparable to the KTR run. The smallest rms error was obtained from using all observation types (KTRB). When applying analysis system modifications as proposed by this thesis, the assimilation of brightness temperatures alone even provides better results

| | | Root zone soil moisture (vol. %) | Layer 1 soil moisture (vol. %) | Layer 2 soil moisture (vol. %) | Layer 3 soil moisture (vol. %) | Latent heat flux ($W/m^2$) | Sensible heat flux ($W/m^2$) |
|---|---|---|---|---|---|---|---|
| CTRL | | 0.19 | 1.80 | 0.89 | 0.38 | 21.9 | 23.0 |
| REF | KTR | 2.15 | 1.64 | 1.30 | 2.62 | 17.6 | 20.3 |
| | KTRB | 2.13 | 1.33 | 1.18 | 2.67 | 15.0 | 18.0 |
| | KB | 0.45 | 1.47 | 1.05 | 0.56 | 19.0 | 19.1 |
| Q | KTR | 1.14 | 2.15 | 1.56 | 1.14 | 20.8 | 22.5 |
| | KTRB | 1.16 | 1.61 | 1.54 | 1.25 | 18.1 | 20.0 |
| | KB | 0.40 | 1.50 | 1.11 | 0.45 | 18.9 | 18.6 |
| BCO | KTR | 1.39 | 1.98 | 0.85 | 1.72 | 24.1 | 26.2 |
| | KTRB | 1.57 | 1.73 | 0.89 | 1.98 | 23.4 | 25.3 |
| | KB | 0.24 | 1.68 | 0.93 | 0.40 | 21.9 | 22.4 |
| PCB | KTRB | 1.15 | 1.62 | 1.61 | 1.18 | 18.7 | 20.7 |
| | KB | 0.34 | 1.46 | 1.05 | 0.42 | 17.5 | 18.1 |

Table 4.4: Bias-corrected rms errors of model soil moisture and surface fluxes (compared to observations) in all assimilation experiments using observed precipitation and assimilating screen-level variables alone (KTR), brightness temperature alone (KB), or all observation types together (KTRB). [CTRL = no soil moisture analysis applied, REF = reference experiments according to Seuffert et al. (2004), Q = using the revised model errors according to the precipitation sensitivity study (Sec. 4.1), BCO = applying a correction of the assimilation variables based on the innovation biases found from the reference control run (Sec. 4.2), PCB = applying the systematic error correction of observed brightness temperatures based on the profile sensitivity study (including the revised model errors, Sec. 4.3)].

than the KTR (in all cases) and the KTRB runs (in almost all cases) for both soil moisture and fluxes.

The increased rms error of root zone soil moisture mainly relies on worse simulations in layer 2 and 3 whereas the rms error of layer 1 is reduced on average (although layer 1 values should be interpreted with care). Since this behavior results in better fluxes in most cases, the sensible and latent heat transports in the model are apparently mainly determined by the soil characteristics of the top 7-cm layer. The vertical water transport and the transpiration by the

vegetation seem to be of lesser importance in this study, although the model vegetation types which are chosen to represent the LW02 site are characterised by vertical root distributions with significant fractions for layer 2 and 3: for tall grass the root fractions are defined by 27, 37, 27, and 9 % from the top to the bottom layer; for interrupted forest the values are 19, 35, 36, and 10 %. In the light of the dominating impact of the surface layer on the model fluxes as found from the assimilation experiments, it is not surprising that the 1.4 GHz brightness temperature, which essentially depends on the near-surface soil moisture, has proven to be a helpful information source for enhancing the quality of the modelled turbulent fluxes. At the same time, in comparison to the assimilation of the screen-level variables the use of the brightness temperatures provides a better simulation of the soil moisture in the root zone as a whole. Consequently, when looking at both root zone soil moisture and turbulent fluxes the assimilation of brightness temperatures serves best, even when compared to the combined usage of all three observation types.

The net effects of each analysis system modification (i.e. the revised model error and the systematic-error corrections of observations) carried out in this thesis on the simulation of soil moisture and surface fluxes are summarised in Tab. 4.5. Negative values denote a reduction of the rms error and therefore an improved performance of the soil moisture analysis. Each modification reduces the bias-corrected rms error of the root zone soil moisture. At the same time, the simulation of the fluxes gets worse in most cases. Only the revised model error and the rain-event-based correction of the brightness temperature observations in combination with assimilating brightness temperature alone improve both root zone soil moisture and surface fluxes, although these changes are small. Table 4.5 also shows that, similar to the behavior described above, the fluxes seem to be correlated predominantly to the near-surface soil moisture while the deeper root zone soil moisture and the fluxes react contrarily to the analysis modifications applied.

The largest improvements in root zone soil moisture were obtained from using the soil-layer-dependent model error (setup Q in Tab. 4.5) in the KTR and KTRB runs instead of the vertically constant setting as in the reference runs. However, these improvements only rely on model layer 3 where the deterioration of the soil moisture simulation caused by the soil moisture analysis is significantly attenuated; the modelled soil moisture in the top two layers and also the turbulent fluxes get worse in comparison to the reference. The assimilation of brightness temperature alone is able to improve both root zone soil moisture and surface fluxes, but the changes are marginal in comparison to the KTR and KTRB runs. Therefore, a definite statement about which of the model error

| | | Root zone soil moisture (vol. %) | Layer 1 soil moisture (vol. %) | Layer 2 soil moisture (vol. %) | Layer 3 soil moisture (vol. %) | Latent heat flux ($W/m^2$) | Sensible heat flux ($W/m^2$) |
|---|---|---|---|---|---|---|---|
| Q | KTR | −1.01 | +0.51 | +0.26 | −1.48 | +3.2 | +2.2 |
| | KTRB | −0.97 | +0.28 | +0.36 | −1.42 | +3.1 | +0.9 |
| | KB | −0.05 | +0.03 | +0.06 | −0.11 | −0.1 | −0.5 |
| BCO | KTR | −0.76 | +0.34 | −0.45 | −0.90 | +6.5 | +5.9 |
| | KTRB | −0.56 | +0.40 | −0.29 | −0.69 | +8.4 | +7.3 |
| | KB | −0.21 | +0.21 | −0.12 | −0.16 | +2.9 | +3.3 |
| PCB | KTRB | −0.01 | +0.01 | +0.07 | −0.07 | +0.6 | +0.7 |
| | KB | −0.06 | −0.04 | −0.06 | −0.03 | −1.4 | −0.5 |

Table 4.5: Net changes of bias-corrected rms errors of model soil moisture and surface fluxes (compared to observations) resulting from each assimilation experiment using observed precipitation (for the acronyms see Tab. 4.4).

settings applied here is preferable can not be given. While atmospheric models primarily need correct heat flux simulations hydrologic applications rather rely on well-determined soil moisture values. Nevertheless, from the significant effects in the assimilation runs using screen-level variables the importance of a correct setting of the model error covariance matrix becomes clear. A further future consideration of radiation and wind speed forcing in a sensitivity study like the one performed with precipitation may prove helpful in this context.

The pre-assimilation correction of the screen-level and microwave observations based on the innovation biases (setup BCO) also shows positive net effects on root zone soil moisture especially for the runs where the screen-level variables are used (KTR and KTRB). Different from the effects of setup Q, not only the bias-corrected rms error of layer 3 but also of layer 2 is reduced. The net increase of the rms error of the surface flux simulations is higher, though, in the BCO runs than in the Q runs. However, when looking only on the state variable, which is soil moisture, accounting for biases from observations, forward operators and the model background by correcting for the innovations found from regular forecast runs is an appropriate and, in the sense of least-squares optimality, a necessary means to improve the quality of the model simulations.

The innovations resulting from the reference assimilation experiments were

found to have large contributions from a significant dry soil moisture bias in the top soil model layer during SGP97. Since SGP97 lasted only four weeks, it is unclear whether this state vector bias is a persistent systematic error of the soil model TESSEL or whether it is a specific characteristic of the SGP97 period. Therefore, the innovation values found from the SGP97 period can hardly be transfered to an operational long-term forecast system. If a persistent state vector bias does not exist or is removed by separate correction schemes, the results of the additional control run with observation-driven soil moisture and soil temperature values (Sec. 4.2.2) indicate that the screen-level forward operators are essentially unbiased so that only the brightness temperature innovations caused by the microwave forward operator LSMEM need to be taken into account. Further studies comprising a full annual cycle are necessary and will be carried out in the context of a subsequent project supported by the Deutsche Forschungsgemeinschaft (see outlook in Sec. 5).

In the profile sensitivity study (setup PCB) it was shown that the vertical distribution of the soil water content and the soil temperature can have a significant effect on the corresponding brightness temperature. A mean uncertainty of up to $\pm$ 5 K was found from the artificial profile ensembles. The magnitude and sign of the error depends on the history of precipitation events and drying periods. In case of assimilating only brightness temperatures, the positive effect of correcting observations due to the insufficient vertical resolution of the soil model has been proven (PCB-KB in Tab. 4.5); in the KTRB run, however, it is attenuated by the influence of the screen-level variables. In general, the benefits of applying such a simple correction scheme have been, although visible, comparitively small in the setup used here. A further refinement of the method, e.g. by accounting for the rain amounts and soil characteristics like texture might lead to more significant improvements.

Finally, Tab. 4.4 and 4.5 show that it is not possible with TESSEL to better adjust simulations of both root zone soil moisture and turbulent heat fluxes significantly closer to the observations at the same time, whatever assimilation setup is chosen. Independent of the apparently prevailing correlation between surface layer soil moisture and surface heat fluxes already described before, this behavior could hint to inconsistent observations or to deficiencies in the physics and parameterisations of the soil model (the Q-KTR run, for instance, improves the fluxes in comparison to the CTRL run although, at the same time, the soil moisture rms errors increase in all model layers (see Tab. 4.4)). However, the best compromise for site LW02 in summer seems to be to assimilate brightness temperature alone with applying the observation correction resulting from the profile sensitivity study and using the revised model error covariance matrix.

An additional correction of the brightness temperature observations, based on an innovation bias determined over a full annual cycle at least, would probably further improve the quality of the soil moisture analysis. In any case, the results show that passive microwave remote sensing can be a valuable information source for soil moisture analyses.

# Chapter 5

# Conclusions and Outlook

Passive microwave remote sensing has been identified as a suitable technology to monitor land surface soil moisture on scales used in current global numerical weather prediction models (10 – 50 km spatial resolution). Especially microwave observations below 5 GHz are able to penetrate the atmosphere (including clouds and rain) and, to a lesser degree, a vegetation canopy and can therefore deliver valuable information about the surface wetness. In the near future, space-borne 1.4 GHz microwave brightness temperatures will become available for the first time on a global scale through the Soil Moisture and Ocean Salinity (SMOS) mission. These new observations are expected to prove helpful in adjusting the soil moisture in hydrological models and numerical weather prediction systems, supplementing other proxy data sources like screen-level atmospheric variables, active microwave measurements, stream flow observations, infrared-derived heating rates, etc.

Due to the limited penetration depth of microwaves in soils, the technique of passive microwave remote sensing only provides information about the top centimetres of the soil whereas applications in hydrology and meteorology depend on the water distribution in the whole root zone. Therefore, brightness temperature observations have to be combined with a hydrological model that integrates their information content vertically, constrained by the model physics. The assimilation procedure relies on well-defined specifications of the model's and observation's uncertainties in order to optimally weight model background and measurements. This study has addressed different systematic and random errors affecting the soil moisture analysis of ECMWF's operational land surface model TESSEL when using L-band brightness temperature observations. For that purpose, the single-column assimilation experiments described in Seuffert et al. (2004) have been revisited with a set of modified error specifications and compared against the former assimilation runs. The types of errors discussed in

this thesis are:

- the uncertainty of the model's precipitation forcing (a random error source which can be integrated in the model error covariance matrix)
- biases caused by observations, forward operators, and the background state vector which degrade the optimality (and quality) of the soil moisture analysis (they can be assessed by the easy-to-determine innovation biases)
- the insufficient representation of the near-surface soil moisture and temperature profiles (which determine the brightness temperature value) in the soil model TESSEL (a systematic error which can be captured by correcting the brightness temperature observations).

At first, the effect of a revised model error covariance matrix has been investigated. The model error in the reference experiment described by Seuffert et al. (2004) was assumed to be 0.005 $m^3/m^3$ for each of the three root zone soil layers. An error propagation study with perturbed rainfall resulted in soil moisture uncertainties of 0.010 $m^3/m^3$ for the two top model layers and 0.0015 $m^3/m^3$ for the third layer. The impact of the modified model error is rather small when assimilating only brightness temperature (KB), but in the KTRB-setup (combined assimilation of screen-level variables and brightness temperatures) the revised model error covariance matrix leads to an improved description of analysed volumetric root zone soil moisture. The rms error was reduced by approximately 45 %. The accuracy of the analysed fluxes and of the surface and middle-layer soil moisture, however, decreases, but to a much lesser percentage. A reduced model error for the third layer gives the modelled first guess a larger weight and makes it more difficult for the screen-level variables to deteriorate root zone soil moisture for the correction of the surface fluxes. Although a preferred setting of the model error covariance matrix can not be given at the moment, it became clear that a correct definition is essential for a well-functioning analysis system.

Secondly, the innovations of the assimilation variables, i.e. the deviations of the measurements of 2-metre air temperature, 2-metre relative humidity and 1.4 GHz brightness temperature from their model equivalents, have been examined. Biases of +2.18 K for air temperature, −9.71 % for relative humidity and +9.55 K for brightness temperature have been found in the reference control run. The microwave bias can be attributed to deficiencies in the microwave radiative transfer model LSMEM, caused by uncertainties about some input parameters and imperfect parameterisations, but to a high degree also to the large dry bias of the model soil moisture in the surface layer during the SGP97 simulation period. At

the same time, this systematic state vector error contributes most to the innovation biases of the screen-level variables whereas their forward operators and the observations seem to be basically free of systematic errors. Forcing the model with observed soil moisture and soil temperatures to minimise the state vector bias reduces the innovation biases to +0.56 K for the 2-metre temperature and −0.27 % for the relative humidity. The resulting innovation bias of the brightness temperature indicates that the microwave forward operator as used in the SGP97 assimilation experiments causes a bias of −12.88 K. Since an accurate grid-box calibration of the LSMEM and TESSEL proved to be difficult and would not be feasible for every grid box in a large-scale model, a correction of measured brightness temperatures and screen-level variables by the innovation biases found from the reference run has been applied before they are assimilated into the model. This procedure is also necessary to maintain the optimality of the soil moisture analysis in the sense of the least-square estimation. As expected, the systematic corrections of the assimilation variables improve the analysis of the root zone soil moisture (compared to observations). The simulations of the surface heat fluxes, however, again do not benefit from that. In operational applications the observation correction can be easily realised to account for observation, forward operator and model background (soil moisture) biases in the soil moisture analysis. When the background soil moisture can be assumed to be bias-free over a longer period of time (e.g. a year) or when a serious background bias as occurring during SGP97 is captured by a separate correction procedure, the adjustment of the brightness temperature observations would be sufficient for a well-defined assimilation system (provided that systematic errors from screen-level observations and forward operators are negligible as generally assumed and supported by the results presented in this thesis).

The vertical distribution of surface soil moisture, its effects on the land surface microwave emissivity, and the implications on the data assimilation system is the third and main topic of this study. Based on SGP99 observations, realistic surface soil moisture and soil temperature profiles have been generated. It was found that the poor vertical near-surface resolution of current operational weather prediction models can introduce mean brightness temperature errors of ± 5 K. This model shortcoming could be corrected by upgrading the soil scheme with additional near-surface soil layers, but such a modification requires elaborate re-calibration and validation of the soil model. Therefore, a correction method in observation space has been presented, which depends on the time period between an observation and the antecedent rainfall event. The correction function has been derived from SGP99 observations and has been applied to the data assimilation experiment carried out for SGP97. For the KTRB experiments,

the correction scheme does not have a consistent impact but in the KB assimilation runs both soil moisture and the turbulent fluxes are more accurate when the correction scheme is applied. However, improvements are small yet, but this can probably be traced back to the simple approach which relies on observations averaged over a large area with partly very different initial rain amounts. A refinement of the correction scheme is expected to give a better representation of the local near surface infiltration and evapotranspiration. It would be possible to introduce more parameters, e.g. the amount of rainfall, soil texture, or vegetation characteristics, as additional constraints in the profile generation process. For a given area, this would reduce the variability in the profile ensemble and consequently results in a narrower brightness temperature distribution (compared to the data shown in Fig. 4.12).

Seuffert et al. (2004) showed that it was not possible in the ELDAS data assimilation system to obtain optimal soil moisture and optimal turbulent surface fluxes at the same time and for the entire period. The improved error description in the revised data assimilation runs described in this study could not overcome this problem. However, for hydrological applications screen-level variables are of limited use since (computationally expensive) coupled land-atmosphere models are required. The majority of hydrological data assimilation systems will probably be similar to the North American LDAS configuration comprising off-line land surface models (Mitchell et al., 2004). These data assimilation systems will benefit from the correction method presented in this study as the results from the KB runs clearly indicate. But even in weather prediction models, the results of the assimilation experiments indicate that the brightness temperature alone can provide better soil moisture and heat flux simulations than the use of 2-metre temperature and humidity, whether in combination with the microwave data or separately. At least, this can be said for a low-to-moderately vegetated land surface during summer conditions.

This study is restricted to a single location covering only four weeks in total and is additionally based on a very limited number of brightness temperature observations. Therefore, to gain a better insight into the error characteristics of a land data assimilation system that makes use of passive microwave data, it is essential to expand such studies like this to a longer period covering at least one year and to areas representing different land use conditions. The extension to a longer time frame is currently done at the Meteorological Institute of the University of Bonn in a project supported by the Deutsche Forschungsgemeinschaft (DFG). Assimilation studies are carried out for the same location in Oklahoma as used in this thesis. Brightness temperature measurements are obtained from the Tropical Rainfall Measuring Mission (TRMM) Microwave Imager (TMI) which

was launched in late 1997. This work will also address the different soil moisture statistics in model space (constrained by the wilting point and field capacity) and observation space (which usually shows higher amplitudes). Observation operators as presented by Drusch et al. (2005) will be applied. Furthermore, the differences in performance and feasibility of assimilating brightness temperatures directly or assimilating soil moisture retrievals derived offline from the brightness temperature observations will be investigated. In future studies, it has to be investigated if the extended Kalman filter, which requires more computing resources than the currently used optimal interpolation procedure, can be applied in an operational weather prediction environment. This work showed that microwave brightness temperatures can be of high value for adjusting soil moisture in hydrological and meteorological models and carried out a further step towards the assimilation of future L-band satellite observations.

# Bibliography


Ament, F. and C. Simmer, 2006: Improved representation of land-surface heterogeneity in a non-hydrostatic numerical weather prediction model. *Boundary Layer Meteorology*, **121**, 153–174.

Barrett, E. C. and D. Kniveton, 1995: Overland precipitation. *Passive Microwave Remote Sensing of Land-Atmosphere Interactions*, B. J. Choudhury, Y. H. Kerr, E. G. Njoku, and P. Pampaloni, eds., VSP International Science Publishers, 571–598.

Bouttier, F. and P. Courtier, 1999: Data assimilation concepts and methods. Lecture Note, ECMWF.

Bundesanstalt für Gewässerkunde, 2002: Das Augusthochwasser 2002 im Elbegebiet. Technical report, Bundesanstalt für Gewässerkunde, Koblenz, Germany, download version available at `http://elise.bafg.de/servlet/is/3967/`.

Calvet, J.-C., J. Noilhan, and P. Bessemoulin, 1998: Retrieving the root-zone soil moisture from surface soil moisture or temperature estimates: A feasibility study based on field measurements. *Journal of Applied Meteorology*, **37**, 371–386.

Choudhury, B. J., T. J. Schmugge, A. Chang, and R. W. Newton, 1979: Effect of surface roughness on the microwave emission from soils. *Journal of Geophysical Research*, **84**, 5699–5706.

Courtier, P., 1997: Variational methods. *Data Assimilation in Meteorology and Oceanography: Theory and Practice*, M. Ghil, K. Ide, A. Bennett, P. Courtier, M. Kimoto, M. Nagata, M. Saiki, and N. Sato, eds., Meteorological Society of Japan, 101–108.

Crow, W. T. and E. van Loon, 2006: Impact of incorrect model error assumptions on the sequential assimilation of remotely sensed surface soil moisture. *Journal of Hydrometeorology*, **7**, 421–432.

Crow, W. T. and E. F. Wood, 2003: The assimilation of remotely sensed soil brightness temperature imagery into a land surface model using Ensemble Kalman filtering: A case study based on ESTAR measurements during SGP97. *Advances in Water Resources*, **26**, 137–149.

Dee, D. P. and A. M. da Silva, 1998: Data assimilation in the presence of forecast bias. *Quarterly Journal of the Royal Meteorological Society*, **124**, 269–295.

Dingman, S. L., 2002: *Physical Hydrology*. Prentice-Hall, Inc., New Jersey, 2nd edition.

Dirmeyer, P. A., F. J. Zeng, A. Ducharne, J. C. Morrill, and R. D. Koster, 2000: The sensitivity of surface fluxes to soil water content in three land surface schemes. *Journal of Hydrometeorology*, **1**, 121–134.

Dobson, M. C., F. T. Ulaby, M. T. Hallikainen, and M. A. El-Rayes, 1985: Microwave dielectric behavior of wet soil — Part II: Dielectric mixing models. *IEEE Transactions on Geoscience and Remote Sensing*, **GE-23**, 35–46.

Douville, H., P. Viterbo, J.-F. Mahfouf, and A. C. M. Beljaars, 2000: Evaluation of the Optimal Interpolation and Nudging techniques for soil moisture analysis using FIFE data. *Monthly Weather Review*, **128**, 1733–1756.

Drusch, M., 1998: *Fernerkundung von Landoberflächen mit multispektralen Satellitendaten*. Ph.D. thesis, Meteorological Institute of the University of Bonn, Bonn, Germany.

Drusch, M. and P. Viterbo, 2006: Soil moisture analysis in ECMWF's Integrated Forecast System — Assimilation of screen level variables. *Submitted to Monthly Weather Review*.

Drusch, M., E. F. Wood, and H. Gao, 2005: Observation operators for the direct assimilation of TRMM microwave imager retrieved soil moisture. *Geophysical Research Letters*, **32**, L15403, doi:10.1029/2005GL023623.

Drusch, M., E. F. Wood, H. Gao, and A. Thiele, 2004: Soil moisture retrieval during the Southern Great Plains Hydrology Experiment 1999: A comparison between experimental remote sensing data and operational products. *Water Resources Research*, **40**, w02504, doi:10.1029/2003WR002441.

Drusch, M., E. F. Wood, and T. J. Jackson, 2001: Vegetative and atmospheric corrections for the soil moisture retrieval from passive microwave remote sensing data: Results from the Southern Great Plains Hydrology Experiment 1997. *Journal of Hydrometeorology*, **2**, 181–192.

ECMWF, 2001: *IFS Documentation — Cycle 23r4*. ECMWF, Reading, UK, download version available at `http://www.ecmwf.int/research/ifsdocs/`.

Entekhabi, D., E. Njoku, P. Houser, M. Spencer, T. Doiron, Y. Kim, J. Smith, R. Girard, S. Belair, W. Crow, T. Jackson, Y. Kerr, J. Kimball, R. Koster, K. McDonald, P. O'Neill, T. Pultz, S. Running, J. Shi, E. Wood, and J. van Zyl, 2004: The Hydrosphere State (HYDROS) mission: An Earth system pathfinder for global mapping of soil moisture and land freeze/thaw. *IEEE Transactions on Geoscience and Remote Sensing*, **42**, 2184–2195.

Gao, H., E. F. Wood, M. Drusch, W. Crow, and T. J. Jackson, 2004: Using a microwave emission model to estimate soil moisture from ESTAR observations during SGP99. *Journal of Hydrometeorology*, **5**, 49–63.

Gao, H., E. F. Wood, T. J. Jackson, M. Drusch, and R. Bindlish, 2006: Using TRMM/TMI to retrieve surface soil moisture over the southern United States from 1998 to 2002. *Journal of Hydrometeorology*, **7**, 23–38.

Garratt, J. R., 1992: *The atmospheric bounday layer*. Cambridge University Press, 316 pp.

Hartmann, D. L., 1994: *Global Physical Climatology*. Volume 56 of International Geophysics Series, Academic Press.

Hess, R., 2001: Assimilation of screen-level observations by variational soil moisture analysis. *Meteorology and Atmospheric Physics*, **77**, 145–154.

Hollinger, J. P., R. C. Lo, G. A. Poe, R. Savage, and J. L. Peirce, 1987: Special Sensor Microwave/Imager user's guide. Technical report, Naval Research Laboratory, Washington, D.C., 120 pp.

Jackson, T. J., D. M. Le Vine, A. Y. Hsu, A. Oldak, P. J. Starks, C. T. Swift, J. D. Isham, and M. Haken, 1999: Soil moisture mapping at regional scales using microwave radiometry: The Southern Great Plains Hydrology Experiment. *IEEE Transactions on Geoscience and Remote Sensing*, **37**, 2136–2151.

Jones, A. S., I. C. Guch, and T. H. Vonder Haar, 1998a: Data assimilation of satellite-derived heating rates as proxy surface wetness data into a regional atmospheric mesoscale model. Part I: Methodology. *Monthly Weather Review*, **126**, 634–645.

— 1998b: Data assimilation of satellite-derived heating rates as proxy surface wetness data into a regional atmospheric mesoscale model. Part II: A case study. *Monthly Weather Review*, **126**, 646–667.

Jung, T. and A. Tompkins, 2003: Systematic errors in the ECMWF forecasting system. Technical Memorandum 422, European Centre for Medium-Range Weather Forecasts.

Kawanishi, T., T. Sezai, Y. Ito, K. Imaoka, T. Takeshima, Y. Ishido, A. Shibata, M. Miura, H. Inahata, and R. W. Spencer, 2003: The Advanced Microwave Scanning Radiometer for the Earth Observing System (AMSR-E), NASDA's contribution to the EOS for global energy and water cycle studies. *IEEE Transactions on Geoscience and Remote Sensing*, **41**, 184–194.

Kerr, Y. H. and E. G. Njoku, 1990: A semiempirical model for interpreting microwave emission from semiarid land surfaces as seen from space. *IEEE Transactions on Geoscience and Remote Sensing*, **28**, 384–393.

Kerr, Y. H., P. Waldteufel, J.-P. Wigneron, J.-M. Martinuzzi, J. Font, and M. Berger, 2001: Soil moisture retrieval from space: The Soil Moisture and Ocean Salinity (SMOS) mission. *IEEE Transactions on Geoscience and Remote Sensing*, **39**, 1729–1735.

Kirdyashev, K. P., A. A. Chukhlantsev, and A. M. Shutko, 1979: Microwave radiation of the earth's surface in the presence of a vegetation cover. *Radio Engineering and Electronic Physics*, **24**, 37–44.

Kummerow, C., W. Barnes, T. Kozu, J. Shiue, and J. Simpson, 1998: The Tropical Rainfall Measuring Mission (TRMM) sensor package. *Journal of Atmospheric and Oceanic Technology*, **15**, 809–817.

Liebe, H. J., 1989: MPM — an atmospheric millimeter-wave propagation model. *International Journal of Infrared and Millimeter Waves*, **10**, 631–650.

Mahfouf, J.-F., 1991: Analysis of soil moisture from near-surface parameters: A feasibility study. *Journal of Applied Meteorology*, **30**, 1534–1547.

Margulis, S. A., D. McLaughlin, D. Entekhabi, and S. Dunne, 2002: Land data assimilation and estimation of soil moisture using measurements from the Southern Great Plains 1997 Field Experiment. *Water Resources Research*, **38**, 1299, doi:10.1029/2001WR001114.

Meyers, T. P., 2001: A comparison of summertime water and $CO_2$ fluxes over rangeland for well watered and drought conditions. *Agricultural and Forest Meteorology*, **106**, 205–214.

Mitchell, K. E., D. Lohmann, P. R. Houser, E. F. Wood, J. C. Schaake, A. Robock, B. A. Cosgrove, J. Sheffield, Q. Duan, L. Luo, R. W. Higgins, R. T. Pinker, J. D. Tarpley, D. P. Lettenmaier, C. H. Marshall, J. K. Entin, M. Pan, W. Shi, V. Koren, J. Meng, B. H. Ramsey, and A. A. Bailey, 2004: The multi-institution North American Land Data Assimilation System (NLDAS): Utilizing multiple GCIP products and partners in a continental distributed hydrological modeling system. *Journal of Geophysical Research*, **109**, d07S90, doi:10.1029/2003JD003823.

Njoku, E. G. and D. Entekhabi, 1996: Passive microwave remote sensing of soil moisture. *Journal of Hydrology*, **184**, 101–129.

Oki, T., 1999: The global water cycle. *Global Energy and Water Cycles*, K. A. Browning and R. J. Gurney, eds., Cambridge University Press, 10–27.

Peixoto, J. P. and A. H. Oort, 1992: *Physics of Climate*. Springer-Verlag, New York, 520 pp.

Raju, S., A. Chanzy, J.-P. Wigneron, J.-C. Calvet, Y. Kerr, and L. Laguerre, 1995: Soil moisture and temperature profile effects on microwave emission at low frequencies. *Remote Sensing Environment*, **54**, 85–97.

Reece, C. F., 1996: Evaluation of a line heat dissipation sensor for measuring soil matric potential. *Soil Science Society of America Journal*, **60**, 1022–1028.

Reichle, R. H. and R. D. Koster, 2005: Global assimilation of satellite soil moisture retrievals into the NASA catchment land surface model. *Geophysical Research Letters*, **32**, l02404, doi:10.1029/2004GL021700.

Richter, H., A. W. Western, and F. H. S. Chiew, 2004: The effect of soil and vegetation parameters in the ECMWF land surface scheme. *Journal of Hydrometeorology*, **5**.

Robinson, D. A., K. F. Dewey, and R. R. Heim Jr., 1993: Global snow cover monitoring: An update. *Bulletin of the American Meteorological Society*, **74**, 1689–1696.

Rossow, W. B. and R. A. Schiffer, 1999: Advances in understanding clouds from ISCCP. *Bulletin of the American Meteorological Society*, **80**, 2261–2287.

Schär, C., D. Lüthi, U. Beyerle, and E. Heise, 1999: The soil-precipitation feedback: A process study with a regional climate model. *Journal of Climate*, **12**, 722–741.

Seuffert, G., P. Gross, C. Simmer, and E. F. Wood, 2002: The influence of hydrologic modeling on the predicted local weather: Two-way coupling of a mesoscale weather prediction model and a land surface hydrologic model. *Journal of Hydrometeorology*, **3**, 505–523.

Seuffert, G., H. Wilker, P. Viterbo, M. Drusch, and J.-F. Mahfouf, 2004: The usage of screen-level parameters and microwave brightness temperature for soil moisture analysis. *Journal of Hydrometeorology*, **5**, 516–531.

Seuffert, G., H. Wilker, P. Viterbo, J.-F. Mahfouf, M. Drusch, and J.-C. Calvet, 2003: Soil moisture analysis combining screen-level parameters and microwave brightness temperature: A test with field data. *Geophysical Research Letters*, **30**, 1498, doi:10.1029/2003GL017128.

SGP97 Experiment Plan, 1997: *Southern Great Plains 1997 (SGP97) Hydrology Experiment Plan*. `http://hydrolab.arsusda.gov/sgp97/documents.html`.

SGP99 Experiment Plan, 1999: *Southern Great Plains 1999 (SGP97) Experiment Plan*. `http://hydrolab.arsusda.gov/sgp99/sgp99b.htm`.

Shutko, A. M., E. A. Reutov, and S. P. Golovachev, 1995: Estimation of soil moisture profiles and root zone moisture content by means of microwave radiometry and *a priori* information. *Passive Microwave Remote Sensing of Land-Atmosphere Interactions*, B. J. Choudhury, Y. H. Kerr, E. G. Njoku, and P. Pampaloni, eds., VSP, Utrecht, The Netherlands, 461–474.

Talagrand, O., 1997: Assimilation of observations, an introduction. *Data Assimilation in Meteorology and Oceanography: Theory and Practice*, M. Ghil, K. Ide, A. Bennett, P. Courtier, M. Kimoto, M. Nagata, M. Saiki, and N. Sato, eds., Meteorological Society of Japan, 81–99.

Ulaby, F., R. Moore, and A. Fung, 1981: *Microwave Remote Sensing: Active and Passive – Volume I: Microwave Remote Sensing Fundamentals and Radiometry*. Artech House, Norwood, Michigan, 456 pp.

— 1982: *Microwave Remote Sensing: Active and Passive – Volume II: Radar Remote Sensing and Surface Scattering and Emission Theory*. Artech House, Norwood, Michigan, 608 pp.

— 1986: *Microwave Remote Sensing: Active and Passive – Volume III: From Theory to Applications*. Artech House, Norwood, Michigan, 1098 pp.

Uppala, S. M., P. W. Kållberg, A. J. Simmons, U. Andrae, V. Da Costa Bechtold, M. Fiorino, J. K. Gibson, J. Haseler, A. Hernandez, G. A. Kelly, X. Li, K. Onogi, S. Saarinen, N. Sokka, et al., 2005: The ERA-40 re-analysis. *Quarterly Journal of the Royal Meteorological Society*, **131**, 2961–3012.

van den Hurk, B. J. J. M., P. Viterbo, A. C. M. Beljaars, and A. K. Betts, 2000: Offline validation of the ERA40 surface scheme. Technical Memorandum 295, European Centre for Medium-Range Weather Forecasts, Reading, UK.

van Genuchten, M. T., 1980: A closed-form equation for predicting the hydraulic conductivity of unsaturated soils. *Soil Science Society of America Journal*, **44**, 892–898.

Wang, J. R. and B. J. Choudhury, 1981: Remote sensing of soil moisture content over bare field at 1.4 GHz frequency. *Journal of Geophysical Research*, **86**, 5277–5282.

Wegmüller, U. and C. Mätzler, 1999: Rough bare soil reflectivity model. *IEEE Transactions on Geoscience and Remote Sensing*, **37**, 1391–1395.

Wegmüller, U., C. Mätzler, and E. G. Njoku, 1995: Canopy opacity models. *Passive Microwave Remote Sensing of Land-Atmosphere Interactions*, B. J. Choudhury, Y. H. Kerr, E. G. Njoku, and P. Pampaloni, eds., VSP International Science Publishers, 375–387.

Wilheit, T. T., Jr., 1978: Radiative transfer in a plane stratified dielectric. *IEEE Transactions on Geoscience Electronics*, **GE-16**, 138–143.

# Appendix A

# Overview of LSMEM input data

- General radiation parameters:
  - Microwave frequency
  - Incidence angle (or viewing angle)
- Soil characteristics:
  - Soil temperature (optional: soil temperature profile)
  - Soil water content (optional: profile of soil water content)
  - Soil water salinity (of minor importance)
  - Soil texture (i.e. sand and clay fraction)
  - Soil porosity (i.e. bulk and specific soil density (of minor importance))
  - Roughness height of the soil surface (i.e. $h$-parameter or standard deviation of surface height)
- Vegetation characteristics:
  - Vegetation coverage
  - Vegetation temperature
  - Vegetation water content
  - Vegetation structure coefficient
  - Salinity of the vegetation water (of minor importance)
  - Single-scattering albedo
  - Optional: dry matter fraction of vegetation (of minor importance at L-band)

  - Optional: leaf thickness (of minor importance at L-band)

- Atmospheric characteristics:
  - Air temperature profile
  - Relative humidity profile
  - Air pressure profile

# Appendix B

# Time series of assimilation runs

On the following pages, the modelled daily means of 2m temperature, 2m relative humidity, brightness temperature, soil moisture, soil temperature, and surface heat fluxes as well as the daytime evaporative fraction from all SGP97 assimilation runs addressed in this thesis are shown in comparison to the corresponding observations. The respective results are presented for four different assimilation procedures: no assimilations, assimilation of 2-metre temperature and relative humidity alone, of microwave brightness temperature alone, and of all three observation types together. The different assimilation system setups applied are:

1. Reference assimilation runs according to Seuffert et al. (2004) (Sec. 3.3).
2. Application of the modified model error covariance matrix with depth-varying model errors due to the error propagation experiment based on perturbed precipitation amounts (Sec. 4.1).
3. As setup 1. but with precipitation set to zero.
4. Application of the modified model error covariance matrix in the zero-precipitation setup (Sec. 4.1).
5. Pre-assimilation correction of observations by the innovation biases found from the reference control run (Sec. 4.2).
6. Pre-assimilation correction of observed brightness temperatures depending on the occurence of rain due to the profile sensitivity study (using the modified model error; Sec. 4.3).

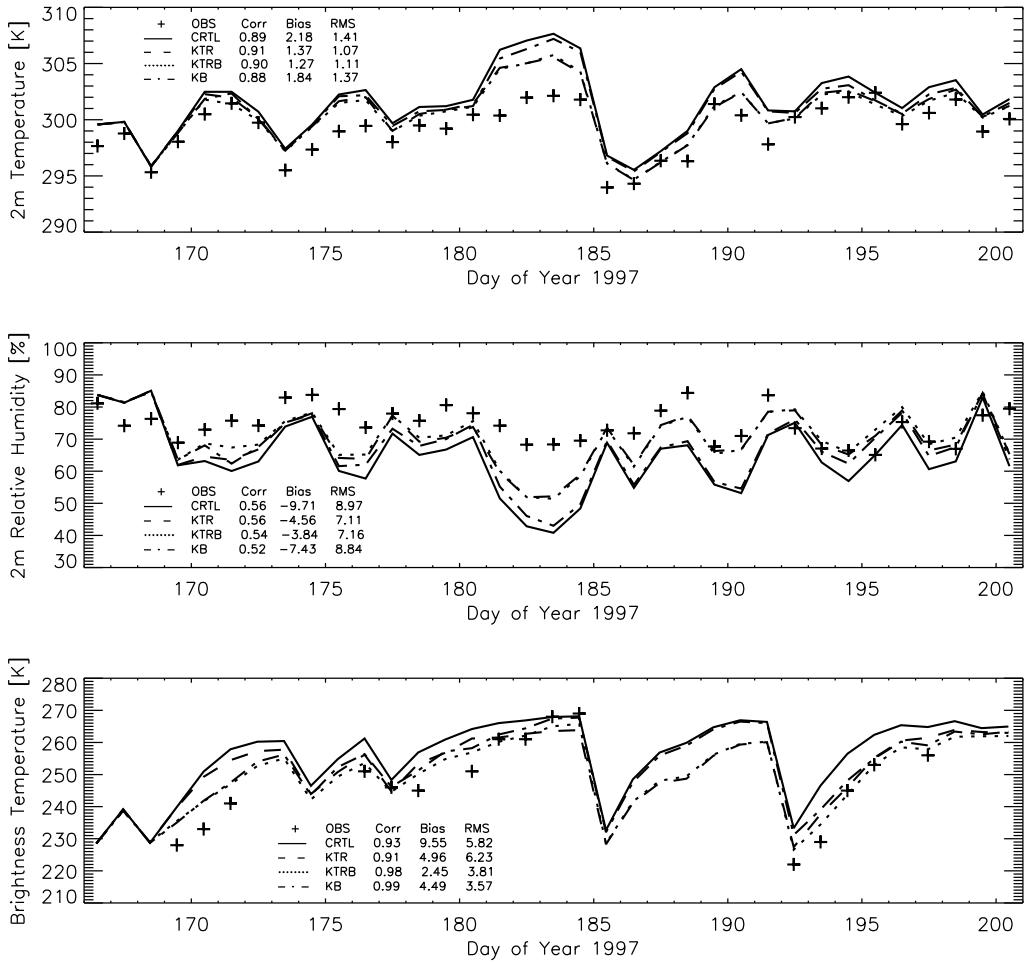


Figure B.1a: Daily means of observed and modelled 2m temperature, relative humidity and microwave brightness temperature from 15 June to 20 July 1997 in the reference data assimilation runs. The plus signs stand for observations [OBS] (brightness temperature observations are from about 11 LST only); lines denote results from model runs (solid = no assimilation [CTRL], dashed = assimilation of 2m temperature and relative humidity alone [KTR], dash-dotted = assimilation of brightness temperature alone [KB], dotted = assimilation of all observation types together [KTRB]). Specified statistic quantities are correlation coefficient [Corr], bias [Bias] and bias-corrected root-mean-square error [RMS] of the modelled variables with respect to the observed values.

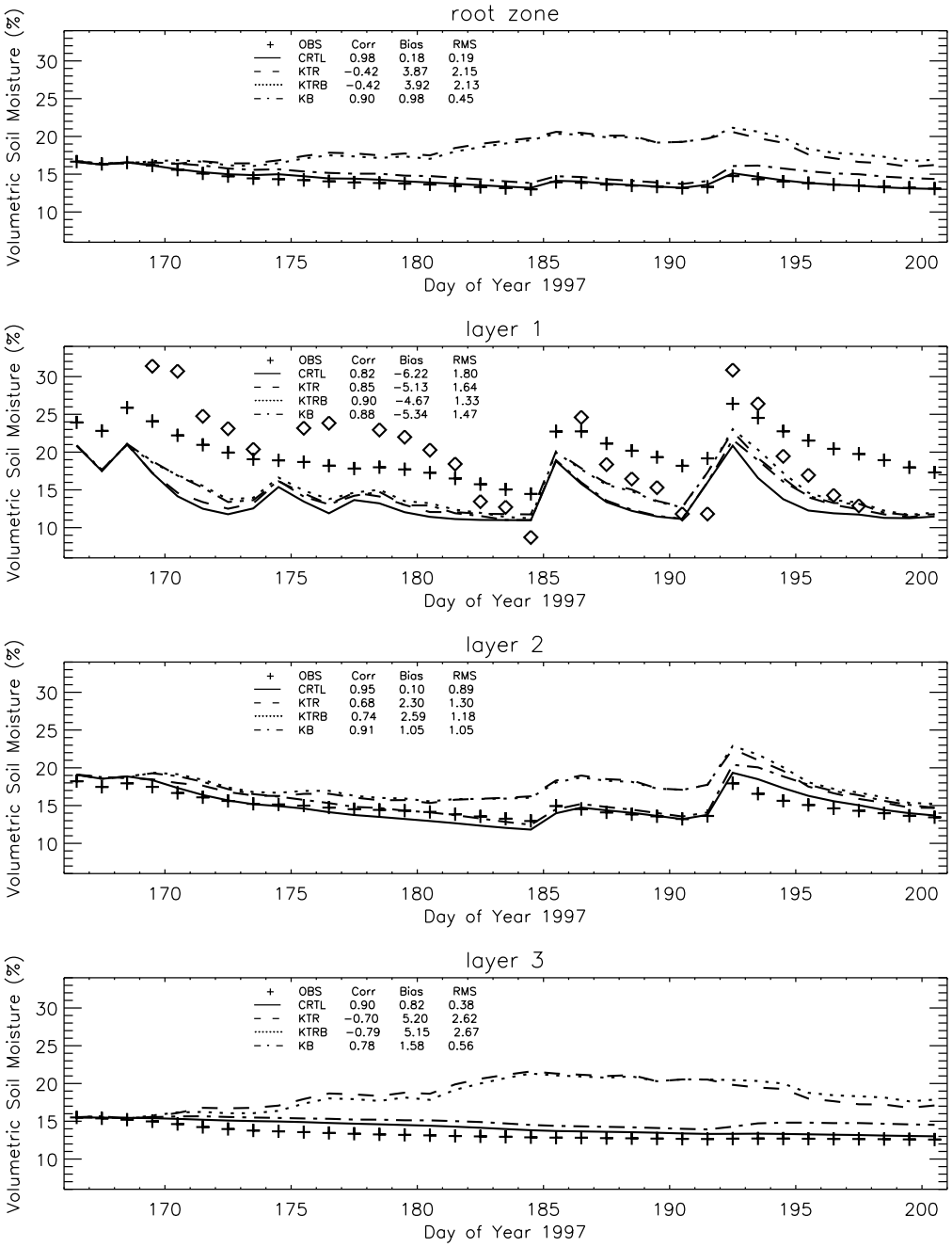


Figure B.1b: Daily means of observed and modelled soil moisture in the root zone and in the single root zone layers from 15 June to 20 July 1997 in the reference data assimilation runs. Plus signs denote SHAWMS observations: values from a depth of 5 cm are chosen to represent model layer 1; the mean from 10, 15, 20 and 25 cm corresponds to layer 2; the 60-cm measurement stands for layer 3. The diamonds represent water contents derived from the gravimetric probes whenever available (not used for calculation of error statistics). For the meaning of the lines and the statistic data see Fig. B.1a.

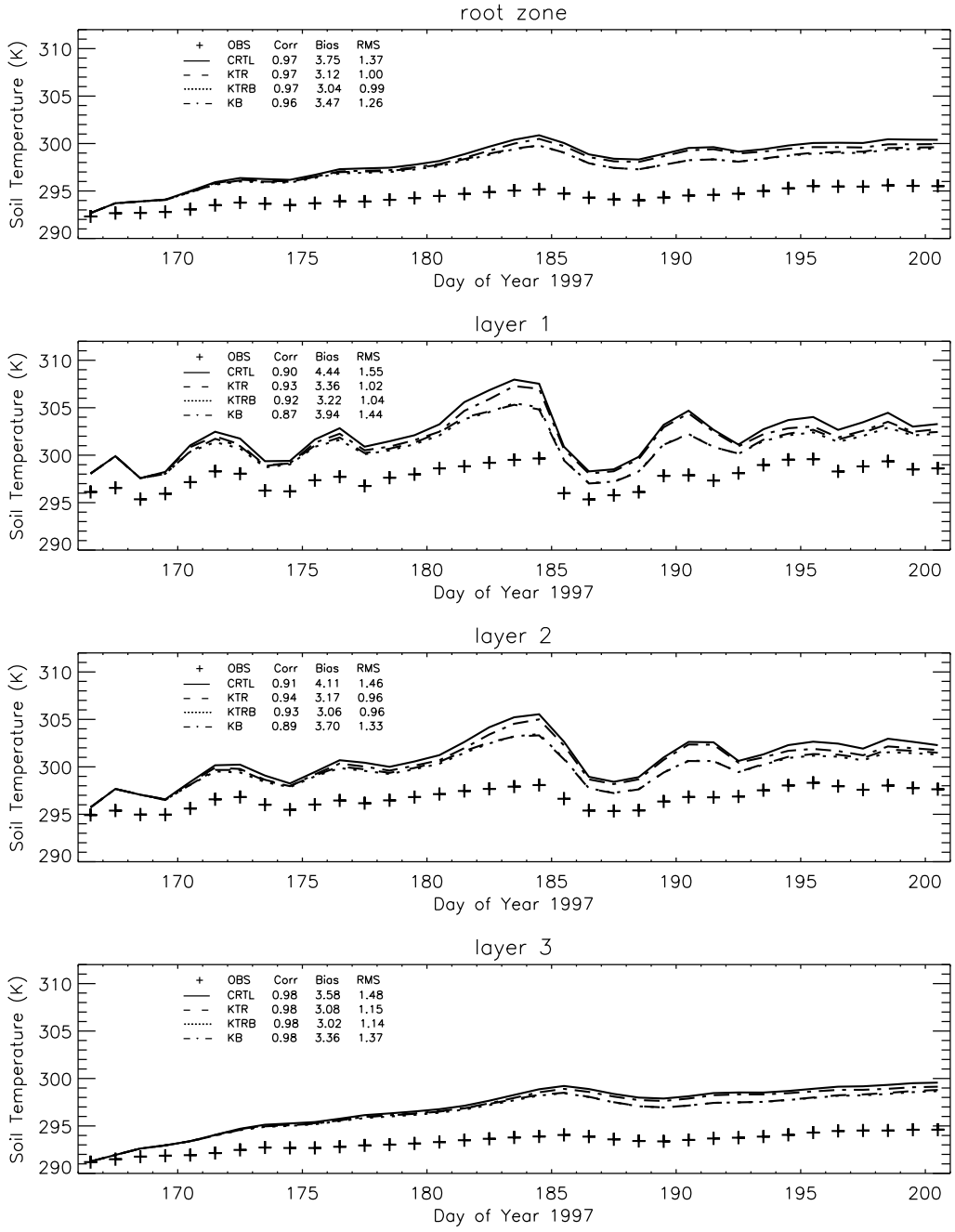


Figure B.1c: Daily means of observed and modelled soil temperature in the root zone and in the single root zone layers from 15 June to 20 July 1997 in the reference data assimilation runs. Plus signs denote measurements from the NOAA/ATDD station: the mean of the values from depths of 2 and 4 cm are chosen to represent model layer 1; the measurement from a depth of 16 cm corresponds to layer 2; the 64-cm measurement stands for layer 3. For the meaning of the lines and the statistic data see Fig. B.1a.

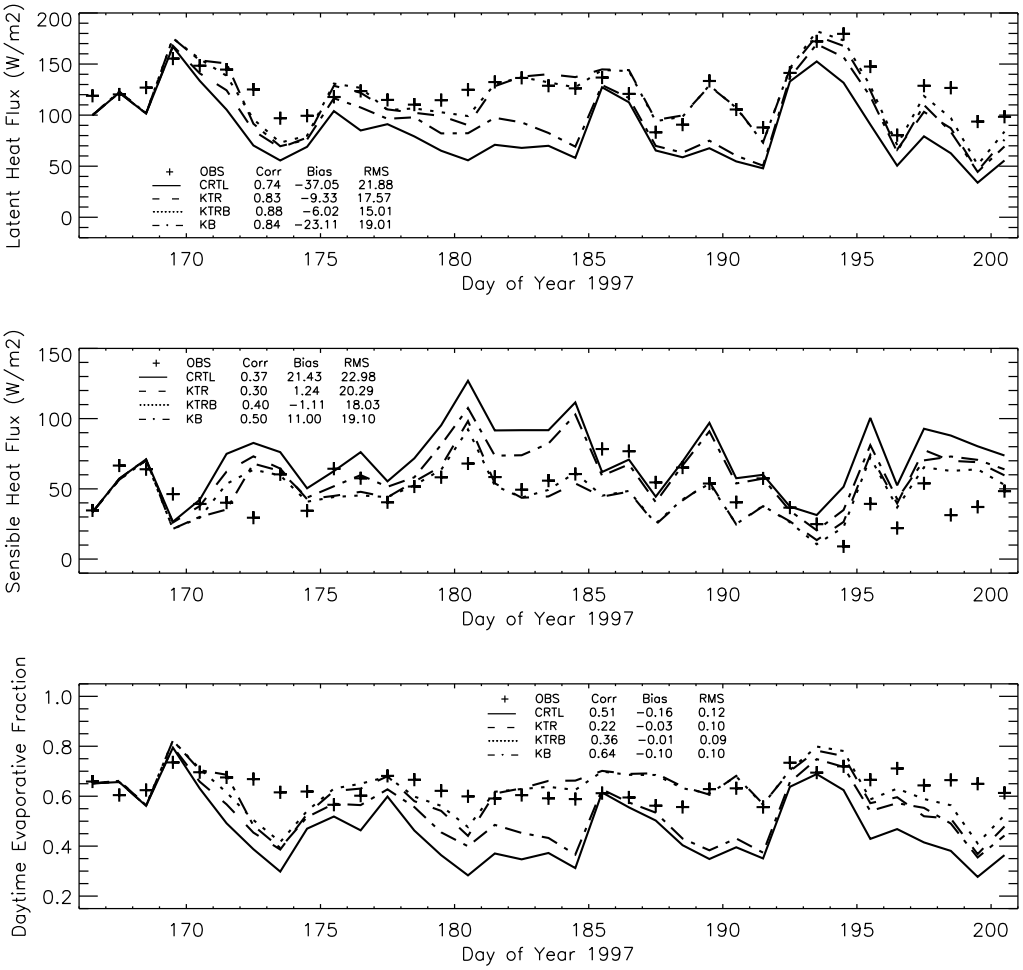


Figure B.1d: Daily means of observed and modelled latent heat and sensible heat flux and daytime mean of observed and modelled evaporative fraction from 15 June to 20 July 1997 in the reference data assimilation runs. For the meaning of the lines and the statistic data see Fig. B.1a.

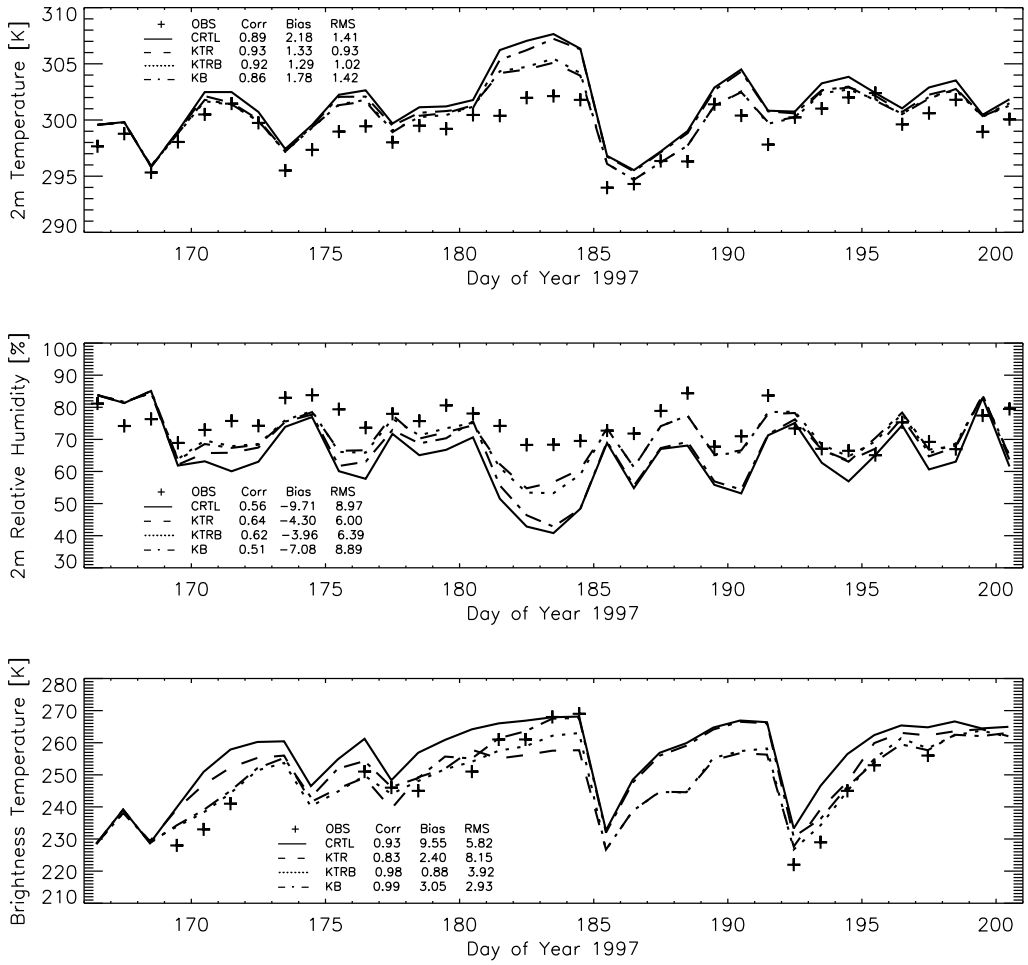


Figure B.2a: Simulations with modified, depth-varying model errors (everything else as in Fig. B.1a).

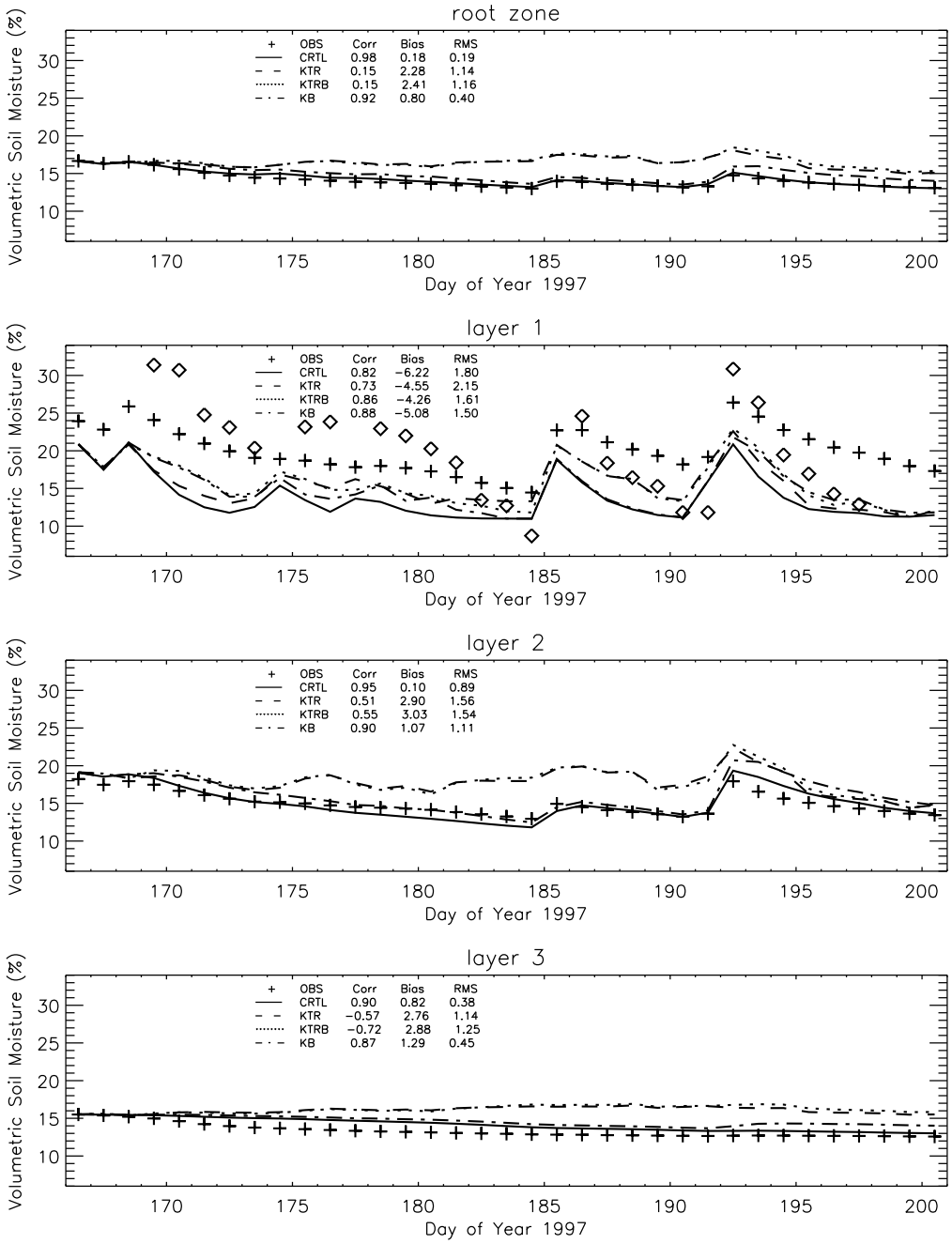


Figure B.2b: Simulations with modified, depth-varying model errors (everything else as in Fig. B.1b).

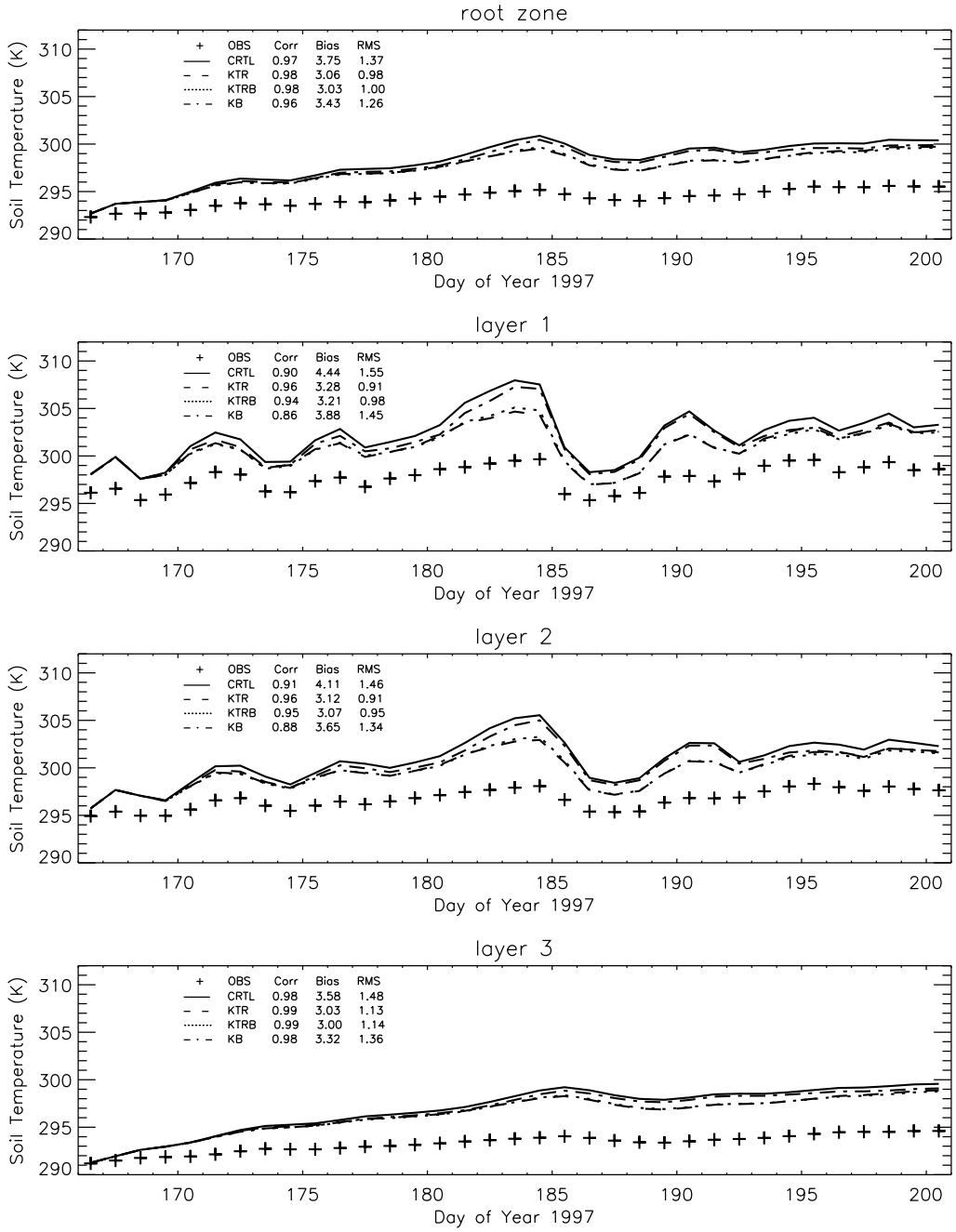


Figure B.2c: Simulations with modified, depth-varying model errors (everything else as in Fig. B.1c).

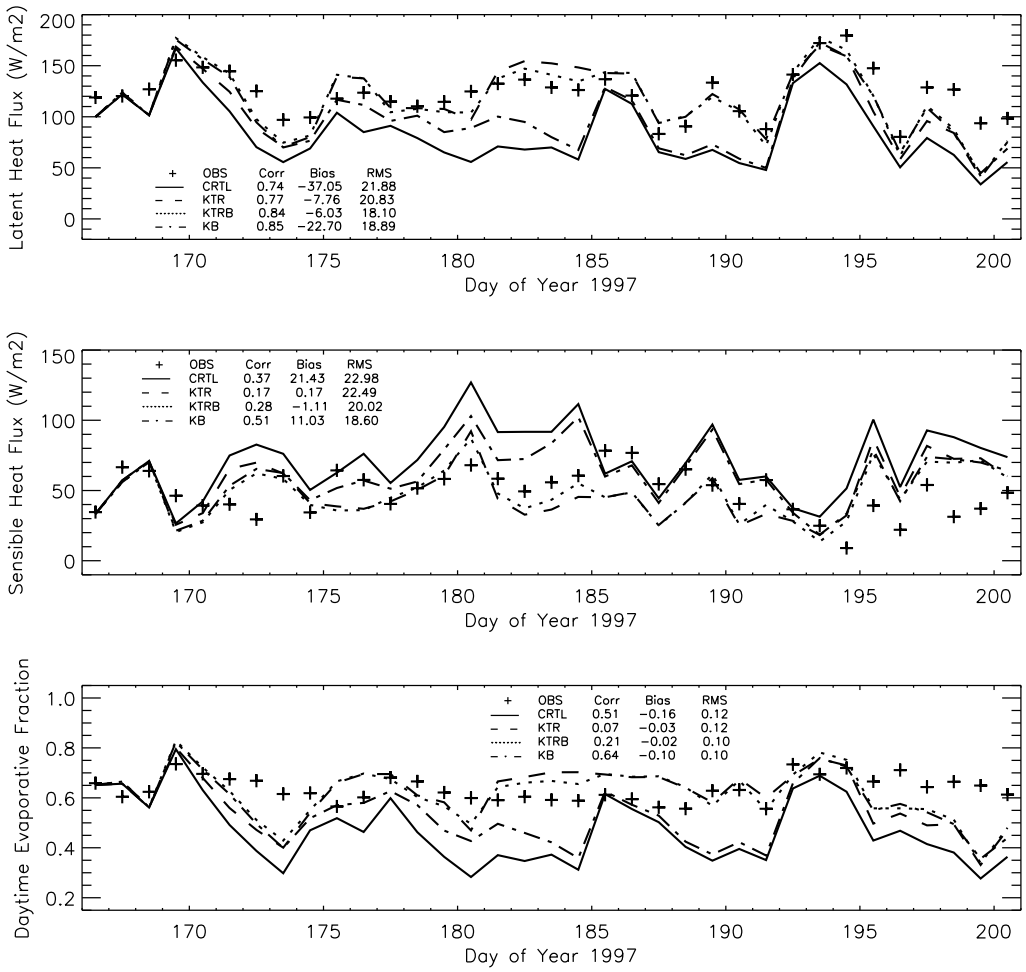


Figure B.2d: Simulations with modified, depth-varying model errors (everything else as in Fig. B.1d).

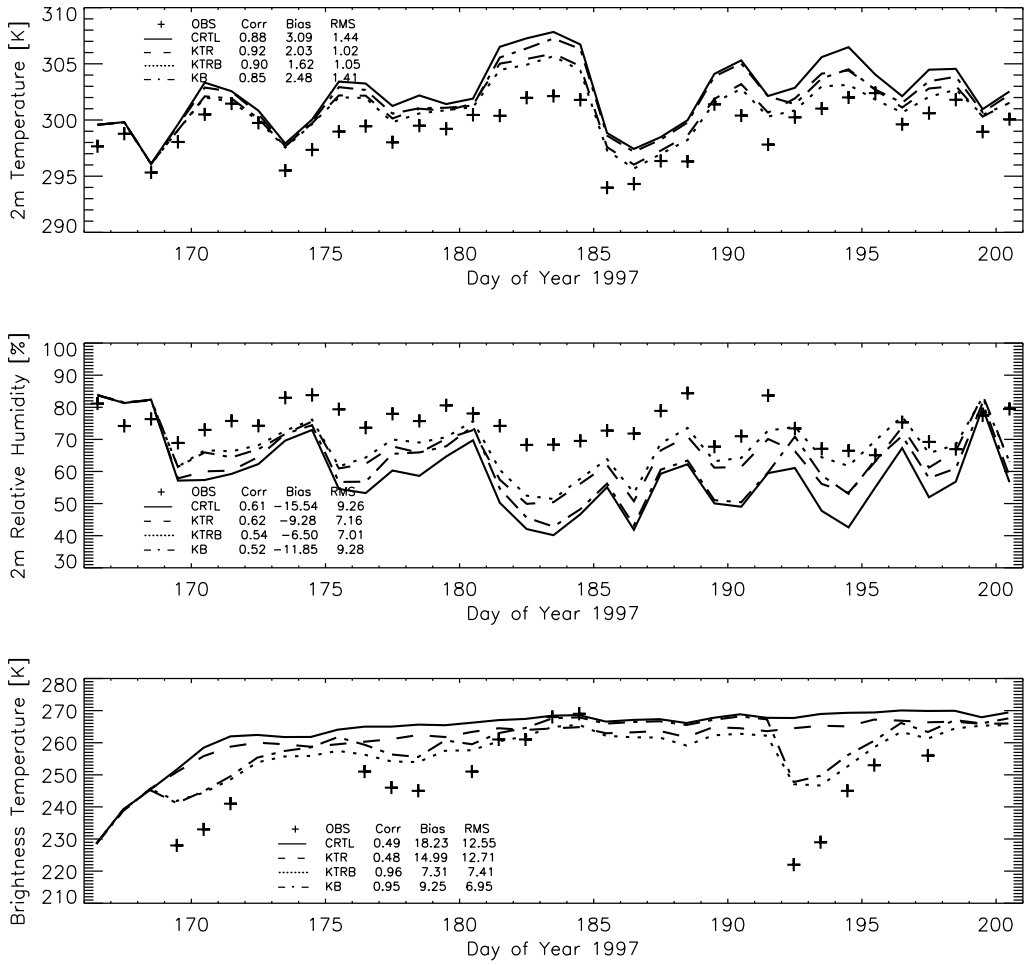


Figure B.3a: Simulations with precipitation set to zero (everything else as in Fig. B.1a).

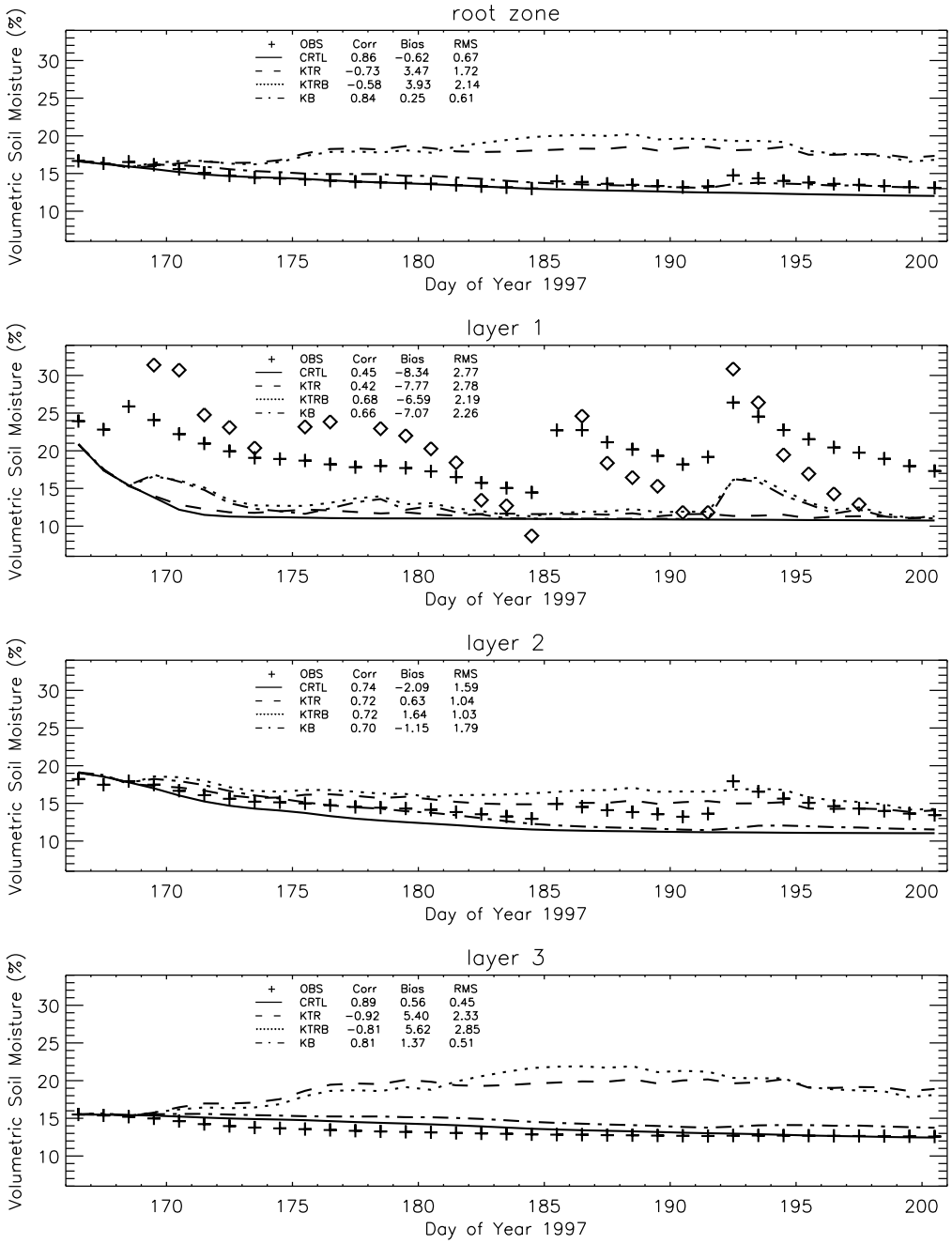


Figure B.3b: Simulations with precipitation set to zero (everything else as in Fig. B.1b).

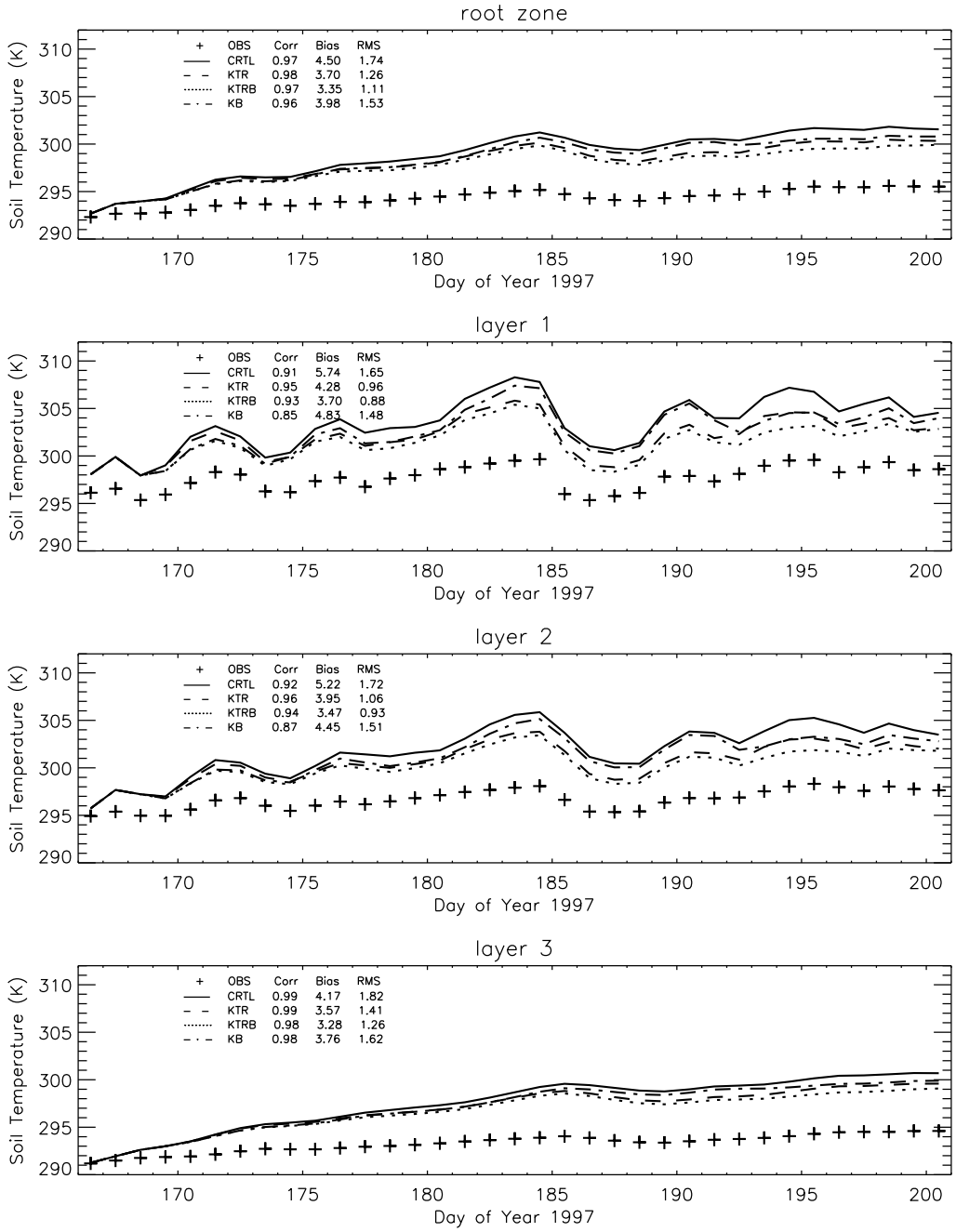


Figure B.3c: Simulations with precipitation set to zero (everything else as in Fig. B.1c).

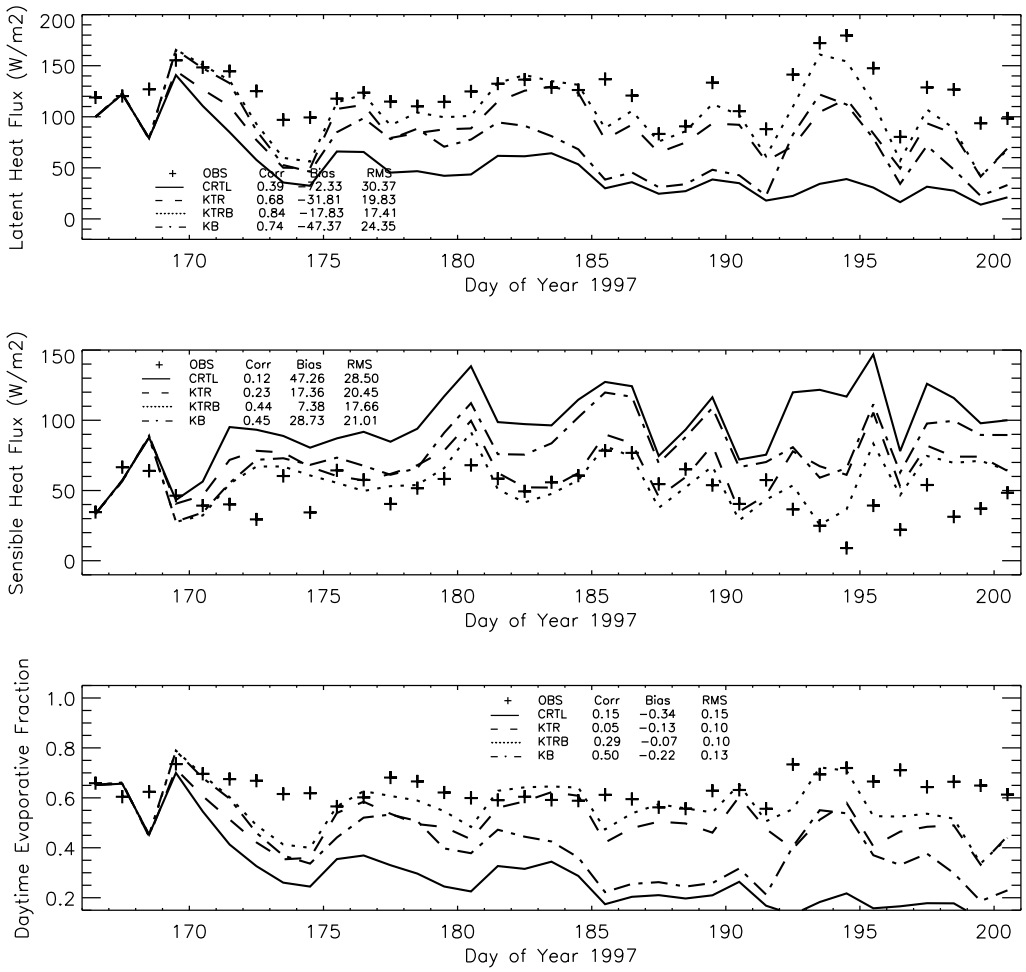


Figure B.3d: Simulations with precipitation set to zero (everything else as in Fig. B.1d).

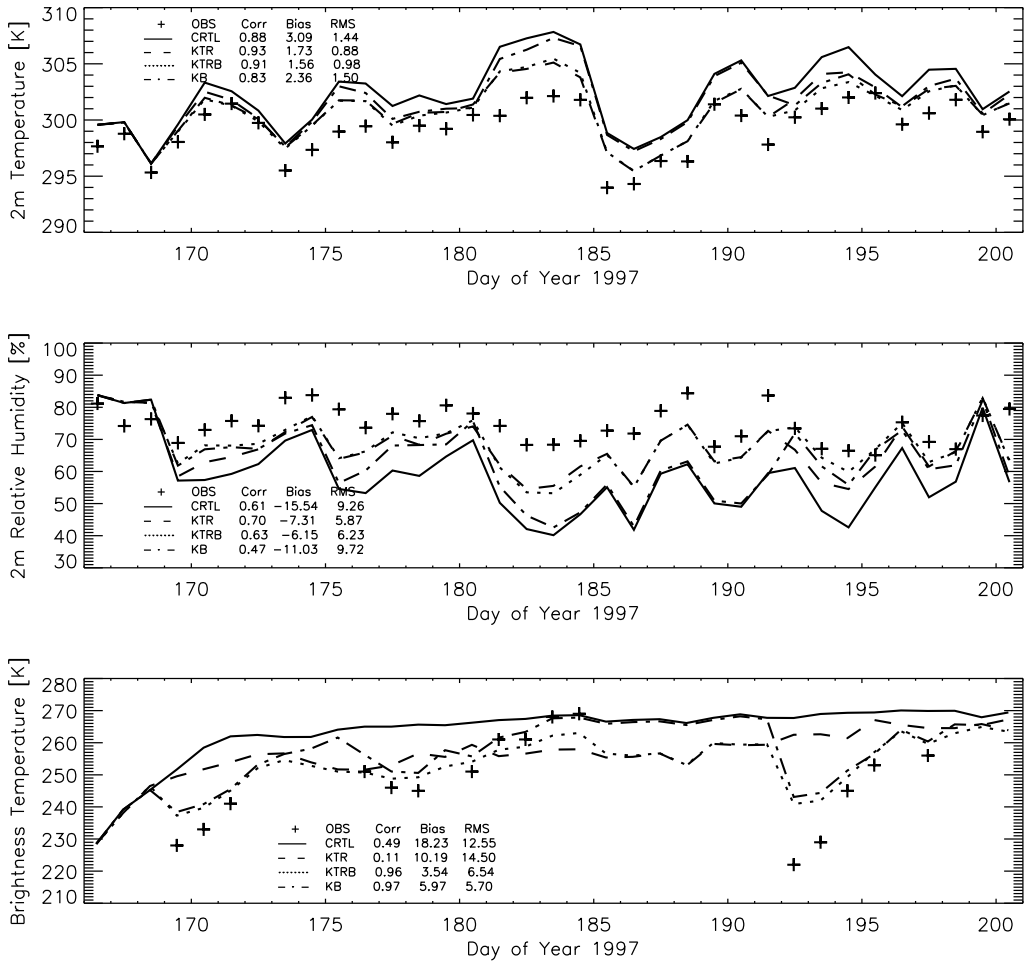


Figure B.4a: Simulations with modified, depth-varying model errors and precipitation set to zero (everything else as in Fig. B.1a).

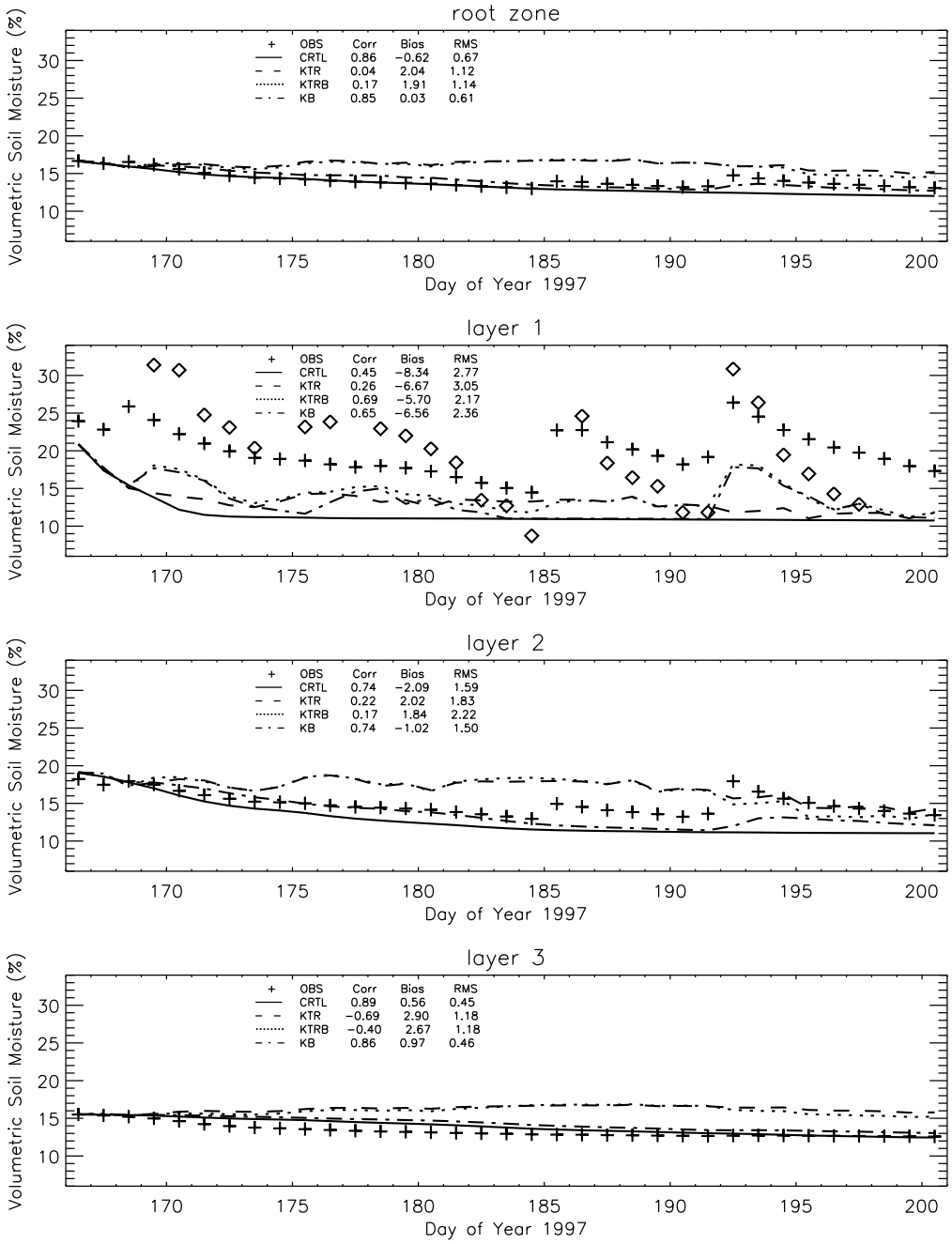


Figure B.4b: Simulations with modified, depth-varying model errors and precipitation set to zero (everything else as in Fig. B.1b).

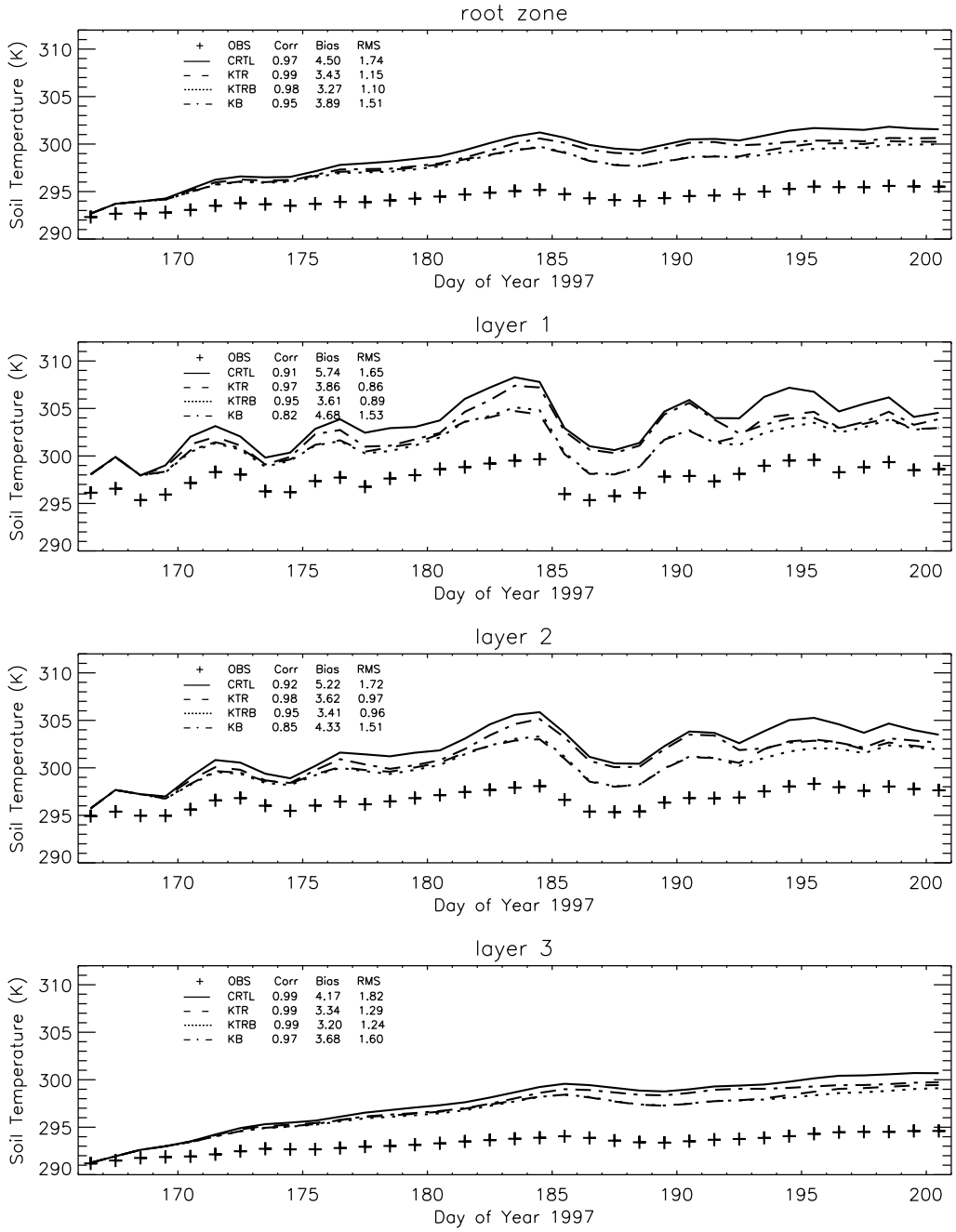


Figure B.4c: Simulations with modified, depth-varying model errors and precipitation set to zero (everything else as in Fig. B.1c).

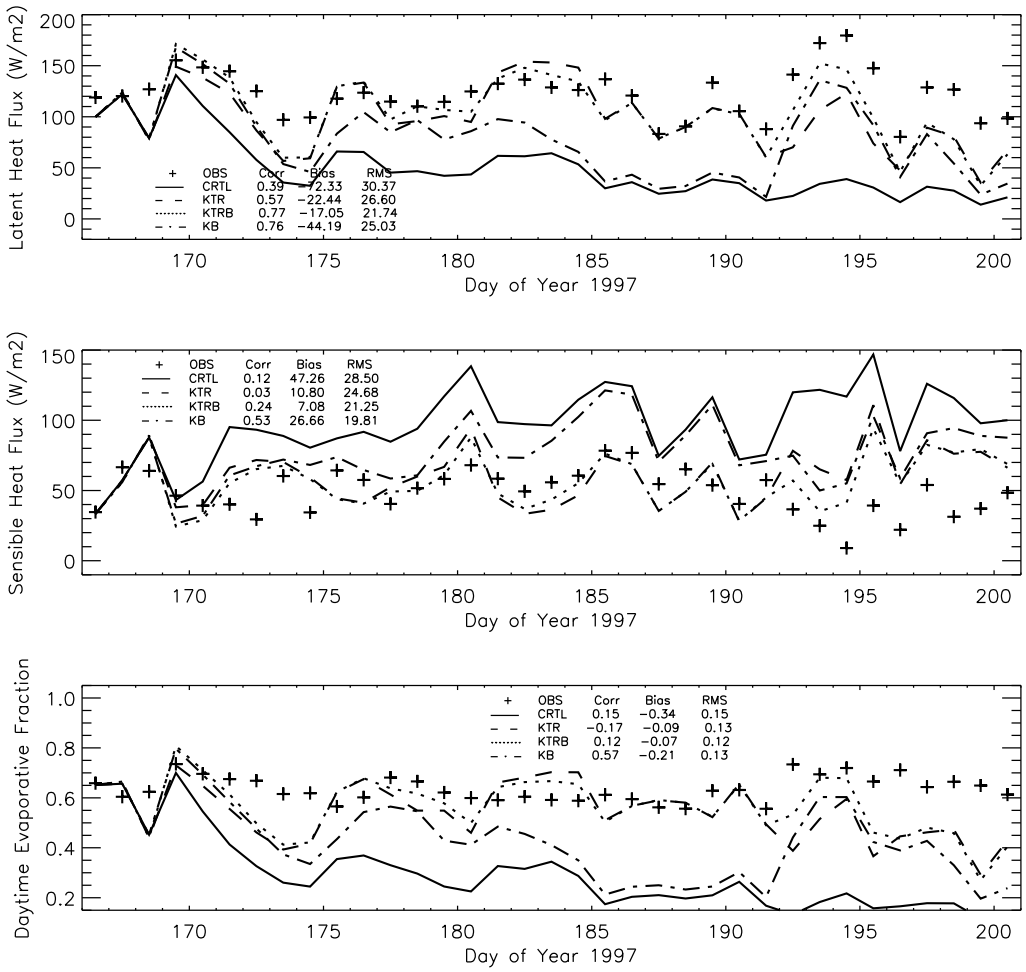


Figure B.4d: Simulations with modified, depth-varying model errors and precipitation set to zero (everything else as in Fig. B.1d).

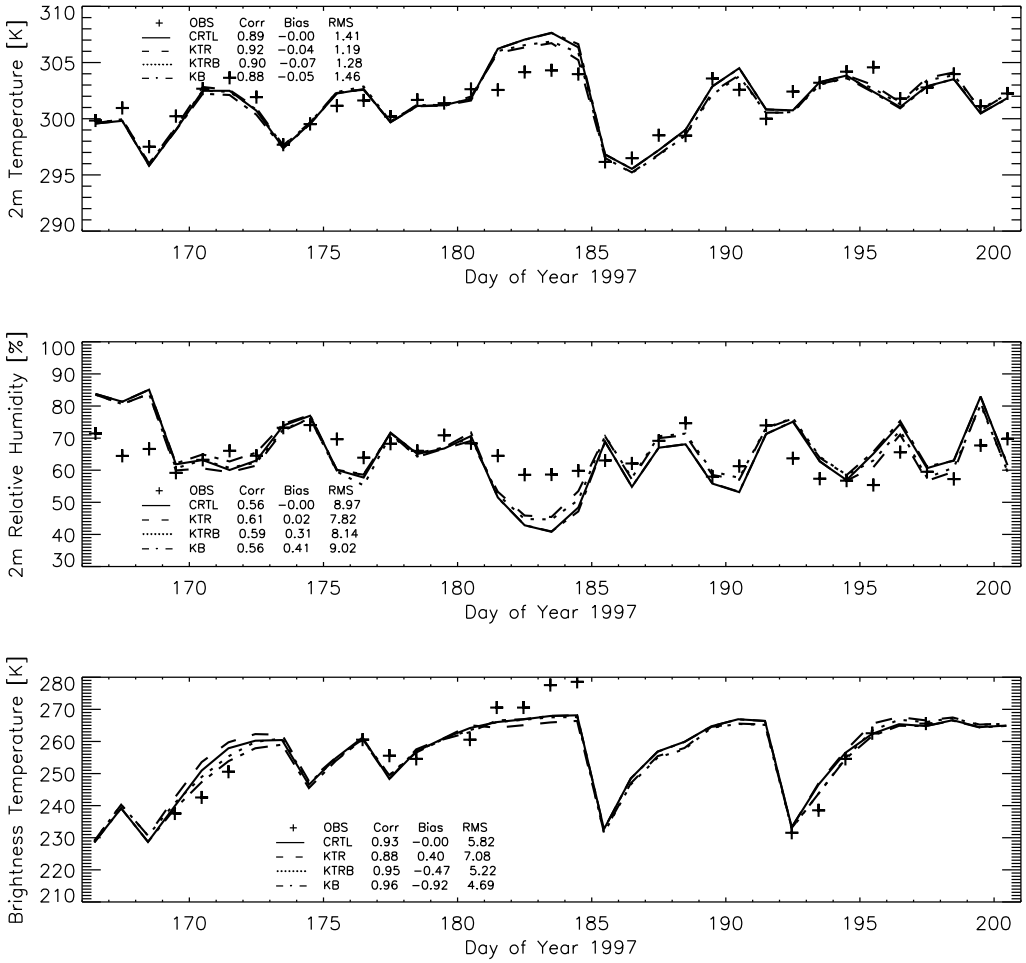


Figure B.5a: Simulations in which observations are corrected by the innovation biases found from the reference CTRL run before they are assimilated (everything else as in Fig. B.1a).

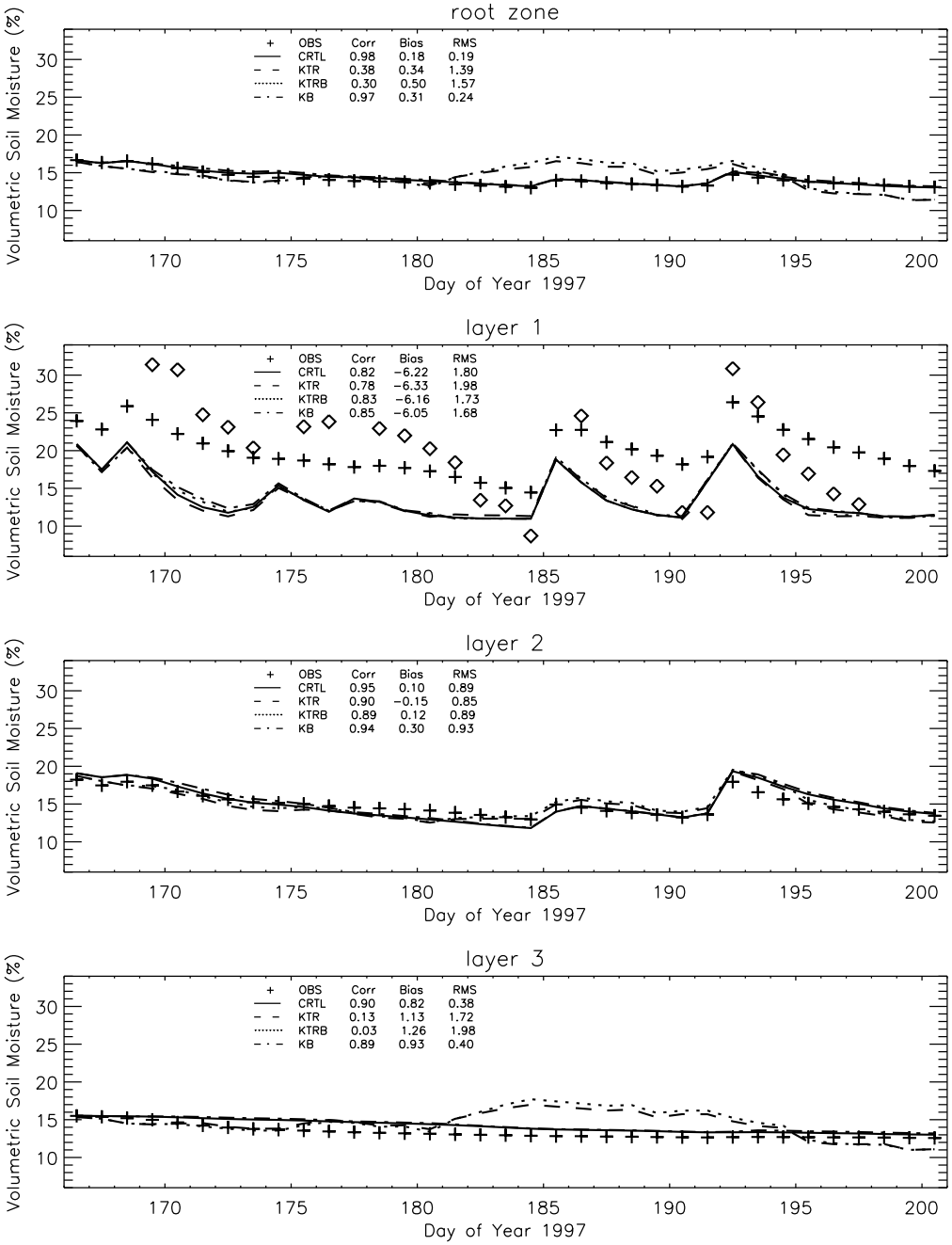


Figure B.5b: Simulations in which observations are corrected by the innovation biases found from the reference CTRL run before they are assimilated (everything else as in Fig. B.1b).

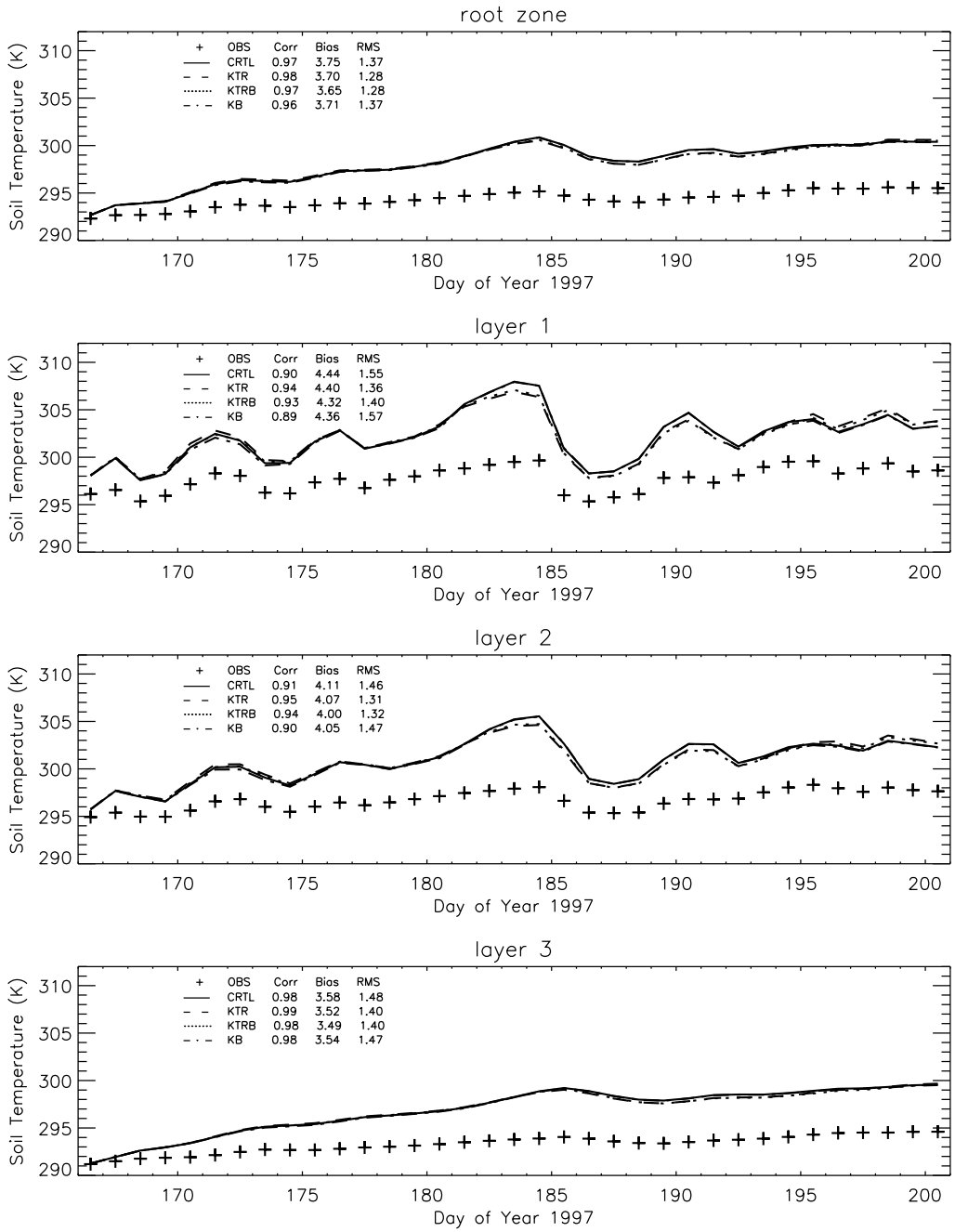


Figure B.5c: Simulations in which observations are corrected by the innovation biases found from the reference CTRL run before they are assimilated (everything else as in Fig. B.1c).

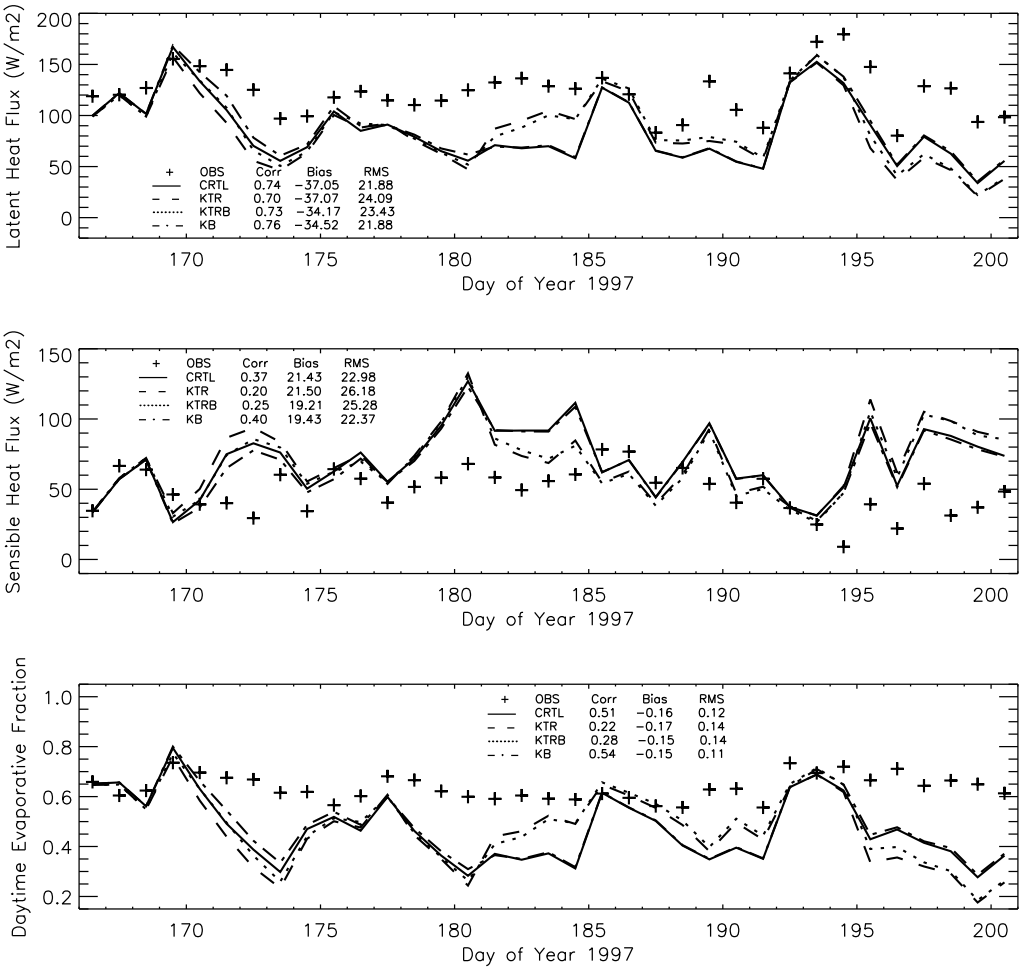


Figure B.5d: Simulations in which observations are corrected by the innovation bias found from the reference CTRL run before they are assimilated (everything else as in Fig. B.1d).

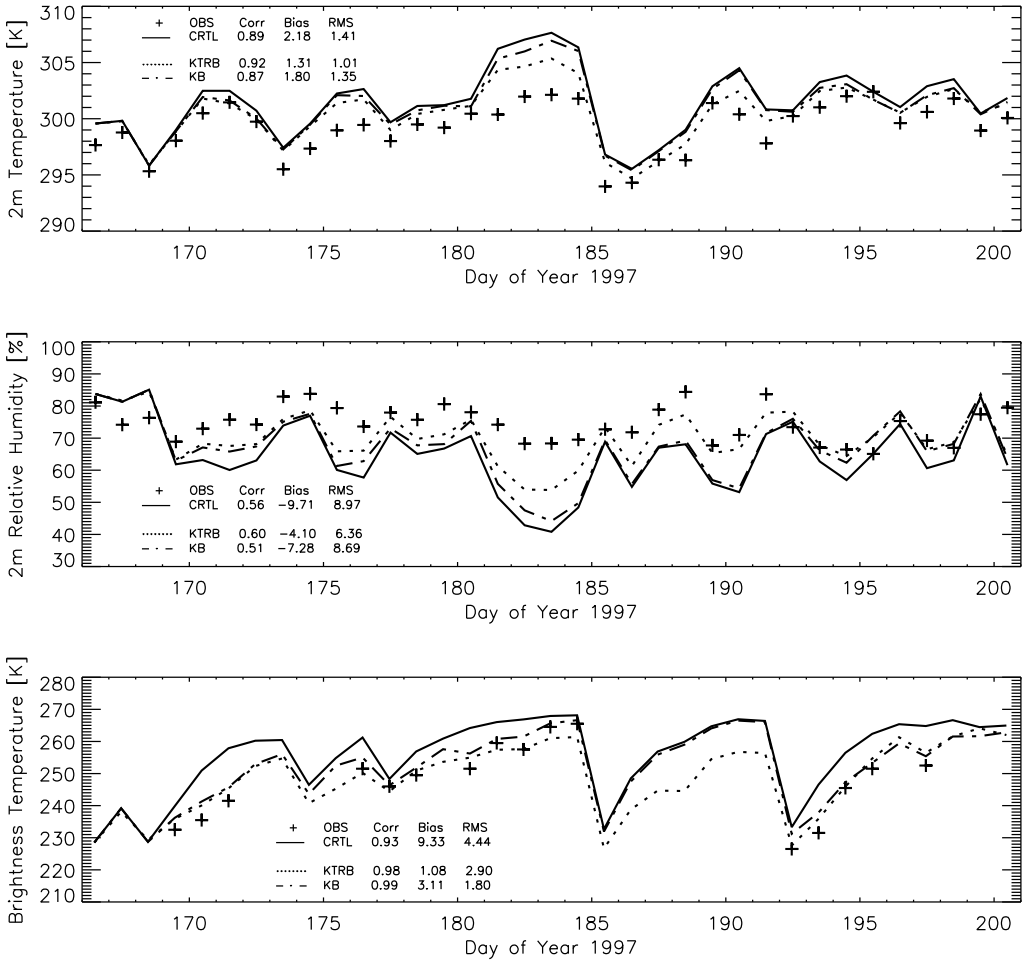


Figure B.6a: Simulations with modified, depth-varying model errors and brightness temperature observations corrected due to the profile sensitivity study before they are assimilated (everything else as in Fig. B.1a).

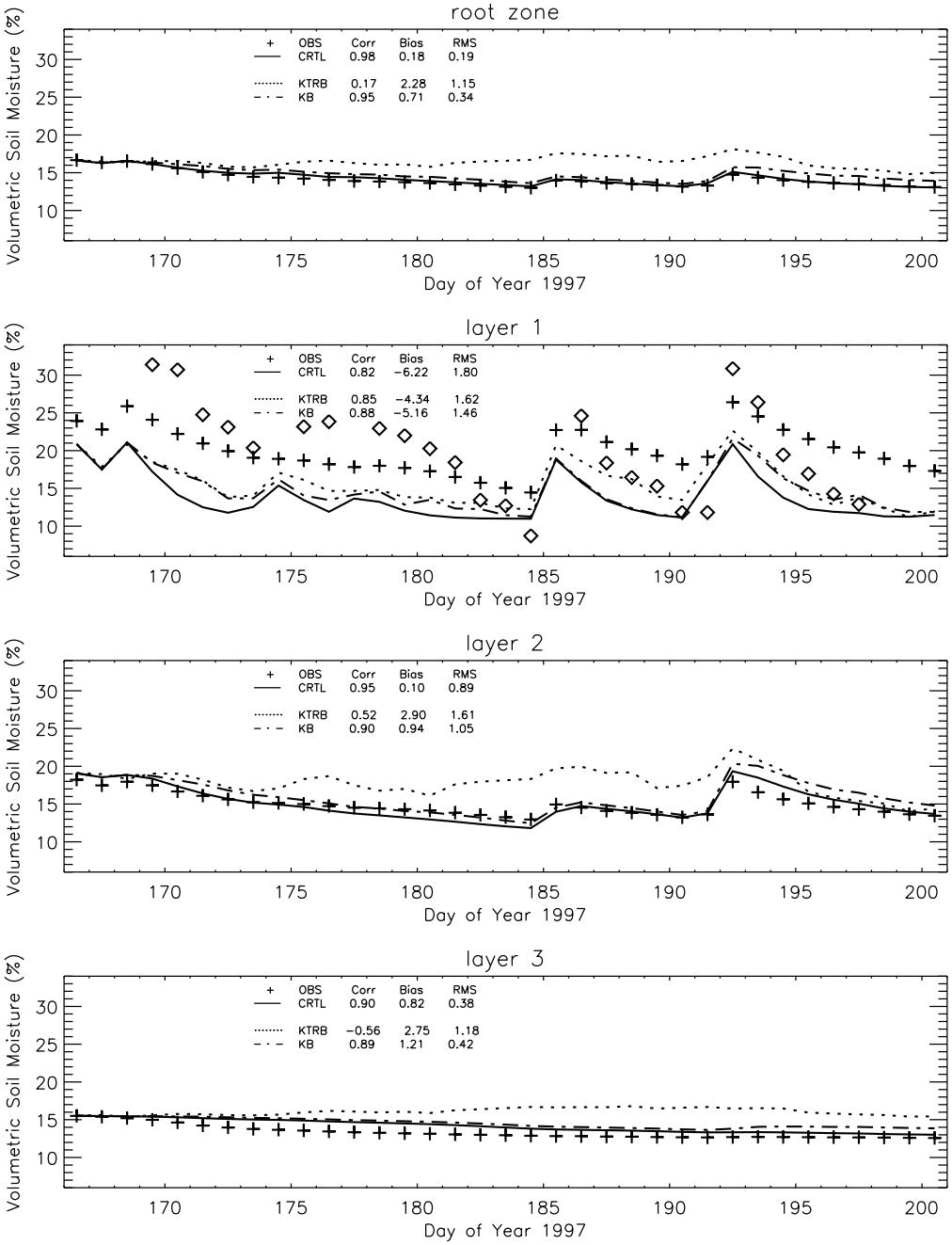


Figure B.6b: Simulations with modified, depth-varying model errors and brightness temperature observations corrected due to the profile sensitivity study before they are assimilated (everything else as in Fig. B.1b).

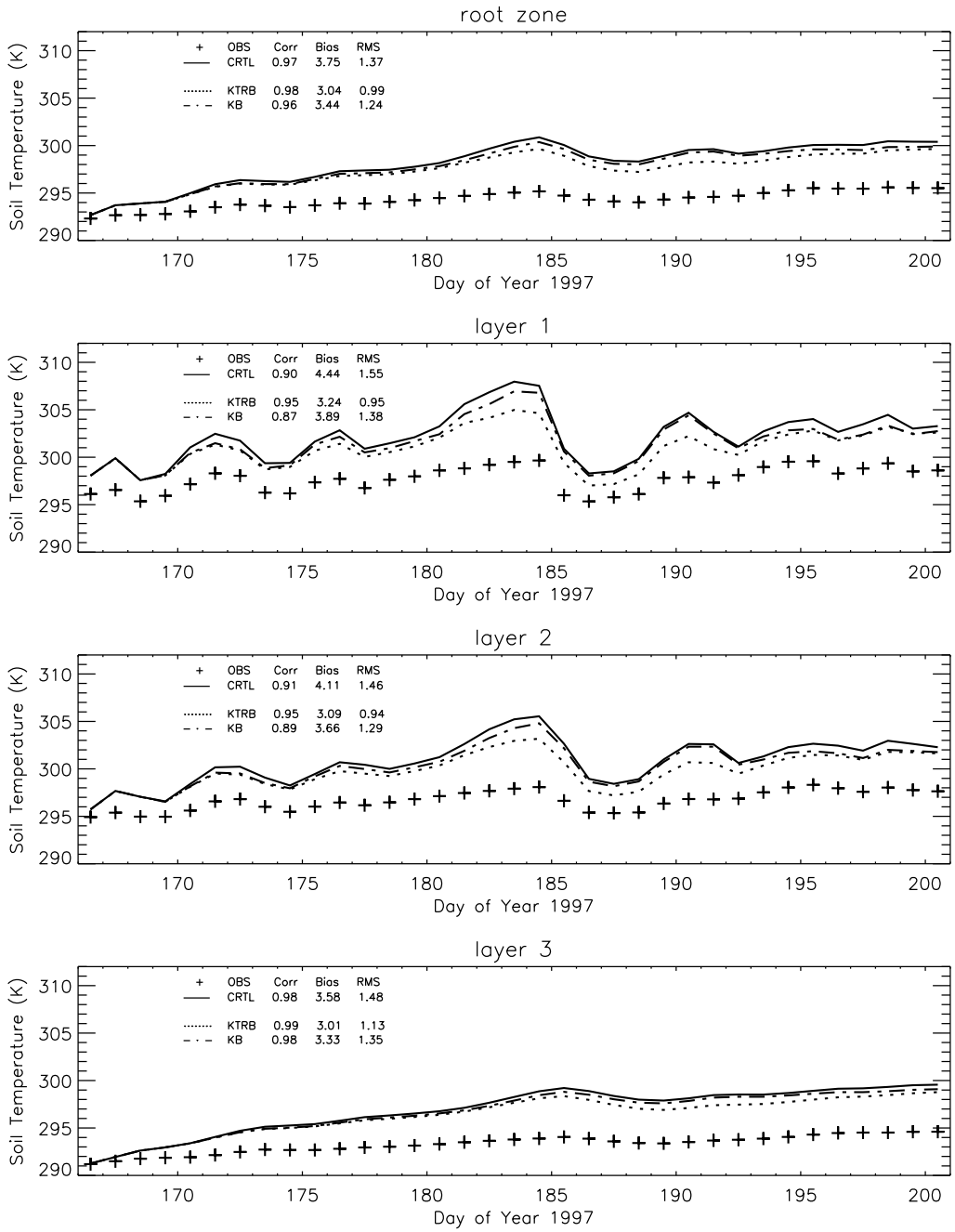


Figure B.6c: Simulations with modified, depth-varying model errors and brightness temperature observations corrected due to the profile sensitivity study before they are assimilated (everything else as in Fig. B.1c).

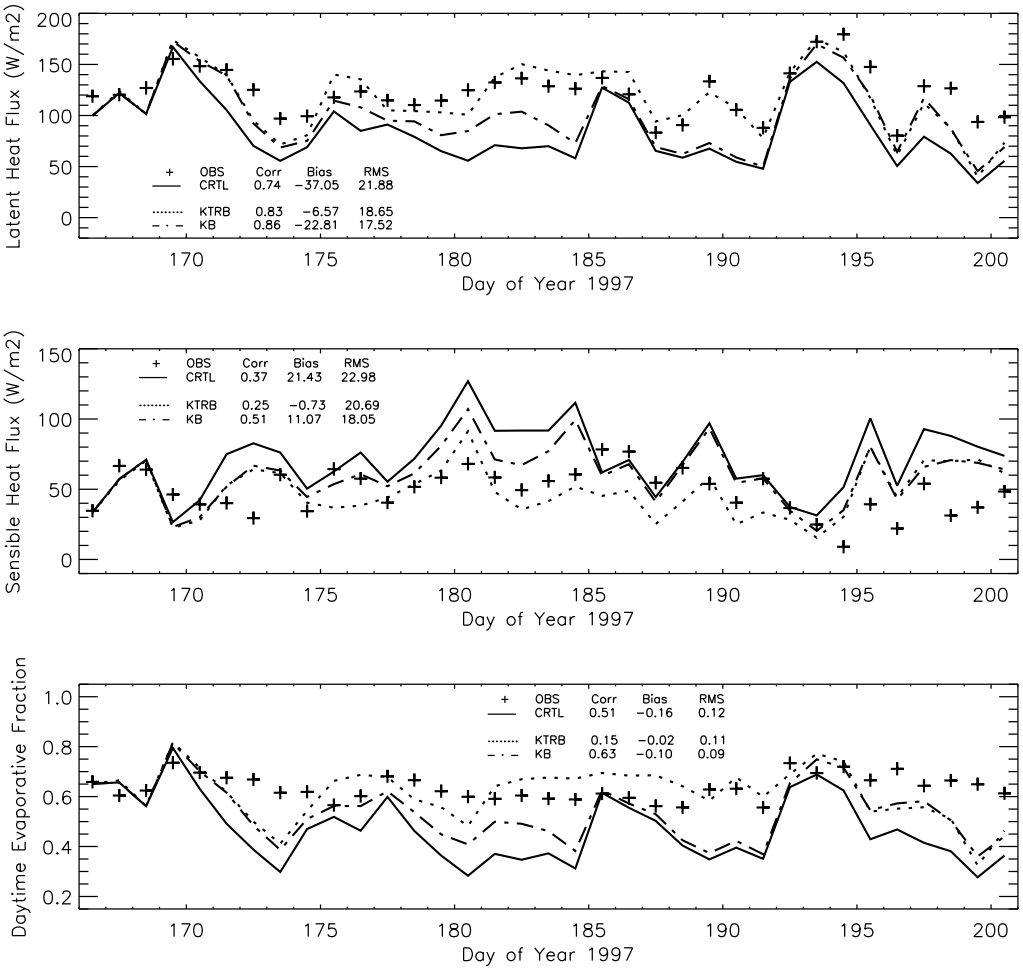


Figure B.6d: Simulations with modified, depth-varying model errors and brightness temperature observations corrected due to the profile sensitivity study before they are assimilated (everything else as in Fig. B.1d).

# Danksagung

An dieser Stelle möchte ich mich herzlich bei Prof. Dr. Clemens Simmer und Dr. Matthias Drusch für das in mich gesetzte Vertrauen und die Betreuung der Arbeit bedanken.

Privatdozent Dr. Hendrik Elbern danke ich für seine Bereitschaft, die Zweitbegutachtung dieser Dissertation zu übernehmen.

Bedanken möchte ich mich auch bei den Mitarbeiterinnen und Mitarbeitern des Meteorologischen Instituts für ein immer angenehmes Arbeitsklima. Stellvertretend seien hier insbesondere meine derzeitigen und ehemaligen "Mitbewohner" des Büros 215 genannt: René Graßelt, Marco Milan, Daniel Simonis, Linda Smoydzin, Malte Diederich und Ralf Schmitz.

Schließlich gilt mein Dank den Mitarbeitern des Europäischen Zentrums für Mittelfristige Wettervorhersage (im Speziellen Gisela Seuffert und Matthias Drusch) und all jenen, die an der Erfassung und unkomplizierten Weitergabe von Messungen im Rahmen der *Southern Great Plains Hydrology Experiments* mitgewirkt haben.

Diese Arbeit entstand im Rahmen des Forschungsprojektes ELDAS, finanziert von der Europäischen Union im Fünften Rahmenprogramm (Referenznummer EVG1-CT-2001-00050).